TECHNO-ECONOMIC EVALUATION OF ZINC AIR FLOW BATTERY IN OFF-GRID COMMUNITIES TO ACHIEVE 100% RENEWABLE PENETRATION

by

Masoud Meshkini

A Thesis Submitted in Partial Fulfillment
of the Requirements for the Degree of

MASTER OF APPLIED SCIENCE

in the department of Mechanical Engineering

Supervisory Committee

TECHNO-ECONOMIC EVALUATION OF ZINC AIR FLOW BATTERY IN OFF-GRID COMMUNITIES TO ACHIEVE 100% RENEWABLE PENETRATION

by

Masoud Meshkini

Supervisory Committee

Dr. Curran Crawford, Supervisor
Department of Mechanical Engineering

Dr. Brad Buckham, Departmental Member
Department of Mechanical Engineering

Abstract

In Canada, more than 1.11 TWh of energy per year is generated by diesel generators in off-grid remote areas. Delivering energy to these territories always has a high cost for the local and federal governments both financially and environmentally. Substituting fossil fuels with clean energies is the solution. However, the unreliability and intermittency of renewable energies (RE) are always challenging issues that need to be solved. Zinc air flow battery (ZAFB) with decoupled power and energy capacity can bring sustainability and reliability for microgrids. In this study, an efficient model was developed for ZAFB, which is applicable for large-scale modeling, and incorporated in microgrid modeling. A bilevel optimization approach was implemented in the microgrid model to find the optimal size and control of the microgrid simultaneously over the project lifetime. Using model predictive control (MPC) and based on user-defined foresight horizon and known information like energy demand and RE resources, the control model decides the future changes in microgrid components. This tool is used to propose the best microgrid design for these communities to reduce or eliminate their dependency on fossil fuels. The functionality of this tool was evaluated by three case studies in British Columbia: Blind Channel, Hot Springs Cove and Moresby Island. Zero CO_2 emission and zero fuel consumption were achieved by a 100% RE microgrid consisting of wind and tidal turbines and large ZAFB. The net present cost (NPC) of this system and cost of energy are 39 – 46 % and 55 – 60 % less than the base case costs in which diesel is the main energy source. ZAFB with a longer storage duration (50 – 60 hours) satisfies 17 – 23% of annual energy demand in these case studies.

Table of Contents

List of Tables

List of Figures

Nomenclature

Abbreviations

CAPEX	Capital Expenditure
CCOS	Cycle Charging Operation Strategy
DG	Distributed Generation
EMS	Energy Management System
ESS	Energy Storage System
GHI	Global Horizontal Irradiance
HER	Hydrogen Evolution Reaction
HOMER	Hybrid Optimization of Multiple Energy Resources
HRES	Hybrid Renewable Energy System
HVAC	Heating Ventilation and Air conditioning
LCOE	Levelized Cost of Energy
LFOS	Load Following Operation Strategy
MILP	Mixed Integer Linear Programming
MINLP	Mixed Integer Nonlinear Programming
MIQCP	Mixed Integer Quadratically Constrained Programming
MIQP	Mixed-Integer Quadratic Programming
MPC	Model Predictive Control
NLP	Nonlinear Programming
NPC	Net Present Cost
NPV	Net Present Value
O&M	Operation and Maintenance
ODE	Ordinary Differential Equation
OER	Oxygen Evolution Reaction
OPEX	Operational Expenditure
ORR	Oxygen Reduction Reaction
PRIMED	Pacific Regional Institute for Marine Energy Discovery
RE	Renewable Energies
SoC	State of Charge
VRFB	Vanadium Redox Flow Battery
ZAFB	Zinc Air Flow Battery
Zn	Zinc
ZnO	Zinc Oxide

Symbols

A_{cell}	Cell active area

A_i	Anisotropy index
α_{air}	Charge transfer coefficient of forward reactions in air electrode
α_{zn}	Charge transfer coefficient of forward reactions in zinc electrode
β	Slope of the surface
β_{air}	Charge transfer coefficient of backward reactions in air electrode
β_{zn}	Charge transfer coefficient of backward reactions in zinc electrode
$C_{Fuel-annual}$	Annual fuel cost
$C_{O\&M-annual}$	Annual O&M cost
$C_{Replacement}$	Replacement cost
$C_{capital}$	Capital cost
$C_{capital-Generator-kW}$	Capital cost per kW of generator
$C_{capital-Regenerator-kW}$	Capital cost per kW of regenerator
$C_{capital-Storage-kWh}$	Capital cost per kWh of energy storage
$C_{capital-kW}$	Capital cost per kW
$C_{carbon\ tax}$	Carbon tax cost
C_t	Cost of the system at time t
$d_{r,N}$	Nominal discount rate
$d_{r,real}$	Real discount rate
d_r	Discount rate
E_B	Stored energy for the ZAFB
E_R'	Energy demand to regenerate the zinc from zincate
E_{act}^B	Battery activation loss energy
E_{act}^R	Regenerator activation loss energy
E_{annual}	Total annual energy production
E_{ch}	Charge energy
E_{dis}	Discharge energy
E_{in}	Input energy
E_{losses}^B	Battery losses energy
E_{losses}^R	Regenerator losses energy
E_{max}	Total energy capacity
E_{ohmic}^B	Battery ohmic loss energy
E_{ohmic}^R	Regenerator ohmic loss energy
E_{out}	Output energy
E_{served}	Total delivered energy over the project lifetime
η	Efficiency

η_{dis}	Battery efficiency
η_B	Battery efficiency
η_R	Regenerator efficiency
η_{act}^{Zinc}	Zinc electrode activation loss
η_{act}^{air}	Air electrode activation loss
η_{ch}	Charge efficiency
η_{ch}^{max}	Maximum discharge efficiency
η_{ch}^{min}	Minimum discharge efficiency
η_{dis}^{max}	Maximum discharge efficiency
η_{dis}^{min}	Minimum discharge efficiency
η_{ohmic}	Ohmic loss
η_{sys}	System efficiency
F	Faraday constant
f	Inflation rate
F_0	Fuel curve intercept
F_1	Fuel curve slope
F_d	Diesel fuel consumption
f_{PV}	Derating factor
f_b	Horizon brightening factor
$FV_{n,fuel}$	Future value of fuel price
F_{annual}	Annual fuel consumption
$\bar{G}$	Global Horizontal Irradiance
$\bar{G}_{T,STC}$	Incident radiation at standard test conditions
$\bar{G}_T$	Global radiation incident on the PV array
$\bar{G}_b$	Beam radiation
$\bar{G}_d$	Diffuse radiation
i_0^{zinc}	Zinc electrode exchange current density
i_{H}	Hydrogen Evolution Reaction current density
i_{Zn}	Zinc electrode current density
i_{air}	Air electrode current density
i_0^{air}	Air electrode exchange current density
i_{cell}	Cell current density
I_B	Battery current
i_{fuel}	Fuel escalation rate
I_R	Regenerator current
I_{stack}	Stack current
m	Number of microgrid components
n	Project lifetime
n_e	Number of electrons

N_{series}	Number of series cells
N_P	Number of parallel modules
$N_{total,Zn}$	Total moles of zinc
P	Turbine output power
$\hat{P}$	Dimensionless variable of turbine output power
P_{PV}	Solar PV output power
P_{cell}	Cell power
P_{gen}	Output power of the generator
P_r	Rated power of the turbine
P_{r-Gen}	Rated power of battery
$P_{r-Regen}$	Rated power of regenerator
R	Gas constant
R_{ohmic}	Ohmic resistance
ρ_g	ground reflectance
SoC_B	Battery state of charge
SoC_R	Regenerator state of charge
T	Temperature
V_B	Battery voltage
V_R	Regenerator voltage
V_{cell}	Cell current density
V_{oc}	Open-circuit voltage
V_{stack}	Stack voltage
$\widehat{\lvert v \rvert}$	Dimensionless variable of wind speed
$\lvert v \rvert^*$	Design speed
Y_{PV}	Rated capacity of PV array
Y_{gen}	Rated capacity of the diesel generator
$ZAFB_{energy\ cap}$	Energy storage capacity of ZAFB

Acknowledgments

I would like to thank:

My supervisor, Dr. Curran Crawford, for believing in me, his support and kindness, and his supervision. Dr. Crawford is fantastic and nice mentor. He is always supportive and problem solver. Working with Curran and being his student was a great honor for me.

Chapter 1

1. Introduction

1.1 Background

In the 21st century, the most challenging issue in the world is global warming. Given that 80% of the total world energy demand is currently met by fossil fuels and that global energy demand is forecast to increase by 30% by 2040, the current situation is expected to deteriorate even further [1]. Most developed countries are planning to achieve net-zero CO_2 emission by 2050 through various policies and technologies like the carbon tax, electrification, clean energies, and carbon capture. Canada is one of the leading countries in this field. Electrification is a decent way to achieve this goal. However, the energy source in this process is very important, and using renewable energies (RE) can be a solution for this goal. Renewable energies are clean and environmentally friendly, but they are not always reliable and sustainable, which means that natural resources may not always be available, for example, there may be enough solar radiation at noon during the summer days but not at night, and there may not be windy days during the week. So, applying an appropriate energy storage system (ESS) can improve the reliability and sustainability of renewable energies. Microgrids in which RE are the primary energy source are the future of outdated central grids and transmission lines.

In Canada, there are 204 off-grid communities with a total population of 114000, in which diesel electric generators are the main source of energy. The total capacity of these generators is around 586 MW, with an annual energy generation of more than 1.11 TWh/yr emitting approximately 0.277 Mtonnes CO_2/yr [2]–[4]. Figure 1.1 shows Canada's remote communities. Delivering energy for these territories always has a high cost for the local and federal governments both financially and environmentally.

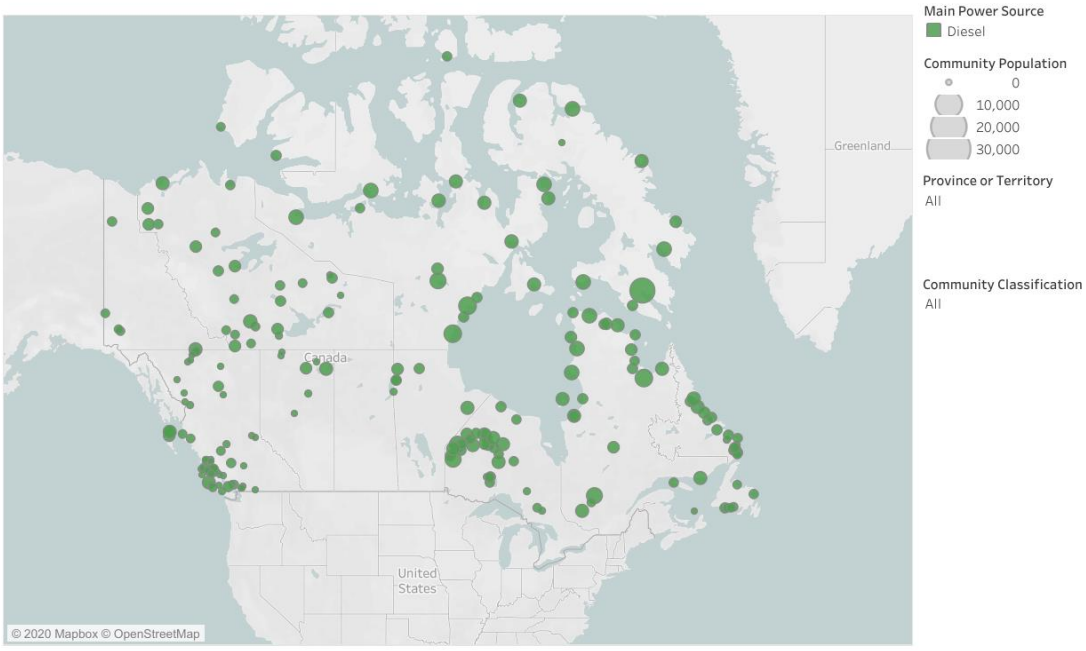

Figure 1.1. Canada's off-grid communities [3]

Renewable energies are a clean substitute for diesel generators in these areas. Figure 1.2 shows the average annual wind speed all over Canada. It can be seen that mean wind speed in these off-grid regions is between 6 – 7 m/s, which presents the opportunity for a significant portion of energy demand in these remote areas to be satisfied by harnessing this source of clean energy through wind turbines. The solar energy map in Canada is shown in figure 1.3. It can be seen that a huge amount of solar energy (1000 – 1100 kWh/kW/yr) can be produced annually in most of these off-grid areas. Therefore, solar energy can be the second good option, along with wind energy, to replace diesel. In addition, most of these remote areas are coastal and have access to ocean water and abundant tidal energy. Therefore, wind, solar and tidal energies can be used in these territories.

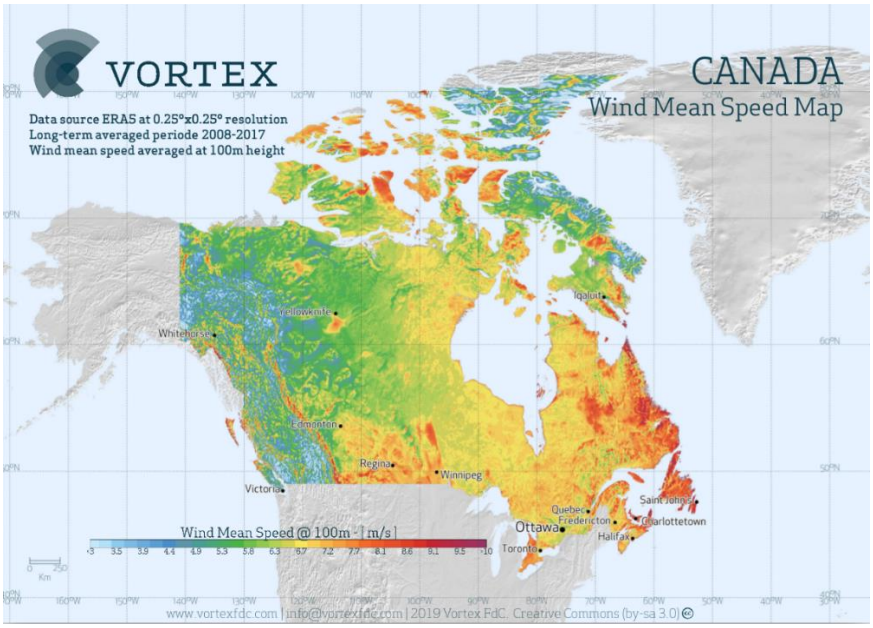

Figure 1.2 Annual mean wind speed in Canada [5]

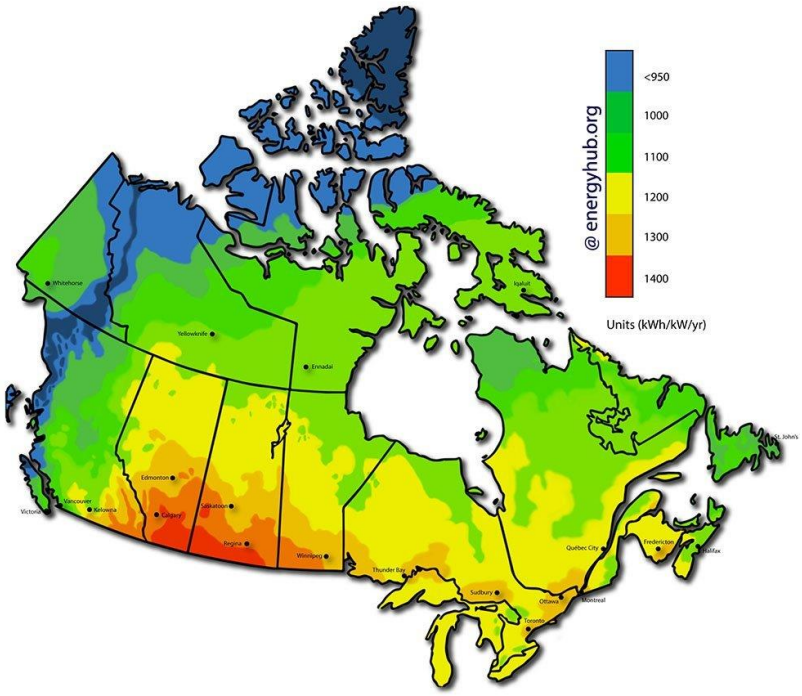

Figure 1.3 Solar energy production potential in Canada [6]

Microgrids, in which RE are the primary energy source, are the best solution to reduce/eliminate the Canadian off-grid communities' dependency on diesel by incorporating maximum RE penetration. However, RE are intermittent and unreliable. Using an efficient ESS can solve this issue and bring reliability and sustainability to the microgrid. Batteries are generally used in microgrids, particularly, Lead Acid, Li-ion, and Vanadium Redox Flow Batteries (VRFB). Li-ion batteries are typically used as a short duration ESS which means that they are not a good option for longer discharge duration like 24 hours to few days, and power and energy storage are coupled means that there is no specific separate unit for charge/discharge. Unfortunately, the degradation rate of Li-ion batteries is much greater than flow batteries. Safety and high cost are other issues with Li-ion batteries. VRFB are typically used for longer-term applications. Although the energy capacity and the power unit are decoupled in VRFB, which makes it well suited for a microgrid, it has low energy density and expensive components and electrolyte, and it is not environmentally friendly, and it is toxic to animals and humans. Zinc air flow battery as a type of metal-air flow battery is a promising solution for microgrids due to its outstanding features.

The most important factor that makes the ZAFB suitable for microgrids is the cheap raw material. As shown in figure 1.4, ZAFB has a much cheaper raw material for energy storage than Li-ion batteries and VRFB. Zinc, the raw material of ZAFB, costs around 10 $/kWh [7], whereas VRFB has the most expensive material (for energy storage) cost of 125 $/kWh. Also, there are no environmental issues with zinc, and it has a high energy density.

The second feature of ZAFB is the capability for longer-term applications and its lowest capital cost for long-duration energy capacity. Figure 1.5 shows the capital expenditure (CAPEX) of three different technologies with respect to storage duration. It can be seen that ZAFB has the lowest capital cost for energy storage capacity above 8 hours, and CAPEX is reduced significantly by increasing the storage duration. For longer storage duration, more electrolyte is added to the tank for such a small amount of money, whereas Li-ion requires new cells to be added.

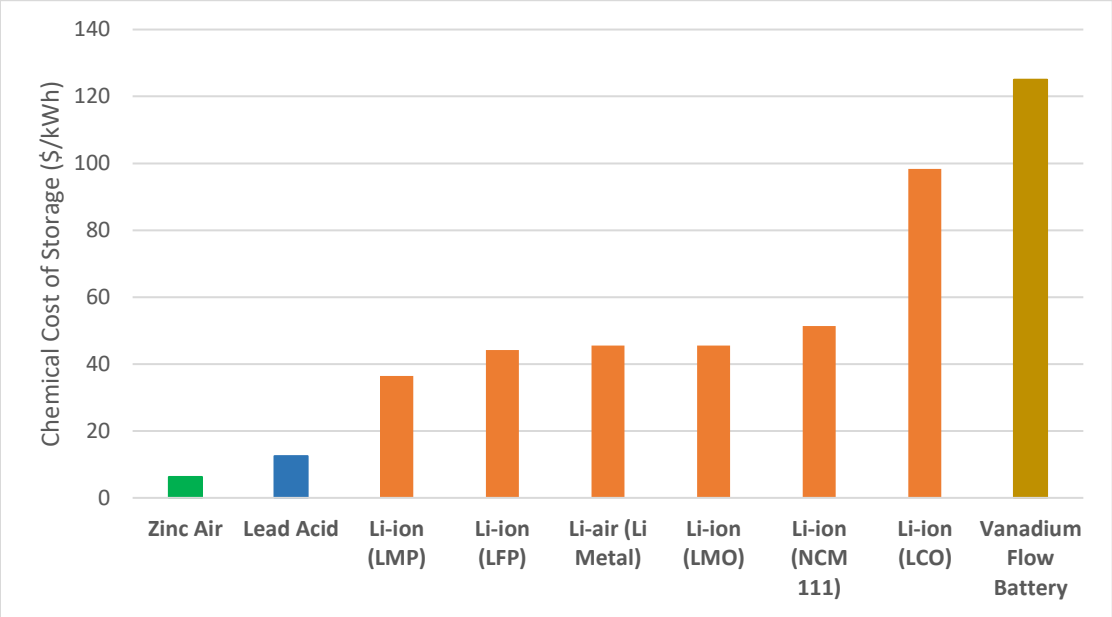

Figure 1.4 Material cost of different battery technologies [8]

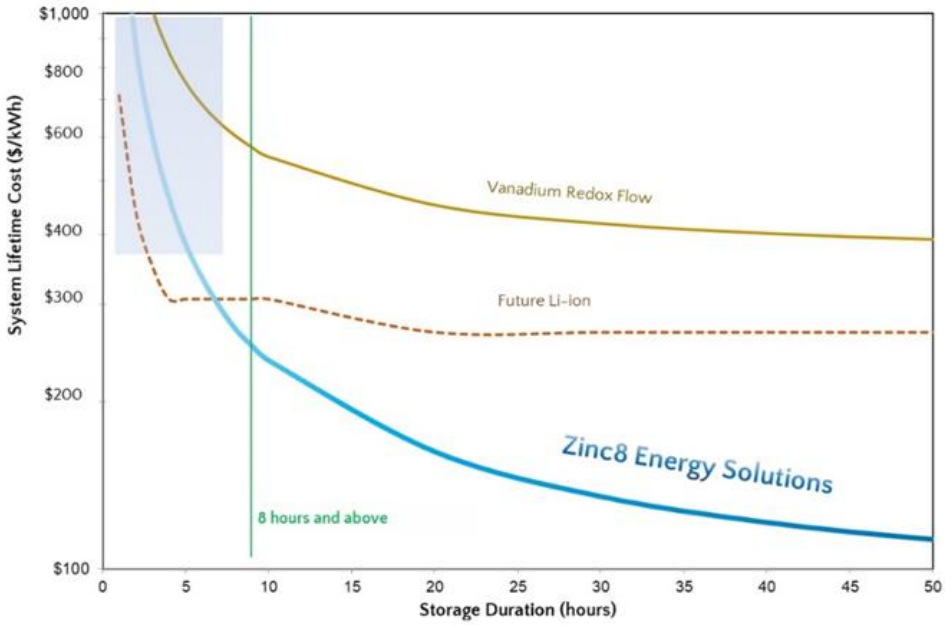

Figure 1.5 Capital cost of ZAFB, VRFB, and Li-ion battery (image credit: Zinc8) [9]

The last reason that makes the ZAFB system the best choice is its scalability. Because this system's main parts, including energy storage, charge, and discharge units, are decoupled, which means that there is a distinct unit for charging the battery (regenerator)

and a distinct unit for discharging (generator) and a distinct unit for energy storage, each one can separately be scalable for different conditions, requirements, and applications.

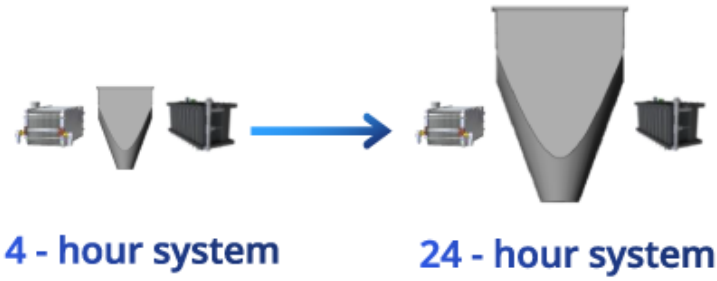

Figure 1.6 Scalable main parts of ZAFB (image credit: Zinc8) [9]

1.1.1. Microgrid

The idea of microgrid originated from the distributed generation (DG) concept in which energy generators are close to the customers and consumers rather than centrally located at a single power plant. DG is a solution for central grid capacity issues with lower investment and higher efficiency. One of the most important factors in the DG concept is the ability to use RE in the grid. Microgrids are small energy systems, shown in figure 1.7, in which renewable energies are the main energy source, and they can be applied in school/university campuses, military bases, office parks, hospitals, and residential or any remote areas [10], [11]. As shown in the figure, microgrids can be grid-connected or off-grid. In this study, off-grid microgrids have been evaluated.

Microgrid configuration and Characteristics

Microgrid components can include:

- Renewable energy plants such as wind turbines, solar photovoltaic (PV), tidal and hydro turbines, etc.
- An ESS such as a battery, pumped hydro storage, or hydrogen storage, etc.
- Fuel cell stacks and green hydrogen plants
- Heat pumps for converting renewable plants' excess production (curtailment) to heat for heating the spaces and hot water.

- A controller which controls the input and output of all these units to achieve optimal operation
- Diesel generators as a spinning reserve are used when RE production and ESS discharge cannot satisfy the demand.

Specifications of microgrids are listed as below [12]:

1. Local: The microgrid covers the local clients' energy demand by generating energy by harnessing the available local natural resources, including solar, wind, tidal, wave, etc. With local production, there is no need for long-distance transmission lines due to their proximity. So, the transmission line losses are almost eliminated.
2. Independent: Islanding and localizing reduce the dependency of these small grids on the central grid. Consequently, microgrids won't be affected by the central grid. However, sometimes, microgrids can have a connection to the central grid to exchange energy to enhance reliability and lower costs.
3. Smart: Microgrids have an advanced controller which controls the energy flow from each source (RE, ESS, generator, . . .) based on available resources to meet the customers' energy demand and always chooses the optimum fleet of energy sources.

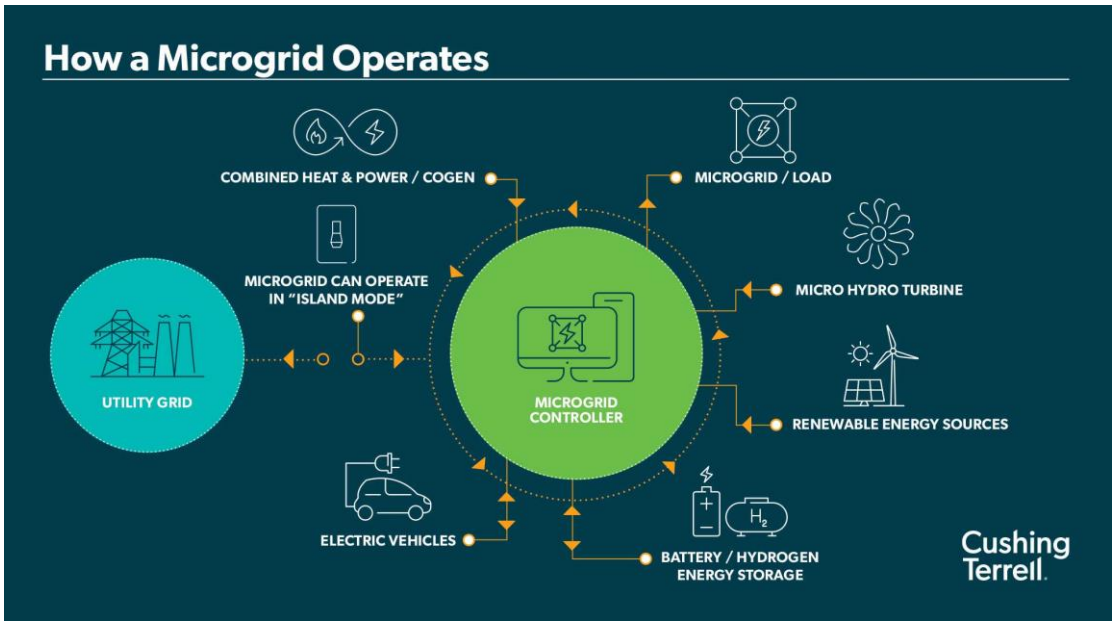

Figure 1.7. Microgrid components [12]

1.1.2. Modeling

Many studies are available in the literature in which microgrids and hybrid systems consist of diesel, wind turbine, solar PV, and a battery with various sizes and load profiles and locations were evaluated. Most of these microgrid modelings were done using the established modeling tools. These microgrid modeling tools, along with their features and weaknesses, are listed as below [10]:

1. HOMER:

   In 1993, North-American National Renewable Energy Laboratory (NREL) proposed the Hybrid Optimization Model for Electric Renewables (HOMER). HOMER is one of the most commonly used tools in microgrid modeling and is used for optimizing the operation and investment of the microgrid to reach minimum net present cost (NPC). HOMER doesn't solve any optimization problem. It uses an accounting method to simulate all feasible solutions of the system in the search domain then finds the system with the lowest cost among these solutions.

   Weaknesses:

   - HOMER PRO is not free.
   - Simple solution method (accounting method) for optimization problems

2. DER-CAM:

   Distributed Energy Resources Customer Adoption Model (DER-CAM) was developed by Lawrence Berkeley National Laboratory (LBNL). It is based on a General Algebraic Modeling System (GAMS) for solving Mixed Integer Linear Programming (MILP) microgrid models via CPLEX solver. DER-CAM is applied for microgrid design, reliable grid components operation, and assessing the potential market for microgrids economically and environmentally. DER-CAM optimizes the operation and investment costs.

   Weaknesses:

   - It is only used for MILP
   - GAMS is needed, which is not free
   - Short-term analyses (1 year) not used for long-term

- Limited output

3. EAM:

   Asano, Bando, and Watanabe developed Economic Evaluation of Microgrids (EAM) in Japan. EAM is used for solving Mixed Integer Nonlinear Programming (MINLP) to minimize the costs of the microgrid by optimization of operation and investment. It is very similar to DER-CAM.

   Weaknesses:

   - Unavailable
   - Short-term analyses (1 year)

4. MARKAL/TIMES:

   Market Allocation model (MARKAL) and The Integrated MARKAL-EFOM (Energy Flow Optimization Model) System (TIMES) are widely used in industry and academia for energy systems long-term analyses, specifically microgrid modeling, and optimization. Environment, economics, and energy are the main fields assessed by this tool. MARKAL/TIMES solves the MILP by CPLEX in GAMS and only minimizes the investment costs.

   Weaknesses:

   - Commercial license
   - GAMS needed
   - No operation optimization
   - It is used for MILP
   - Limited output

5. RETScreen:

   In 1996, RETScreen Clean Energy Project Analysis Software was developed by the government of Canada, Industry, and Academia by Natural Resources Canada. It is free and for public use. RETScreen analyses the grids costs, energy generation, energy savings, emission, and project feasibility and risks. RETScreen compares the conventional and RE cases for the given scenarios to determine the best option. RETScreen is used for optimizing the investment costs for both small and large-scale projects. RETScreen has an accounting

method for finding the minimum cost and doesn't solve any optimization problem.

Weaknesses:

- Unavailable for further developments and update
- No operation optimization
- Limited and simple solution method for the optimization method
- Large time resolution, monthly time step

6. H_2RES

Instituto Superior Técnico (IST-UTL) and University of Zagreb (UZagreb) developed the H_2RES in 2000. This modeling tool is applied for off-grid communities to maximize the RE integration by optimizing the operation of components. Its solution method is based on energy balancing. H_2RES includes the models for wind, solar, hydro, geothermal, biomass, and fossil fuels plants, and even central grid connection except tidal and nuclear power. Also, it contains most energy storage systems (ESS) except compressed air. Hydrogen storage and fuel cell models are available in this tool.

Weaknesses:

- Unavailable
- Limited solution method
- No investment optimization

Among the microgrid modeling tools, HOMER is the most popular one, which is applied as a modeling and optimization tool in most studies for sizing and energy management. Some of these studies are shown in the table 1-1.

Table 1-1 Microgrid (off-grid) models using HOMER

Authors	System	Location	Findings
Kamel et al. [13]	Wind turbine (200kW)+solar PV (1kW)+battery(80kwh)+diesel gen (100kW)	Egypt	- 37% reduction on system NPC compared with the base case - LCOE of HRES is 0.11 $/kWh - LCOE of the base case is 0.16

	Base case: diesel gen (100kW)		$/kWh
Himri et al. [14]	Wind turbine + diesel gen	Algeria	- NPC and LCOE of the hybrid system are less than the base case
Fantidis et al. [15]	Wind turbine (150kW)+solar PV (8kW)+battery(1450kwh) Base case: diesel gen (100kW)	Greece	- LCOE and system NPC of the base case are 0.494 $/kWh and 1.963 $M - LCOE and system NPC of the 100% RE system case are 1.001 $M and 0.252 $/kWh
Rohani et al. [16]	Hybrid System	UAE	- The hybrid system was cheaper than the base diesel case - LCOE was found between 0.2 – 0.3 $/kWh - Maximum CO_2 emission reduction was 46% - The maximum RE penetration rate was 65%
Rehman et al. [17]	Wind turbine +solar PV+diesel gen	Saudi Arabia	- The cost of energy was cheaper in the hybrid system, 0.212 $/kWh with 35% RE penetration
Schezan et al. [18]	Wind turbine +solar PV+diesel gen	Australia	- NPC and LCOE of the hybrid system was cheaper - LCOE around 0.209 $/kWh
Murugaperumal et al. [19]	Wind turbine +solar PV+battery+ bio-mass gen	India	- The microgrid was found to be a cost-effective solution

Besides microgrid modeling tools like HOMER, there are many efforts in the literature explaining microgrid modeling using different methods. For example, a microgrid control model was developed using the numerical method [20], or in another one, a metaheuristic approach along with a neural network were applied in the microgrid optimal control model [21]. The Monte Carlo method (known as Monte Carlo analytical model in this study) was recently applied in microgrid modeling to consider the uncertainty and risk of parameters [22]. First, HOMER was used for simulation and optimization, and levelized

cost of energy (LCOE) in few feasible cases for Popova Island were found. Then, the probability distribution of possible systems, the LCOE and uncertainty values were found using the HOMER's outputs, and input parameters distribution in the Monte Carlo method. Finally, the hybrid system configuration with the minimum LCOE value was proposed for this off-grid area. LCOE varies between 0.3 $/kWh and 0.71 $/kWh. Maximum RE penetration found in this study was 95% using a huge wind turbine (1000 kW), Solar PV (2814 kW), and battery (5000 kWh). LCOE is first decreases when the RE penetration increases, but after 45.9% penetration, an inflection point is reached, and increased renewables begins to increase LCOE. The stochastic method has also been applied to assess the optimal microgrid control [23]. Uncertainties, including wind turbine and solar PV production, market price, and load demand error, were characterized in this approach. Probability Distribution Function (PDF) and roulette wheel were used for scenario generation. The scenario reduction method was applied for picking the best scenarios, and finally, converted deterministic problems were solved by Adaptive Modified Firefly Algorithm (AMFA). Kafetzis et al. [24] developed a control model for a microgrid in a remote area with few industrial and residential load demand profiles. Wind turbine, solar PV, hydropower plant, and biomass system were delivering the RE in this modeling, Li-ion battery and hydrogen storage were the ESS and fuel cell was another source of energy. Hybrid Automata Algorithm along with Propositional-based Logic was used in this model for switching between operation strategies.

Multiobjective optimization is another approach recently applied in microgrid modeling to minimize/maximize two or more objective functions simultaneously and find a pareto front (set of non-dominated solutions) of optimum solutions for both of them. For example, a stochastic control model was developed by Firouzmakan et al. [25] to minimize the operation cost and maximize the system reliability. A Scenario-based method was used to consider the uncertainty of RE resources, load demand, and market price. A multi-objective Particle Swarm Optimization (MOPSO) algorithm was applied to solve the multi-objective problem in this model to find a set of optimum solutions for operation cost and reliability of the system. The Genetic Algorithm is a meta-heuristics method and one of the stochastic optimization algorithms widely used in microgrid

modeling. Quitoras et al. [26] applied the Nondominated Sorting Genetic Algorithm II (NSGA-II) for multi-objective optimization. Fuel consumption and LCOE of a hybrid system in Sachs Harbour (Canadian Arctic community) were minimized simultaneously. LCOE and RE penetration in this microgrid at the trade-off point in the pareto front were 0.575 $/kWh and 80.45%.

1.1.3. Flow Batteries

The reliability of the system is the most critical factor in microgrids because of their dependency on RE. Applying an efficient ESS with an appropriate size in the microgrid can improve the system's reliability, so ESS sizing is important in hybrid systems modeling. Most of the microgrid modeling for ESS sizing has been done for Lead-acid and Li-ion batteries [27]–[30]. Charge/discharge units and storage are coupled in these types of batteries. Therefore, sizing these types of batteries is typically done by determining the size of energy storage (kWh). Li-ion batteries have three issues. First, they are expensive. Second, they degrade quickly and need to be replaced after a defined replacement time, and third, they are not a good option for a longer time duration ESS due to integrated power and energy storage units in this type of battery. However, flow batteries are another type of ESS used in microgrids that don't have Li-ion battery problems, which means they are cheaper, and they don't degrade as much as Li-ion batteries and can be applied for a longer duration. Longer duration energy storage is the most important specification of flow batteries, affecting microgrids' operation and energy management. Decoupled energy storage and power (separate units for electrolyte and charge/discharge) in flow batteries allow them to be scaled separately, which is very practical for microgrids.

The most common type of flow battery is the VRFB, in which power and storage are decoupled. However, vanadium is expensive, and it is not environmentally friendly. It has only one power unit for both charge and discharge. The sizing of flow batteries in the hybrid system is more challenging than other conventional batteries due to their complex configuration. There are few models of microgrids incorporating VRFB in the literature. Nguyen et al. [31] developed an optimal sizing model for VRFB incorporated in microgrid using dynamic programming (DP) algorithm. The operation cost of the

microgrid integrated with different sizes of VRFB was studied by an optimal operating model and found that a larger flow battery reduces operation cost [32]. HOMER's energy management model has the functionality of using VRFB in the microgrid [33]. Recently, VRFB was also applied in microgrid operation modeling by Mohiti et al. [34]. They developed an energy management system for microgrids incorporated with VRFB. They also proposed a linear model for VRFB. They used the CPLEX solver to solve the MILP and optimize the operation cost. They found an 11.67% reduction in the operation cost of the microgrid.

Another type of flow battery is the Zinc Air Flow Battery (ZAFB) which has impressive specifications that make it one of the best solutions for the reliability and sustainability of RE and microgrids. Recently developed ZAFB, an innovative metal-air type flow battery, is a descendant of the conventional zinc air battery. Zinc air batteries are in different forms, such as Flexible [35], [36], cable-shaped [37], and flow batteries [38].

The decoupling of charge, discharge power units, and energy storage is the most impressive feature of the ZAFB. These three main parts are shown in figure 1.8. The regenerator is responsible for charging, the power unit (generator) provides the discharge, and the storage tank contains the electrolyte. All three parts are separately scalable for various sizes of microgrids. In addition, the zinc metal used in the electrolyte is very cheap. ZAFB is very safe and environmentally friendly and also has a high energy density of around 700 Wh/kg [39]. These advantages of ZAFB make it a promising ESS type for microgrids.

In the battery unit, also known as the generator, power unit, and zinc air fuel cell, electricity is generated by an electrochemical reaction between zinc (Zn) and oxygen. Zincate and zinc oxide are the by-products of this reaction. The electrolyte containing potassium hydroxide (KOH) and zinc particles as reactant (fuel) is continuously pumped into the battery, and products of the reaction return into the tank. In the regenerator (electrolyser), zinc is regenerated by an electrochemical reaction in which zincate is converted to zinc, oxygen, and water. Zincate and zinc oxide are pumped into the

regenerator as reactants and fuel, and charged zinc particles return into the tank. ZAFB configuration and how it operates will be explained in Chapter **2**.

Figure 1.8 Schematic of Zinc Air Flow Battery (image credit: Zinc8) [9]

From 1998 to 2004, ZAFB, also known as Zinc Regenerative Fuel Cell (ZRFC), was developed by Metallic Power Inc. for the first time [40], [41]. In 2007, Smedley et al. developed a pilot plant of ZRFC for emergency backup power [41]. This system included a 12 cells stack with 1.8 kW power capacity, and it was capable of providing 1.1 kW for 24 hours. Another pilot plant with a 1kW power capacity and 4 kWh energy capacity was developed by Amunátegui et al. [42]. This system has three stacks, and each one includes 20 cells. They found the shunt current negatively impacts on efficiency, which resulted in a reduction in coulombic efficiency by 18 %. They also found the 40 % maximum round-trip efficiency during the 2000 cycles.

In the previous studies, there are only a few models and simulations for the ZAFB. In 1992, a mathematical performance model was proposed for primary zinc air batteries for the first time and was validated with experimental data [43]. A numerical model was

developed by Diess et al. [44] to evaluate the galvanostatic three-cycle and discharge experiments. Migration and diffusion processes, electrochemical reactions in cathode and anode, and overpotential were defined in this model. Humidity, CO_2, and oxygen concentration in the air can affect the ZAFB performance. Schröder et al. [45] evaluated these parameters' impact by developing a mathematical model to simulate the galvanostatic cycle. They found carbon dioxide concentration as the most important factor which affects the battery operation significantly, and humidity can cause flooding or water loss. Based on their test results, to have the highest and stable performance in ZAFB, CO_2 must be below 10 ppm, humidity must be around 65%, and pure oxygen can be helpful, but commercial ZAFB operates with standard air. Zinc dendrite growth is the other phenomenon that has a negative impact on zinc air batteries. A numerical model was developed by Wang et al. [46] to simulate this process. Activation loss (overpotential) and electrolyte flow are two factors that can affect and control dendrite propagation. Hydrogen evolution reaction (HER), also known as self-corrosion of the zinc electrode [47], is a parasitic reaction that affects the zinc electrode performance, reduces the system efficiency, and corrodes the zinc electrode [48]. HER effect was considered in a few previous ZAFB modeling and studies [48]–[50]. An integrated ESS including ZAFB and regenerator was simulated by Lao-atiman et al. [48], and an electrochemical model was developed for this system and validated by experimental results. This model evaluated the effect of operating parameters such as the initial concentration of zincate and KOH and the electrolyte flow rate. It was found that higher KOH concentration can reduce the current efficiency, and increasing the zincate concentration results in HER reduction and current efficiency increase in the generator. On the other hand, a higher flow rate and zincate ion concentration can increase the current efficiency of the regenerator. Olaru et al. [51] developed a mathematical model for ZAFB cells, which investigates the behavior and discharge profile of the cell through time.

1.2. Contributions

Research Gap:

Although Microgrid modeling tools like HOMER are available, they have some deficiencies. First and most importantly, there is no ZAFB model in them, HOMER has a model for VRFB, but the structure and features of these two types of flow batteries are different. Secondly, they have simple and limited optimization methods for microgrid optimal design and control. Lastly, they are not open source, and free tools and licenses are needed to use them.

There are few ZAFB models in the previous studies, but they were developed for analyzing the performance of battery cells or systems. However, they are very complex and too computationally expensive to use efficiently in large-scale modeling. Also, the incorporation of ZAFB in microgrids has never been studied before. So ZAFB, with novel specifications and potential for economic value, must be investigated technically and economically through this modeling. In addition, more efforts are required to replace the diesel with clean energies in Canadian off-grid communities.

This research is aimed to develop a microgrid modeling tool and integrate the ZAFB system with microgrids in Canadian off-grid territories to investigate the economic value of ZAFB and the impact of different RE penetration scenarios in microgrids on total system cost, cost of energy, fuel consumption, and CO_2 emission, etc. and explore the possibility of 100% RE microgrids and reduce/eliminate their dependency on diesel fuel. An efficient and accurate model for the ZAFB system was developed to achieve this goal, which is beneficial for large-scale modeling applications. Then a microgrid modeling tool was developed for optimal microgrid operational control and optimal sizing of grid components, including ZAFB, RE power plants, diesel generators. For the last stage, this tool was implemented for evaluating the microgrid and ZAFB in a few case studies in British Columbia. In summary, the contributions of this research are as below:

- A semi-empirical ZAFB performance model was developed and validated through experimental data
- A state of charge (SoC) model was developed for ZAFB.

- An efficiency model was proposed, and a linear efficiency model was developed for use in microgrid modeling.
- Cost models were developed for ZAFB using real-world data
- A microgrid modeling tool for optimal control and sizing using a bilevel optimization approach and model predictive control (MPC) method was developed. All performance and cost models of the wind turbine, solar PV, tidal turbine, diesel generator, and ZAFB were incorporated in this modeling tool.
- The functionality of the microgrid modeling tool, the economic value of ZAFB, energy system cost over the lifetime, and cost of energy were evaluated by three case studies in BC: Blind Channel, Hot Springs Cove, Moresby Island.
- Different RE penetration scenarios, particularly 100% RE were explored through this microgrid modeling tool which was integrated with ZAFB.

1.3. Thesis Structure

The sections of this thesis are described as follows:

Chapter 1 presents the background of the ZAFB integrated systems and microgrids and reviews what modeling and analysis have been done before in the previous studies. Then the motivation, objectives, and contributions of this study will be explained. Information given in this chapter will be discussed in detail in ZAFB modeling (Chapter 2) and microgrid modeling (Chapter 3).

Chapter 2 will describe the developed zinc air flow battery (ZAFB) model. Performance, SoC, efficiency, and cost models will be described in this chapter. Performance model validation will be shown. ZAFB models will be used in microgrid optimal design and control, which will be explained in Chapter 3.

Chapter 3 will present the microgrid components' performance and cost models, optimization approach, and optimal design and control model. This microgrid modeling tool will be evaluated by three case studies in Chapter 4.

Chapter 4 will show the model verification, case studies results, and discussions. ZAFB will be compared with Li-ion batteries in this chapter, and insights into 100% RE microgrids, hybrid renewable energy system (HRES), and ZAFB will be described.

Chapter 5 will summarize all the work done in this research and present the significant achievements and results, future works, and developments.

Chapter 2

2. Battery Energy Storage System: Zinc Air Flow Battery Modeling

2.1. ZAFB Configuration

Zinc Air Flow Battery (ZAFB) is a type of aqueous metal-air battery which is mechanically rechargeable and takes oxygen from the air. Power and energy capacity are decoupled in this system. As shown in Figure 2.1, the charging unit, also known as regenerator and zinc electrolyzer (part 1), the energy storage unit (part 2), and the discharge unit, also known as power unit and generator (part 3), are separate. There is no reactant on the electrodes in this system, and the electrolyte, which is the aqueous solution of KOH, conveys reactants to the reaction area and electrodes. In discharging mode, zinc particles as the reactant are pumped mechanically to the generator, electrochemical reactions generate electricity, and zincate and zinc oxide as the products of these reactions return to the tank. In charging mode, zinc oxide and zincate ions in the electrolyte are transported mechanically to the charge unit, and zinc particles are regenerated by electrochemical reactions and returned to the tank. Three species such as zinc particles, zincate, and zinc oxide are always in the tank, which determine the state of charge (SoC) of the system.

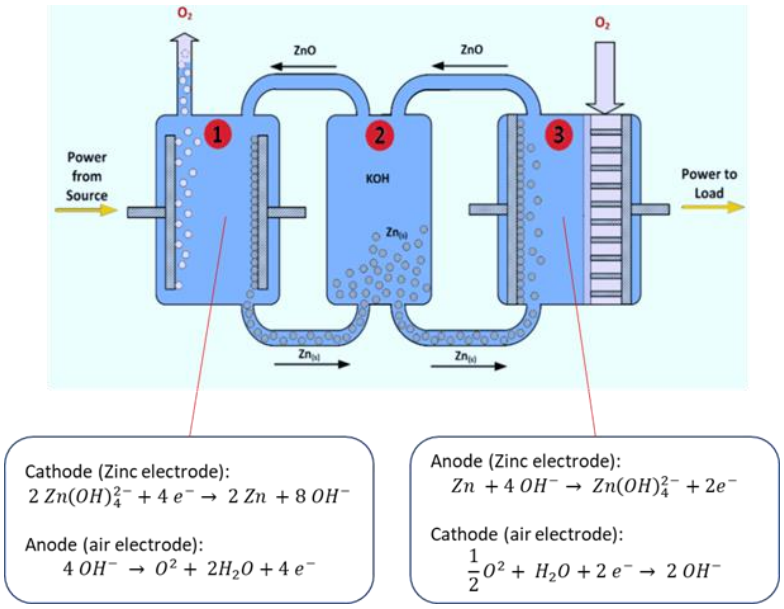

Figure 2.1 schematic of Zinc Air Flow Battery system (image credit: Zinc8) [9]

ZAFB advantages:

- Inexpensive, abundant, safe, and environmentally friendly active material which is zinc
- Decoupled charge, discharge, and energy storage and easily scalable for large scale applications
- Cheaper than other types of batteries, especially for longer-duration use.
- High energy density
- No capacity fade over the lifetime
- Lower depth of discharge (DoD)

Figure 2.2 ZAFB system (image credit: Zinc8) [9]

As shown in figure 2.2, regenerator and generator are fabricated in multiple stacks connected in parallel or series mode. Each stack consists of many cells connected in series. Inside the battery cell, the anode (zinc electrode) and cathode (air electrode) are separated by a separator. The air electrode is fabricated in three layers: gas diffusion layer (GDL), current collector, and catalyst. Inside of regenerator cell, the separator splits the zinc electrode (cathode) and air electrode (anode). The Air electrode has a current

collector and catalyst layer [48]. Electrochemical reactions that happen inside of the cell will be discussed in the next sections.

Battery Cell Reactions

In the anode, zincate ions ($Zn(OH)_4^{2-}$) is produced by the reaction between zinc particles (Zn) in the electrolyte and hydroxide ions (OH^-). Also, two electrons are released in this reaction.

$$Zn + 4\,OH^- \rightarrow Zn(OH)_4^{2-} + 2e^-$$

There is a saturation point for the zincate ions. When zincate concentration in the electrolyte reaches this point, zincate breaks down to zinc oxide (ZnO), water (H_2O), and hydroxide ions.

$$Zn(OH)_4^{2-} \rightarrow ZnO + H_2O + 2\,OH^-$$

Oxygen reduction reaction (ORR) occurs in the cathode and hydroxide ion (OH^-) is produced, as shown below [48];

$$\frac{1}{2}O^2 + H_2O + 2\,e^- \rightarrow 2\,OH^-$$

Regenerator Cell Reactions

In the zinc electrode (cathode), zinc is regenerated by the breaking down process of the zincate.

$$2\,Zn(OH)_4^{2-} + 4\,e^- \rightarrow 2\,Zn + 8\,OH^-$$

When zincate concentration drops below the saturation point, zinc oxide reacts with water and hydroxide ions and produces zincate ions.

$$ZnO + H_2O + 2\,OH^- \rightarrow Zn(OH)_4^{2-}$$

In the anode (air electrode), oxygen is produced by breaking down the hydroxide ion, which is known as the oxygen evolution reaction (OER).

$$4\,OH^- \rightarrow O^2 + 2H_2O + 4\,e^-$$

Parasitic Reactions:

Hydrogen evolution reaction (HER) and zinc dissolution reaction are the two parasitic reactions in the zinc electrode in both the regenerator and the battery. In HER, water consumes the electrons from discharge or charge current and breaks down to hydrogen and hydroxide ions. On the other hand, zinc particles in the electrolyte react with water and hydroxide ions and produced zincate ions and hydrogen. In this reaction, zinc is converted to zincate without releasing any electrons [48].

HER:

$$2H_2O + 2\,e^- \rightarrow H_2 + 2\,OH^-$$

Zinc dissolution reaction:

$$Zn + 2\,OH^- + H_2O \rightarrow Zn(OH)_4^{2-} + H_2$$

2.2. Modeling Approach

Battery modeling includes the SoC model, performance model, temperature model, and degradation model. Depending on the application of the modeling, the type of modeling is determined. For instance, the electrochemical models are the best and the most accurate option for the cell design of the flow batteries. However, they are computationally expensive, making them difficult to use for large systems or long-

duration modeling. In contrast, the energy reservoir model (ERM) and charge reservoir model (CRM) are very efficient options applicable for long-duration operational control modeling[52].

In temperature models, equivalent circuits are assumed for the heating generated by resistivity, overpotential, and entropy changes in the cell. The biggest issue with these thermal models is the nonlinearity that makes them suitable for cell or system design. But using them for large-scale control models is challenging because of the complexity. Also, cell current is required for thermal models.

Degradation models include two types: empirical and physical. Calendar aging and cycle aging are the sub-models of the empirical type in which stress factors are determined experimentally. Chemical side-reaction and material fatigue models are categorized in the physical degradation models. Having an accurate degradation model requires experimental data, whereas this kind of data is considered secret and proprietary by the manufacturers [52]. ZAFB doesn't suffer from a high degradation rate and capacity fade. Based on the information provided by the manufacturer, only the cathodes need to be replaced after 20000 hours of working. So this replacement cost was added to the cost model.

In this modeling work, three main parts of the system, charge, discharge, and energy storage units, were considered and modeled separately. Performance, SoC, efficiency, and cost models were proposed. ZAFB semi-empirical performance model was defined based on the current density of the cell in the generator and regenerator. SoC model is an energy-based model. A dynamic efficiency model was also defined for this system based on the losses inside of the cell. Flow batteries are equipped with the HVAC system, and the temperature is constant inside of the enclosure. So, temperature changes were assumed negligible and ambient temperature was applied in this modeling.

2.3. Performance Model

Semi-empirical models were proposed to predict the output power of the battery and regenerator. These performance models are the function of the cell current density, the number of cells connected in series, and the number of parallel stacks. In these models,

the HER parasitic effect was also defined as current density loss and considered as a function of current density.

2.3.1. ZAFB Cell Potential

ZAFB (generator) is responsible for delivering discharge power and includes several stacks that are typically connected in parallel mode. Each stack is fabricated by many cells connected in series. Inside the cell, the zinc electrode and the air electrode are the anode and cathode, respectively. Overpotentials such as activation losses in each electrode and the total ohmic loss reduce the cell voltage. In this performance model, cell potential is determined by these losses. Equation 2-1 shows the general form of cell voltage [45].

$$V_{cell} = V_{oc} - \eta_{act}^{Zinc} - \eta_{act}^{air} - \eta_{ohmic} \quad 2\text{-}1$$

Where η_{act}^{Zinc} is the activation loss of zinc electrode, η_{act}^{air} is the air electrode activation loss, η_{ohmic} is the ohmic loss and V_{oc} is the open-circuit voltage, which was assumed constant for the battery cell in this model. In battery (power unit), overpotentials reduce the V_{oc} during the discharge.

Activation loss:

Electron drift in the electrode, which includes the forward chemical reaction (electronation) impact and backward reaction (de-electronation) impact, determines the net flow of electrons (current density) in the electrodes. The Butler-Volmer equation considers both effects. The current density of the electrode is calculated using the electrode overpotentials (activation overpotential) [53]. Equation 2-2 shows the generic Butler-Volmer equation.

$$i = i_0 \left[e^{(1-\alpha)\frac{F}{RT}\eta} - e^{-\alpha\frac{F}{RT}\eta} \right] \quad 2\text{-}2$$

Where i and i_0 are the current density and exchange current density of electrode and α is the transfer coefficient. By replacing α and $(1-\alpha)$ with two separate coefficients, the current density of the zinc electrode can be described by equation 2-3.

$$i_{Zn} = i_0^{zinc} \left[e^{\alpha_{zn}\frac{n_e F}{RT}\eta_{act}^{Zinc}} - e^{-\beta_{zn}\frac{n_e F}{RT}\eta_{act}^{Zinc}} \right] \quad 2\text{-}3$$

Where $\boldsymbol{i_{Zn}}$ and i_0^{zinc} are current density and exchange current density of zinc electrode, α_{zn} and β_{zn} are the charge transfer coefficient of forward and backward reactions, respectively, and n_e is the number of electrons.

Equation 4 shows the zinc electrode activation loss change rate [48].

$$\frac{d\eta_{act}^{Zinc}}{dt} = i_{Zn} - (i_{cell} + i_H) \quad 2\text{-}4$$

Where i_{cell} is the cell current density, i_{H} is the HER current density, which is a parasitic reaction effect.

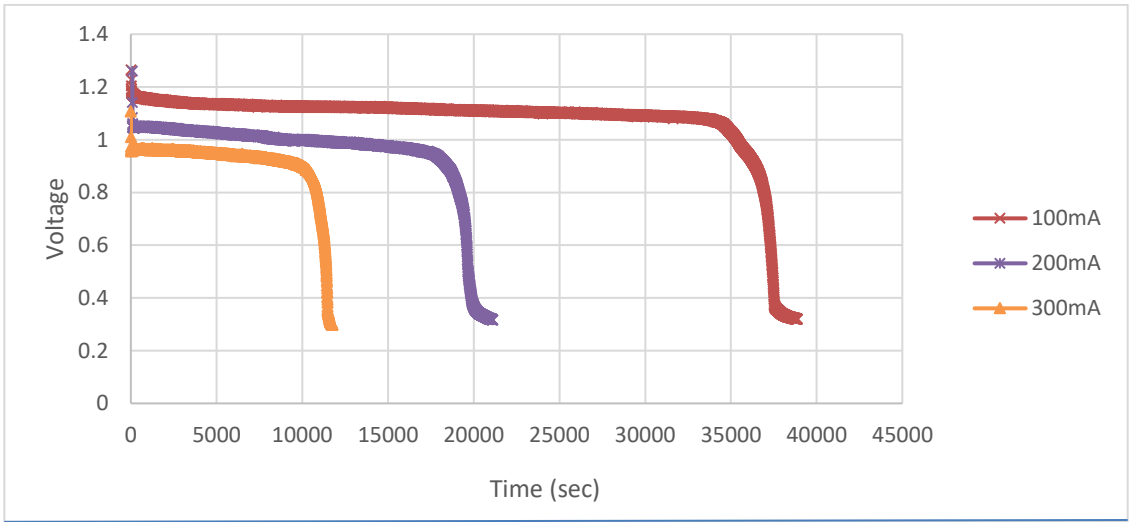

Figure 2.3 cell voltage at constant currents

Based on experimental results [54], [55], shown in figure 2.3, it can be seen that voltages at different currents are almost constant over a time period and changes are negligible, which means that overpotentials are constant throughout the test period because in equation 2-1 open-circuit voltage and ohmic loss are constant at a given current. It's concluded that the change rate of electrode activation losses is negligible.

$$\frac{d\eta_{act}^{Zinc}}{dt} = 0$$

So from equation 2-4 and the equation above, the current density of the zinc electrode is described below.

$$i_{Zn} = i_{cell} + i_H \qquad 2\text{-}5$$

It can be assumed that forward and backward reaction coefficients are equal [56].

$$i_{Zn} = i_0^{zinc}\left[e^{\alpha_{zn}\frac{n_eF}{RT}\eta_{act}^{Zinc}} - e^{-\alpha_{zn}\frac{n_eF}{RT}\eta_{act}^{Zinc}}\right]$$

Activation loss can be calculated by using the equation above and equation 2-3. There are two options to calculate the activation loss of zinc electrode. The first option is converting the Butler-Volmer to Tafel equation [53] and neglecting the backward reaction impact. In this case, the current density will be calculated as below:

$$i_{Zn} = i_0^{zinc}\left[e^{\alpha_{zn}\frac{n_eF}{RT}\eta_{act}^{Zinc}}\right]$$

Therefore, activation loss of zinc electrode will be described by equation 2-6 in logarithmic form.

$$\eta_{act}^{Zinc} = \frac{RT}{\alpha_{zn} n_e F} \, ln\left(\frac{i_{cell} + i_H}{i_0^{zinc}}\right) \quad 2\text{-}6$$

The logarithmic form is simple, can predict the activation loss accurately, but it gives negative values, particularly at low current densities, which physically is meaningless. The hyperbolic sine is the second option. It includes both sides' reactions (electronation and de-electronation) impact, which calculates the activation losses more accurately. Equation 2-7 shows the activation loss of the zinc electrode using the inverse hyperbolic sine.

$$\eta_{act}^{Zinc} = \frac{RT}{\alpha_{zn} n_e F} sinh^{-1}\left(\frac{i_{cell} + i_H}{2 i_0^{zinc}}\right) \quad 2\text{-}7$$

From the Butler-Volmer equation [53], the current density of the air electrode is calculated by Equation 2-8.

$$i_{air} \; = \; i_0^{air}\left[e^{\alpha_{air}\frac{n_e F}{RT}\eta_{act}^{air}} - e^{-\beta_{air}\frac{n_e F}{RT}\eta_{act}^{air}}\right] \quad 2\text{-}8$$

Where i_{air} and i_0^{air} are the current density and the exchange current density of air electrode, α_{air} and β_{air} are the charge transfer coefficient of forward and backward reactions, respectively. Equations 2-8 can be converted to hyperbolic sine form by the same assumptions of zinc electrode activation loss.

$$i_{air} \; = \; 2 \times i_0^{air} \, sinh\left(\alpha_{air} \frac{n_e F}{RT} \eta_{act}^{air}\right) \quad 2\text{-}9$$

Air electrode activation loss change is the difference between the cell and air electrode current densities, and as mentioned earlier, it is concluded that its change rate is negligible [54], [55].

$$\frac{d\eta_{act}^{air}}{dt} = i_{cell} - i_{air} = 0 \quad \text{2-10}$$

$$i_{cell} = i_{air} \quad \text{2-11}$$

The activation loss of the air electrode is calculated using equations 2-9 and 2-11, which is shown in equation 2-12.

$$\eta_{act}^{air} = \frac{RT}{\alpha_{air} n_e F} \, sinh^{-1}\left(\frac{i_{cell}}{2i_0^{air}}\right) \quad \text{2-12}$$

Ohmic loss:

Ohmic's law is used to describe the ohmic loss of ZAFB, which is calculated by the total ohmic resistance of the ZAFB cell.

$$\eta_{ohmic} = R_{ohmic} i_{cell} A_{cell} \quad \text{2-13}$$

Where R_{ohmic} is total ohmic resistance which is assumed a constant value, A_{cell} is the active area of the ZAFB cell.

Using equations 2-1, 2-7,2-10, and 2-12, battery cell voltage can be shown as below.

$$V_{cell} = V_{oc} - \frac{RT}{\alpha_{zn} n_e F} sinh^{-1}\left(\frac{i_{cell} + i_H}{2i_0^{zinc}}\right) - \frac{RT}{\alpha_{air} n_e F} \, sinh^{-1}\left(\frac{i_{cell}}{2i_0^{air}}\right) - R_{ohmic} i_{cell} A_{cell} \quad \text{2-14}$$

Stack total voltage and current depend on its structure, series/series-parallel.

$$I_{stack} = N_P \times i_{cell} \times A_{cell} \quad \text{2-15}$$

$$V_{stack} = N_{series} \times V_{cell} \quad \text{2-16}$$

Where N_P and N_{series} are the total number of parallel modules and series cells, respectively.

2.3.2. Regenerator Cell Potential

Regenerator, also known as electrolyzer, is responsible for charging, and chemical reactions in the regenerator are reverse reactions of ZAFB. The zinc electrode is the cathode, and the air electrode is the anode in the regenerator. Ohmic losses, zinc electrode activation losses, and air electrode activation losses are the overpotentials inside the regenerator cell. The general form of cell potential is shown in equation 2-17.

$$V_{cell} = V_{oc} + \eta_{act}^{Zinc} + \eta_{act}^{air} + \eta_{ohmic} \quad \text{2-17}$$

Where V_{oc} is the open-circuit voltage of the regenerator cell in this model, which is a constant value. In the regenerator, overpotentials increase the open-circuit voltage when charging takes place.

Activation loss:

Using the Butler-Volmer equation (Equation 2-2), zinc electrode current density can be shown below.

$$i_{Zn} = i_0^{zinc}\left[e^{\alpha_{zn}\frac{n_eF}{RT}\eta_{act}^{Zinc}} - e^{-\beta_{zn}\frac{n_eF}{RT}\eta_{act}^{Zinc}}\right]$$

Based on the similar assumption of the previous section, the equation above is converted to hyperbolic sine format.

$$i_{Zn} = 2 \times i_0^{zinc} \sinh\left(\alpha_{zn}\frac{n_eF}{RT}\eta_{act}^{Zinc}\right) \quad \text{2-18}$$

As mentioned earlier, the change rate of zinc electrode activation loss can be neglected [54], [55].

$$\frac{d\eta_{act}^{Zinc}}{dt} = i_{cell} - (i_{Zn} + i_H) = 0 \quad 2\text{-}19$$

$$i_{Zn} = i_{cell} - i_H \quad 2\text{-}20$$

By using equation 2-18 and 2-20, activation loss $\left(\eta_{act}^{Zinc}\right)$ of the zinc electrode is calculated by the inverse of hyperbolic sine.

$$\eta_{act}^{Zinc} = \frac{RT}{\alpha_{zn} n_e F} \, sinh^{-1}\left(\frac{i_{cell} - i_H}{2i_0^{zinc}}\right) \quad 2\text{-}21$$

Air electrode activation loss is described by the same assumptions and equations 2-10, 2-11, and it is shown as follows.

$$\eta_{act}^{air} = \frac{RT}{\alpha_{air} n_e F} \, sinh^{-1}\left(\frac{i_{cell}}{2i_0^{air}}\right) \quad 2\text{-}22$$

Ohmic loss:

Ohmic's law is used to describe the ohmic loss of Electrolyzer (Regenerator), which is shown in equation 2-23.

$$\eta_{ohmic} = R_{ohmic} i_{cell} A_{cell} \quad 2\text{-}23$$

Where R_{ohmic} is total ohmic resistance and A_{cell} is the active area of the regenerator cell. Using equations 2-17,2-21,2-22, and 2-23, the regenerator cell voltage will be calculated by the equation below.

$$V_{cell} = V_{oc} + \frac{RT}{\alpha_{zn} n_e F} sinh^{-1}\left(\frac{i_{cell} - i_H}{2i_0^{zinc}}\right) + \frac{RT}{\alpha_{air} n_e F} sinh^{-1}\left(\frac{i_{cell}}{2i_0^{air}}\right) + R_{ohmic} i_{cell} A_{cell} \quad 2\text{-}24$$

2.3.3. Performance Model Validation

This semi-empirical performance model can predict the system dynamics, including ZAFB and regenerator cell and stack potentials, losses (activation, ohmic, and HER) at various charging/discharging currents. Model accuracy and performance were evaluated and validated by using the experimental data [48] in which a ZAFB integrated with a zinc electrolyzer (regenerator) with an active area of 10 cm^2 was tested. Performance model parameters used in equations 2-14 and 2-24 are shown in table 2-1. These parameters were derived by using the nonlinear least square method and trust-region algorithm in MATLAB R2019b. Known parameters and variables of the performance model are shown in Tables 2-2 and 2-3, respectively.

Table 2-1 Performance model parameters found by best fit to the data

Parameter	Unit	Description	Value for Generator	Value for Regenerator
V_{oc}	V	Open circuit voltage	1.584	1.728
i_0^{zinc}	mA/cm^2	Exchange current density of zinc electrode	69.54	5.896
i_0^{air}	mA/cm^2	Exchange current density of air electrode	7.149e-05	3.997e-05
i_H	mA/cm^2	HER current density	0.006233*i_{cell}	0.00121*i_{cell}
α_{zn}	-	Charge transfer coefficient of zinc electrode	0.5	0.4729
α_{air}	-	Charge transfer coefficient of air electrode	0.4833	0.4681
R_{ohmic}	Ω	Ohmic resistance	0.5613	0.325

Table 2-2 Performance model known parameters

Parameter	Unit	Description	Value for Generator	Value for Regenerator
A_{cell}	cm^2	Active area of cell	10	10
T	K	Temperature	298.15 (25 c)	298.15 (25 c)
n_e	-	Number of electrons	2	2

$\boldsymbol{R}$	J/mol.K	Gas constant	8.314	8.314
$\boldsymbol{F}$	C/mol	Faraday constant	96485	96485

Table 2-3 Performance model variables

Variable	Unit	Description
i_{cell}	mA/cm2	Charge/discharge current density (cell current density)
N_p	-	Number of parallel modules
N_{series}	-	Number of serries cells

Figure 2.4 shows the experimental data of cell voltage at different current densities for ZAFB and regenerator. It can be seen that model can predict the cell voltage accurately. Cell overpotentials of ZAFB and regenerator are shown in Figure 2.5. These losses include activation loss of zinc electrode and air electrode and ohmic loss. Figure 2.6 shows the power density of ZAFB and regenerator at different current densities.

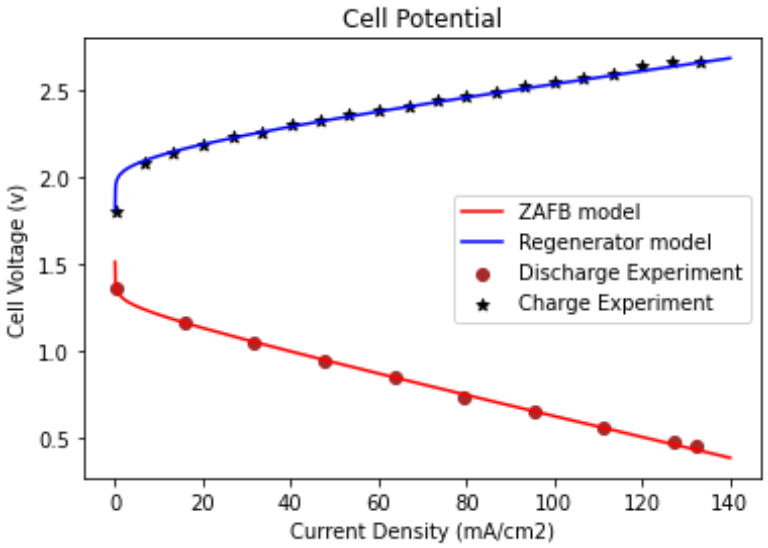

Figure 2.4 Battery (generator) and regenerator cell Potential

(a) (b)

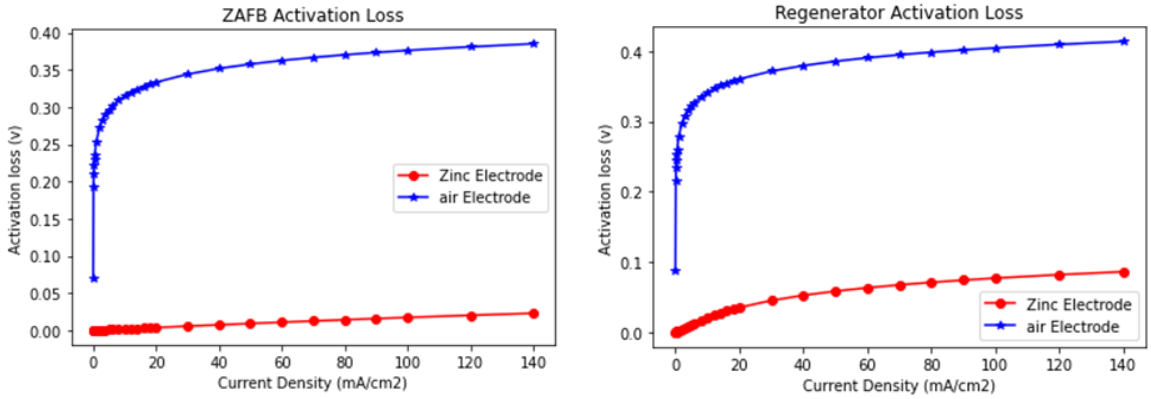

(c)

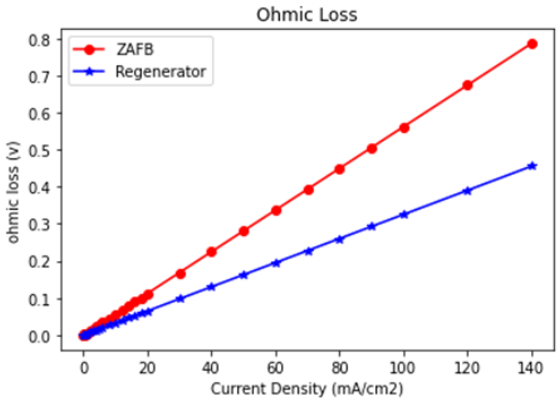

Figure 2.5 Cell overpotentials: Activation loss of (a) ZAFB (b) regenerator and (c) Ohmic loss

(a) (b)

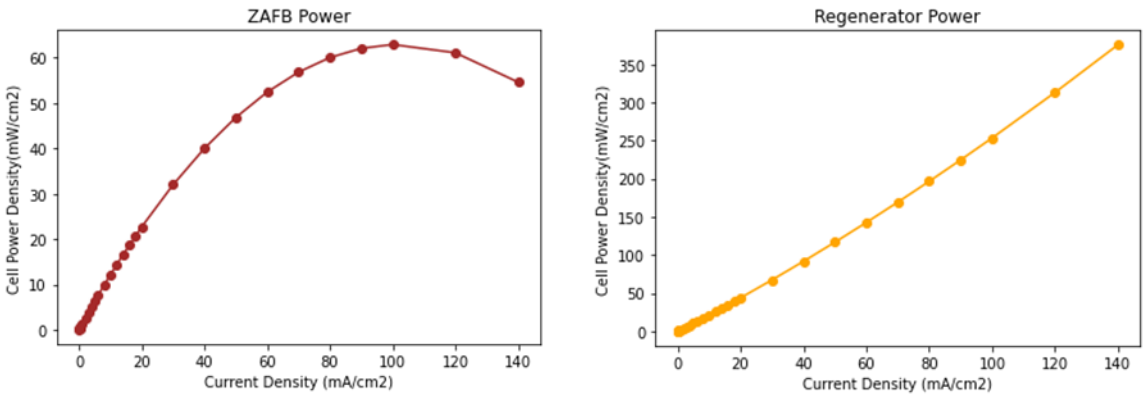

Figure 2.6 Power Density of (a) ZAFB (b) Regenerator

2.4. Efficiency Model

The efficiency of a system can be described as the ratio of output (delivery) energy of the system and input energy of the system. The energy efficiency definition is shown as follows.

$$\eta = \frac{E_{out}}{E_{in}}$$

All systems have some losses, which reduce the efficiency, and the ZAFB system does not exclude. Activation losses of anode and cathode and ohmic loss occur inside of both ZAFB and regenerator cells. HER effect, a parasitic reaction, is also considered in the activation loss equation. Of course, there are other types of losses in this system, such as power loss in pumps, HVAC, etc., but real data of system operation and configuration is required to calculate the system efficiency more accurately. Data will be provided by the manufacturer. Until then, these losses are neglected.

2.4.1. ZAFB Efficiency

The discharge energy of ZAFB is the output of the system, and some losses occur in the system. Therefore, the input energy of the system is the summation of output energy and losses. So ZAFB dynamic efficiency can be defined as below.

$$\eta_B(t) = \eta_{dis}(t) = \frac{E^B_{out}}{E^B_{in}} = \frac{E_{dis}(t)}{E_{dis}(t) + E^B_{losses}(t)} \qquad 2\text{-}25$$

$$= \frac{E_{dis}(t)}{E_{dis}(t) + E^B_{act}(t) + E^B_{ohmic}(t)}$$

$$= \frac{\int V_B I_B \, dt}{\int V_B I_B \, dt + \int \left(\eta^{zinc}_{act}(t) + \eta^{air}_{act}(t)\right) I_B \, dt + \int R^B_{ohmic} I_B^2 \, dt}$$

$$= \frac{\int V_B I_B \, dt}{\int V_{oc} I_B \, dt}$$

Where $\eta_{dis}(t)$ is the efficiency of the ZAFB system/cell, $\eta^{zinc}_{act}(t)$, $\eta^{air}_{act}(t)$ are the activation loss of the zinc electrode and air electrode**,** $E_{dis}(t)$, $E^B_{losses}(t)$, $E^B_{act}(t)$,

$E^{B}_{ohmic}(t)$ are the discharge energy, losses energy, activation loss energy, and ohmic loss energy of the ZAFB, respectively, and V_B and I_B are the battery voltage and current. This dynamic model is the function of the voltage and current of the system. Every system can operate at its maximum or minimum efficiency and can have limits, shown below.

$$\eta_{dis}^{min} \leq \eta_{dis}(t) \leq \eta_{dis}^{max} \quad \text{2-26}$$

2.4.2. Regenerator Efficiency

In the regenerator, charge energy includes the losses and covers the energy demand for regenerating the zinc. So charge energy is the input energy of the system, and regeneration energy which is the charge energy without the losses energy is the output energy of the system. All these definitions can be seen in equation 2-27.

$$\begin{aligned} \eta_R(t) = \eta_{ch}(t) = \frac{E_{out}^R}{E_{in}^R} &= \frac{E_{ch}(t) - E_{losses}^R(t)}{E_{ch}(t)} \\ &= \frac{E_{ch}(t) - E_{act}^R(t) - E_{ohmic}^R(t)}{E_{ch}(t)} \\ &= \frac{\int V_R I_R \, dt - \int \left(\eta_{act}^{zinc}(t) + \eta_{act}^{air}(t)\right) I_R \, dt - \int R_{ohmic}^R I_R^2 \, dt}{\int V_R I_R \, dt} \\ &= \frac{\int V_{oc} I_R \, dt}{\int V_R I_R \, dt} \end{aligned} \quad \text{2-27}$$

Where $\eta_{ch}(t)$ is the efficiency of the regenerator system/cell, $\eta_{act}^{zinc}(t)$, $\eta_{act}^{air}(t)$ are the activation loss of the zinc electrode and air electrode, $E_{ch}(t)$, $E_{losses}^{R}(t)$, $E_{act}^{R}(t)$, $E_{ohmic}^{R}(t)$ are the charge energy, losses energy, activation loss energy, and ohmic loss energy of the regenerator, respectively, and V_R and I_R are the battery voltage and current. The regenerator operates between its maximum and minimum efficiency, which can be changed by voltage and current in this model. Equation 28 shows this definition.

$$\eta_{ch}^{min} \leq \eta_{ch}(t) \leq \eta_{ch}^{max} \quad 2\text{-}28$$

2.4.3. Overall system Efficiency

ZAFB system includes two subsystems, generator (power unit) and regenerator. These subsystems have their own efficiency. Generator (power unit) and regenerator efficiency using equations 2-25 and 2-27 at different current densities are shown in Figure 2.7.

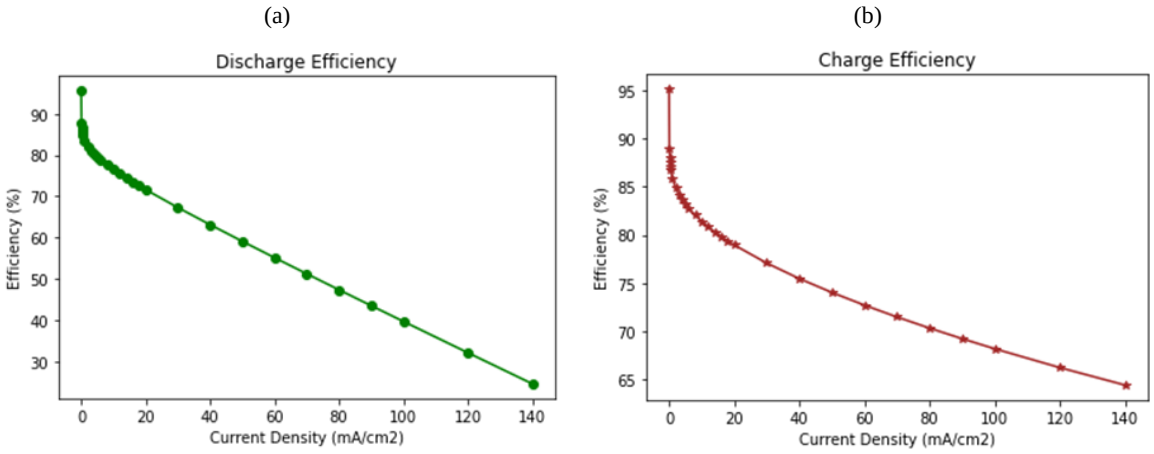

Figure 2.7(a) ZAFB efficiency (b) Regenerator efficiency

So the overall system energy efficiency can be calculated by equation 2-52.

$$\eta_{sys} = \eta_{dis} \times \eta_{ch} \quad 2\text{-}29$$

Overall system efficiency is in a range which is defined as below.

$$\eta_{dis}^{min} \times \eta_{ch}^{min} \leq \eta_{sys} \leq \eta_{dis}^{max} \times \eta_{ch}^{max} \quad 2\text{-}30$$

2.4.4. Linearized Efficiency Model

ESS models must be as simple as possible in large-scale modeling and optimization. Using Nonlinear models is challenging in the optimization process and also computationally expensive. In this study, the developed microgrid model has two levels of optimizations. The upper level optimizes the microgrid design and size of components

to minimize the system cost. The inner level or optimal control model optimizes the operation of microgrid components to have minimum diesel operation time. ZAFB models are used in the control model (inner level). One of the nonlinearities of the control model is the ZAFB SoC model. The discharge and charge efficiency functions determine that ZAFB SoC models would be nonlinear (with respect to current density) or quadratic (with respect to cell charge/discharge power). For this reason, the nonlinear form of the efficiency models was converted to a linear form. By using this linear form, Mixed-Integer Nonlinear Programming (MINLP) in the optimal control model (inner level) is changed to Mixed-Integer Quadratic Programming (MIQP), which is easier and faster to solve in the optimization process. This microgrid modeling approach will be discussed in the next chapter in detail.

From figures 2.4, 2.6, and 2.7, it can be seen that there is one specific voltage for every single current, and consequently, there is one power, and for each power, there is one efficiency. So, efficiency is the function of cell output power. By using the experimental data, power unit (battery) and regenerator efficiencies are plotted as the function cell power, shown as below:

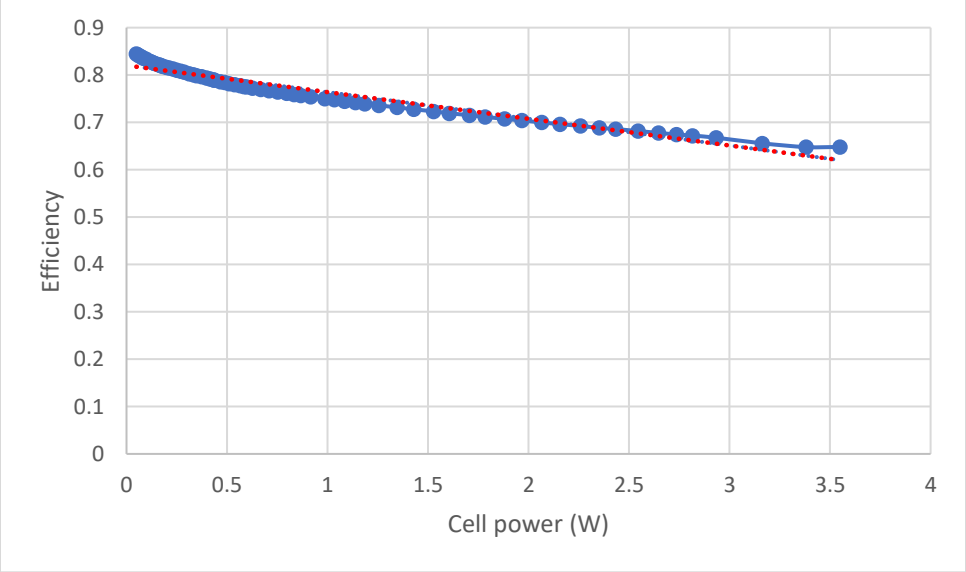

Figure 2.8. The efficiency of the regenerator

Equation 2-31 shows the Linear form of regenerator efficiency as a function of cell power. This form has been used in microgrid modeling.

$$\eta_R(P_{cell}) = -0.0563 \times P_{cell} + 0.8202 \quad \text{2-31}$$

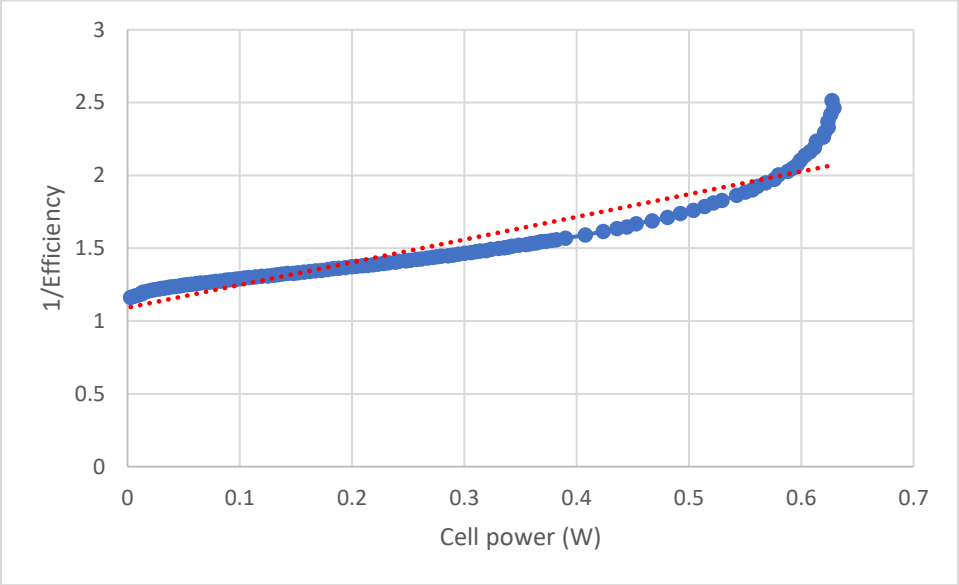

Figure 2.9. The reverse efficiency of ZAFB

The linear form of the reverse of battery efficiency ($\frac{1}{\eta_B}$) as a function of cell power is shown in equation 2-32. The reverse of efficiency would be used in the SoC model, which will be discussed in the next section.

$$\frac{1}{\eta_B}(P_{cell}) = 1.5578 \times P_{cell} + 1.0922 \quad \text{2-32}$$

2.5. SoC Model

Chemical species in the storage tank and their available amount determines the state of charge. The available amount of zinc or charged energy in the storage tank shows the SoC of the ZAFB, and the available amount of zinc oxide and zincate determines the SoC of the Regenerator. Therefore, two types of SoC are defined for the ZAFB system, SoC of the ZAFB and SoC of the regenerator. Equation 2-33 shows both SoCs of the ZAFB system.

$$SoC_B(t) + SoC_R(t) = 1 \qquad \text{2-33}$$

The energy storage or energy capacity of ZAFB (storage tank) can be defined in these forms.

1. Capacity (mole) = maximum total moles of zinc in the tank
2. Capacity (Ah) = $\frac{F \times n_e \times N_{total,Zn}}{3600}$
3. Capacity (Wh)

SoC can be defined based on the energy balance of the ZAFB system. The energy balance of this system is shown in figure 2.10. As shown, there are two types of energy in the storage tank. E_B is the stored energy for ZAFB, which is ready to be used in the ZAFB for discharge. It is the zinc particles in the electrolyte stored in the storage tank. Indeed, it is the electro-chemical energy of zinc particles that will be consumed as reactant or fuel for the battery to generate electricity and provide discharge power. E'_R is the energy demand of available zinc oxide in the tank for charging in the regenerator. Indeed, it is the electrochemical energy demand of zinc oxide and zincate in the electrolyte that will be pumped into the regenerator as a reactant to regenerate the zinc particles. The amount of the equivalent energy of species in the tank determines the SoC of the battery and regenerator. The summation of these energies is always equal to the total capacity of the storage system (E_{max}).

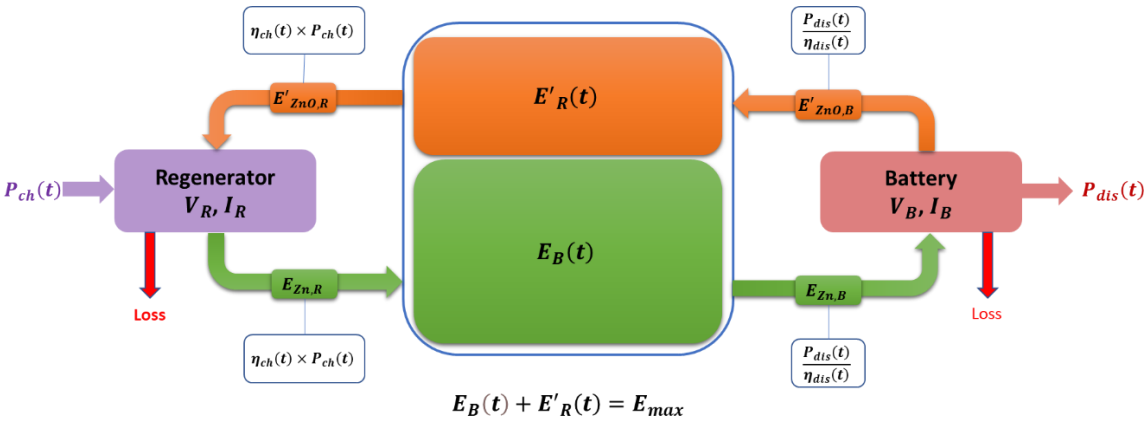

Figure 2.10 Energy balance of ZAFB system

2.5.1. ZAFB SoC

SoC of the ZAFB can be defined by the stored energy that will be used for discharging in ZAFB, and it can be changed by the amount of discharged energy in the ZAFB and the amount of charged energy in the regenerator. As shown in figures 2.1 and 2.10, when the battery operates and delivers discharge power, zinc particles are pumped into the power unit. Electricity is generated by an electrochemical reaction in the cell, and zinc is the reactant of this reaction or fuel for the battery. So, $E_{zn,B}$ is the equivalent energy of pumped zinc particles that are consumed in the battery to provide discharge power, and it is the outlet of the storage tank that reduces the available stored energy for the ZAFB (E_B). When the regenerator operates, zinc oxide is pumped into the regenerator, and charge power is provided from the grid side. A part of the charge energy is wasted by overpotentials inside the cells, and the rest is used to regenerate the zinc particle. The regenerated zinc particles, which contain energy and will be used in the battery for discharging, are returned to the tank and raise the stored energy for the ZAFB (E_B). So the change rate of this energy (E_B) in the tank is determined by the inlet and outlet of the tank during the discharge and charge, and the ordinary differential equation below describes these definitions. Power for pumping the electrolyte to the power units for charging and discharging can be added to this equation. For this purpose, real data from the manufacturer is needed.

$$\frac{dE_B(t)}{dt} = \eta_{ch}(t) \times P_{ch}(t) - \frac{P_{dis}(t)}{\eta_{dis}(t)} \qquad 2\text{-}34$$

By integrating and discretizing the equation above for each time step, battery energy is determined by the equation below. Charge and discharge power and efficiency at each time step are constant.

$$E_B(t) = E_B(t - \Delta t) - \int \frac{(P_{dis})_t}{(\eta_{dis})_t} dt + \int (\eta_{ch})_t \times (P_{ch})_t \, dt \qquad 2\text{-}35$$

SoC of ZAFB and its constraints are defined as follows.

$$SoC_B(t) = \frac{E_B(t)}{E_{max}} \quad 2\text{-}36$$

$$0 \leq E_B(t) \leq E_{max} \quad 2\text{-}37$$

$$0 \leq SoC_B(t) \leq 1 \quad 2\text{-}38$$

2.5.2. Regenerator SoC

The amount of energy that zinc oxide and zincate in the tank need to be regenerated is defined as the SoC of the Regenerator. It can be changed by the amount of discharged energy in ZAFB and the amount of charged energy in the regenerator. It can be seen from Figures 2.1 and 2.10 when the power unit (battery) operates, zincate and zinc oxide as the products of the electrochemical reaction are returned to the tank, which are added to the available amount of these species in the tank and increase the equivalent energy demand of the zincate and zinc oxide (SoC of the regenerator). When the regenerator charges the system, zincate and zinc oxide are pumped into the regenerator to regenerate the zinc particles using the provided charge energy from the grid. These pumped reactants and their equivalent energy demand for charging are the outlets of the tank, which reduce the SoC of the regenerator. So the change rate of this type of energy in the storage tank ($E'_R(t)$) is determined by the inlet and outlet of the tank and calculated by the ODE below. Pumps power demand during the charge and discharge can also be added to this equation.

$$\frac{dE'_R(t)}{dt} = \frac{P_{dis}(t)}{\eta_{dis}(t)} - \eta_{ch}(t) \times P_{ch}(t) \quad 2\text{-}39$$

By integrating and discretizing the equation above for each time step, total energy demand for charging ($E'_R(t)$) is determined by the equation below. Charge and discharge power and efficiency at each time step are constant.

$$E'_R(t) = E'_R(t - \Delta t) + \int \frac{(P_{dis})_t}{(\eta_{dis})_t} dt - \int (\eta_{ch})_t \times (P_{ch})_t dt \quad \text{2-40}$$

SoC of Regenerator and its Constraints are defined as follows.

$$SoC_R(t) = \frac{E'_R(t)}{E_{max}} \quad \text{2-41}$$

$$SoC_R(t) = 1 - SoC_B(t) \quad \text{2-42}$$

$$0 \leq E'_R(t) \leq E_{max} \quad \text{2-43}$$

$$0 \leq SoC_R(t) \leq 1 \quad \text{2-44}$$

2.6. ZAFB System Cost Model

Capital Cost:

Since power and energy storage are decoupled in the ZAFB system, and these units are scalable separately, each part must have a capital cost per unit, and capital cost of charge, discharge units, and energy capacity must be defined. Based on the information provided by the manufacturer [9], the capital cost per kW of regenerator and generator and capital cost per kWh of energy capacity are shown in figure 2.11.

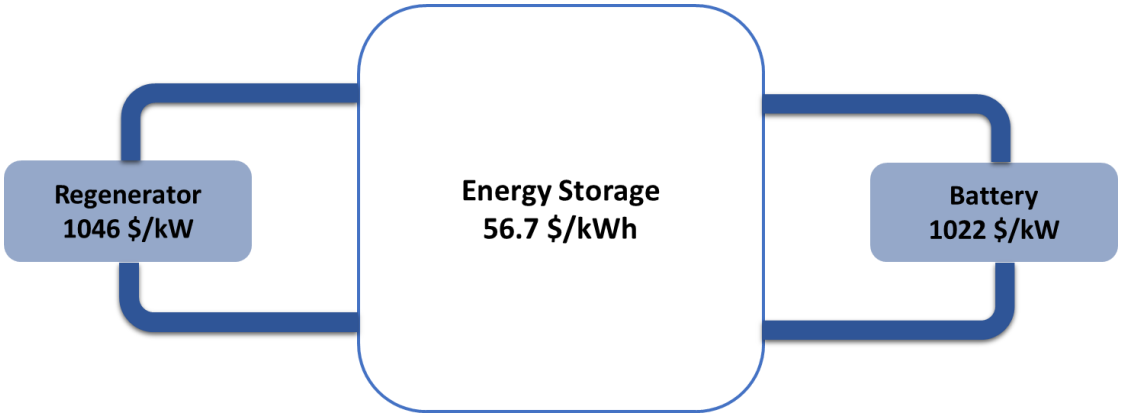

Figure 2.11 CAPEX of power units and energy storage in ZAFB system

Total CAPEX of the ZAFB system can be obtained by the equation below.

$$C_{capital} = P_{r-Regen} \times C_{capital-Regenerator-kW} + P_{r-Gen} \times C_{capital-Generator-kW} + ZAFB_{energy\ cap} \times C_{capital-Storage-kWh}$$

Where $C_{capital}$ is the capital cost and $P_{r-Regen}$ and P_{r-Gen} are the rated power of regenerator and battery (generator) and $C_{capital-Regenerator-kW}$, $C_{capital-Generator-kW}$ capital cost per kW of battery and regenerator and $C_{capital-Storage-kWh}$ is the capital cost per unit energy of the ZAFB system.

O&M Cost:

The operation and maintenance (O&M) cost of the ZAFB system is 1 percent of its capital cost.

$$C_{O\&M-annual} = 1\%\ of\ C_{capital}$$

Replacement Cost:

The most vulnerable parts of the ZAFB system are the cathodes, and they are degraded over time. Cathodes of the ZAFB system must be replaced after defined running hours. The cost of replacement is calculated as follows.

Replacement time: after 20000 hours working at max power

$$C_{Replacement} = 15\%\ of\ Regenerator\ CAPEX\ + 15\%\ of\ Generator\ CAPEX$$

The net present cost of the ZAFB system over its lifetime is shown below:

$$NPC_{ZAFB} = C_{capital} + \sum_{1}^{n} NPV_{O\&M} + \sum_{1}^{n} NPV_{Replacement}$$

As mentioned, the bilevel optimization method was applied in the microgrid model for the optimal design of microgrid configuration to have minimum NPC of the system and optimal control of the operation of microgrid components to have minimum diesel output. ZAFB model was imported to the inner loop (optimal control model). Figure 2.12 shows how ZAFB models are used in the microgrid model.

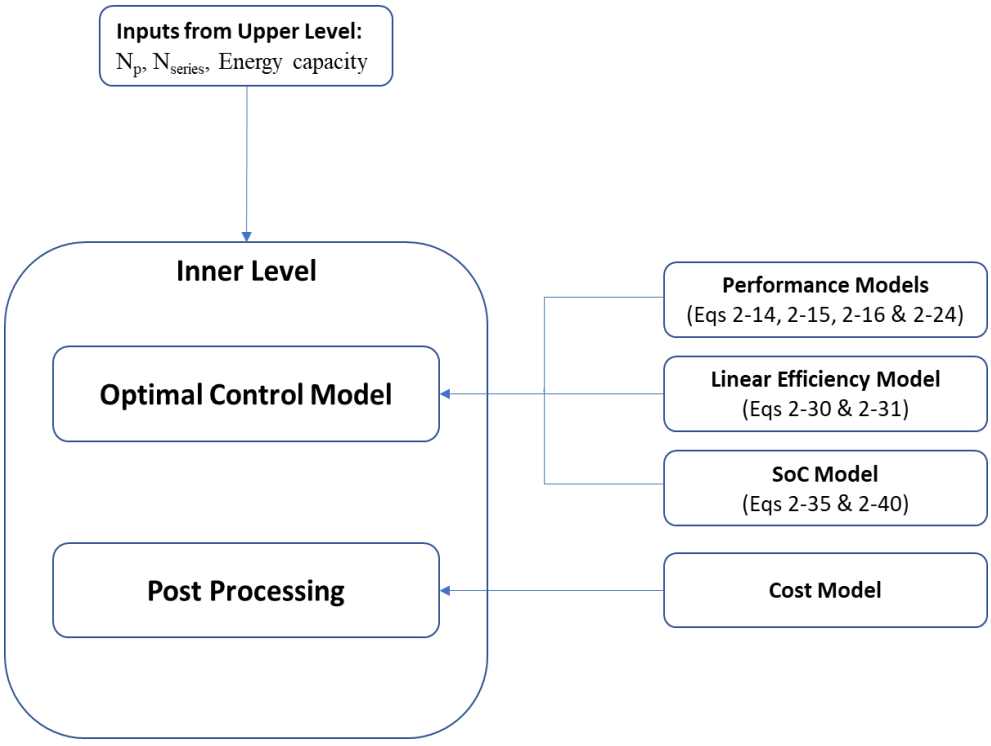

Figure 2.12 Flowchart of ZAFB model in microgrid model

Chapter 3

3. Microgrids Modeling

Integration of local renewable energy sources (RES) with fossil fuel generations in decentralized off-grid communities in which a smart energy management system (EMS) controls the grid components output forms a microgrid. ESS is the inseparable part of microgrids that compensate for the intermittency of RE and improve the reliability and sustainability of the microgrids. In this study, solar PV, tidal, and wind turbines are the RE plants and main energy sources, ZAFB is the ESS, and the diesel generator is the reserve source. Performance and cost models of the components were defined and imported to the microgrid modeling tool. These models will be discussed in the next sections.

3.1. Energy system Performance

3.1.1. Wind Turbine

A generic nondimensionalized performance model was developed at PRIMED by Truelove et al. based on the various wind turbine technologies performance data collected from HOMER Pro's library [57]–[59]. In this work, this model was adopted in microgrid modeling. In this model, two dimensionless variables were defined for the turbine output power and wind speed, $\hat{P}$ and $\widehat{|v|}$. These variables are described as below.

$$\hat{P} = \frac{P}{P_r} \tag{3-1}$$

Where P is the turbine output power and P_r is the rated power of the turbine.

$$\widehat{|v|} = \frac{|v| - |v|^*}{|v|^*} \tag{3-2}$$

Where $|v|$ is the wind speed and $|v|^*$ is the lowest wind speed at which rated power is achieved.

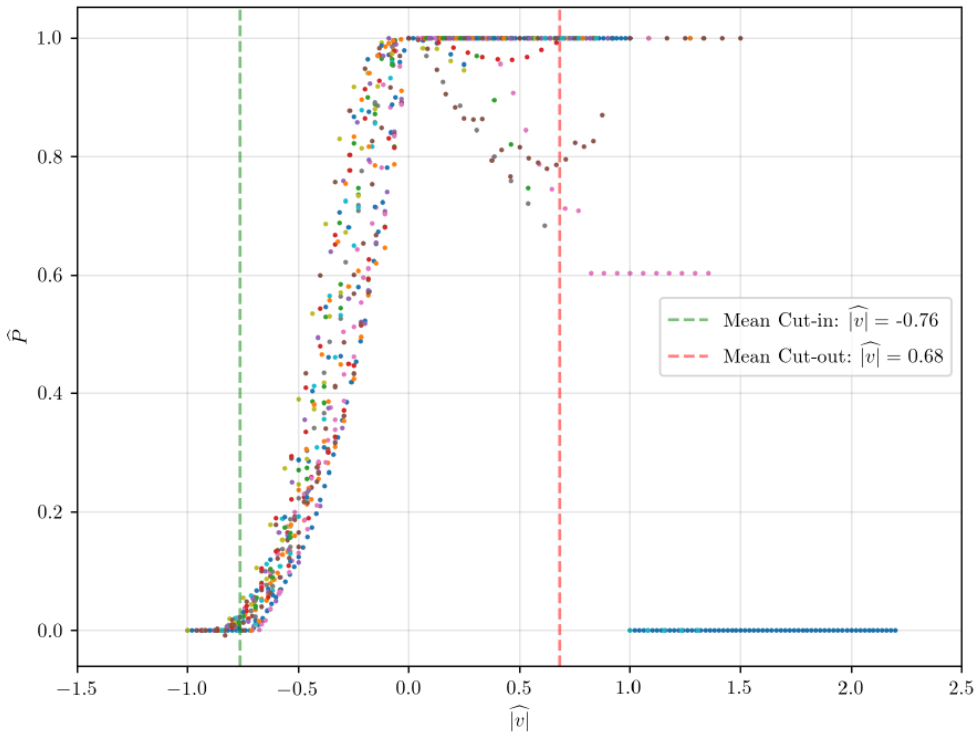

Figure 3.1 dimensionless power of wind turbine technologies [58]

Figure 3.1 shows the collected performance data of different wind turbine performance based on dimensionless variables, each color represent a different technology or model. From data, dimensionless cut-in and cut-out speeds were found – 0.76 and 0.68, respectively. These values are the mean value of the cut-in and cut-out speeds of all technologies in dimensionless format. A general model was proposed for the best fitting of the data;

$$\hat{P}\left(\widehat{|v|}\right) = \begin{cases} 0 & \widehat{|v|} < -0.76 \; or \; \widehat{|v|} > 0.68 \\ a_1 e^{r_1 \widehat{|v|}^2} + b_1 & \widehat{|v|} \in [-0.76, 0] \\ a_2 e^{r_2 \widehat{|v|}^2} + b_2 & otherwise \end{cases} \quad 3\text{-}3$$

In order to find the optimal coefficients in equation 3-3, dual annealing optimization algorithm along with the boundary conditions at cut-in and $\widehat{|v|} = 0$ were used to minimize the maximum absolute error value between the illustrated points in figure 3.1

and the proposed model and find the optimum value of coefficients. Therefore, the resultant coefficients are described in the equation below. The fitted curve for the proposed model with these coefficients is shown in figure 3.2. As shown, an exponential curve was fitted for the wind speed between 0 and 0.68 (cut-out). It's the best fit for all data points in this domain which was found by the optimization process.

$$\hat{P}(\widehat{|v|}) = \begin{cases} 0 & \widehat{|v|} < -0.76 \; or \; \widehat{|v|} > 0.68 \\ 1.03273e^{-5.97588\widehat{|v|}^2} - 0.03273 & \widehat{|v|} \in [-0.76, 0] \\ 0.16154e^{-9.30254\widehat{|v|}^2} + 0.83846 & otherwise \end{cases} \quad 3\text{-}4$$

By using this generic model and having the rated power and design speed, the dimensionless power of the turbine can be calculated at different wind speeds. Then output power of the wind turbine is defined using the equation 3-1 as follows.

$$P(|v|) = P_r \times \hat{P}(\widehat{|v|}) \quad 3\text{-}5$$

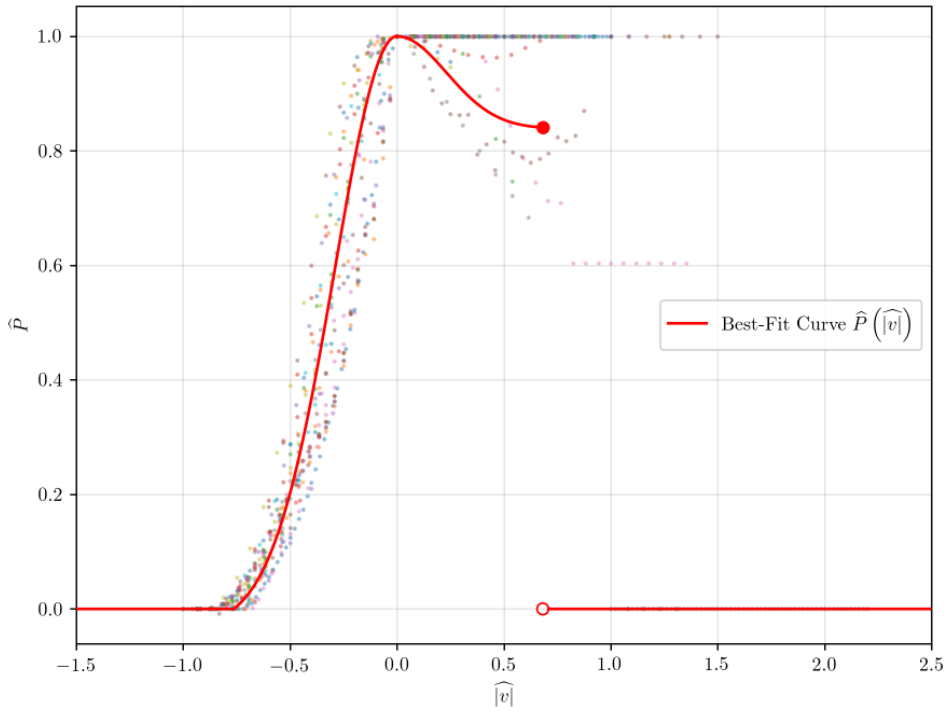

Figure 3.2 Fitted curve using wind turbine generic performance model [58]

3.1.2. Tidal Turbine

The same scaling and nondimensionalizing approach that was explained for the wind turbine was used to propose a general model for the tidal turbine (mostly for bottom fixed turbines) [57]–[59]. For this purpose, performance data of four different tidal turbine technologies and different models and capacities were gathered from the HOMER Pro's library. Two dimensionless variables, $\hat{P}$ and $\widehat{|v|}$ defined by equation 3-1 and 3-2, were used to convert the output power data in nondimensionalized form.

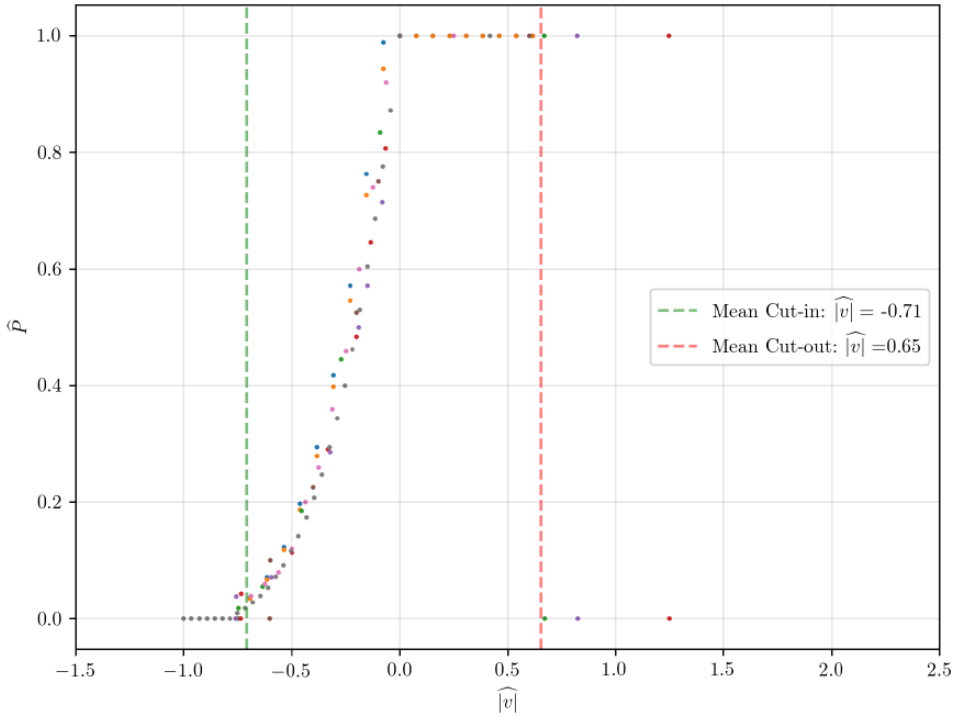

Figure 3.3 Dimensionless power of tidal turbine technologies [58]

Figure 3.3 shows the data in a dimensionless format, and each color in this figure represents a different technology or model. Mean cut-in and cut-out dimensionless speed shown by green and red dash lines were found to be -0.71 and 0.65, respectively. A nondimensionalized generic model proposed for the dimensionless output power of tidal turbine as a function of $\widehat{|v|}$ to fit the given data in the figure.

$$\hat{P}(\widehat{|v|}) = \begin{cases} 0 & \widehat{|v|} < -0.71 \; or \; \widehat{|v|} > 0.65 \\ a_1 e^{r_1 \widehat{|v|}} + b_1 & \widehat{|v|} \in [-0.71, 0] \\ 1 & otherwise \end{cases} \quad 3\text{-}6$$

In order to find the best-fitted curve to the given data, boundary conditions at cut-in and $\widehat{|v|} = 0$ were used to find the b_1 and r_1, and dual annealing optimization algorithm was applied to find the optimal value of a_1 by minimizing the maximum absolute error between the given values and the proposed function. So the resultant scaling model is shown in equation 3-7.

$$\hat{P}(\widehat{|v|}) = \begin{cases} 0 & \widehat{|v|} < -0.71 \; or \; \widehat{|v|} > 0.65 \\ 1.69215 e^{1.25909 \widehat{|v|}} - 0.69215 & \widehat{|v|} \in [-0.71, 0] \\ 1 & otherwise \end{cases} \quad 3\text{-}7$$

Figure 3.4 shows this fitted curve. It can be seen that this model can appropriately predict the $\hat{P}$ of different tidal turbine technologies and be used as a general dimensionless model for all types and models. Using equation 3-5, the output power of the tidal turbine at a specific wind speed can be calculated.

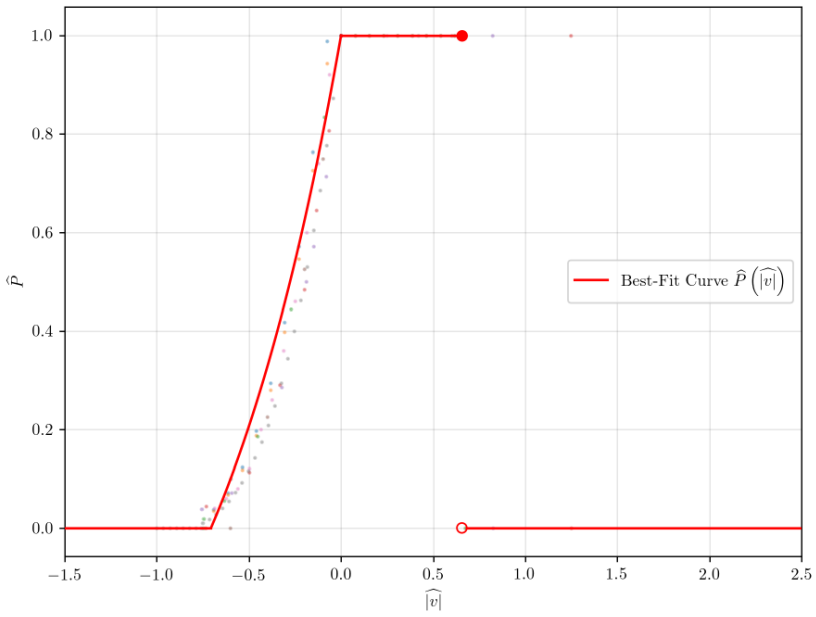

Figure 3.4 Fitted curve using tidal turbine generic nondimensionalized performance model [58]

3.1.3. Solar PV

Solar PV output power is determined by the amount of solar resources potential, which is defined by Global Horizontal Irradiance (GHI). GHI demonstrates the solar radiation on the surface of the earth. This term includes two parameters: Beam radiation, also known as direct radiation, which goes through the atmosphere directly and strikes the earth's surface without scattering and causes the shadow, and diffuse radiation doesn't cause any shadow, and its direction is changed in the sky by the atmosphere components [59].

$$\bar{G} = \bar{G}_b + \bar{G}_d \tag{3-8}$$

Where $\bar{G}$, $\bar{G}_b$ and $\bar{G}_d$ are the GHI, beam radiation, and diffuse radiation, respectively. Using the HDKR model [59]–[61], global radiation incident on the PV array ($\bar{G}_T$) is calculated by equation 3-9.

$$\bar{G}_T = (\bar{G}_b + \bar{G}_d A_i) R_b + \bar{G}_d (1 - A_i) \left(\frac{1 + \cos\beta}{2}\right) \left[1 + f_b sin^3\left(\frac{\beta}{2}\right)\right] + \bar{G}\rho_g \left(\frac{1 - \cos\beta}{2}\right) \tag{3-9}$$

Where A_i is the anisotropy index, which measures the atmospheric transmittance of beam radiation and R_b represents the ratio of beam radiation on a tilted surface to the beam ratio on a horizontal surface, and f_b is the horizon brightening factor, ρ_g is the ground reflectance, also known as albedo, and β is the slope of the surface. It's assumed that solar panels are horizontal, which means that β is zero. Therefore, the equation above is simplified as below.

$$\bar{G}_T = \bar{G}_b + \bar{G}_d \tag{3-10}$$

Equation 3-10 is exactly the same as the equation 3-8, which means global radiation incident on the PV array ($\bar{G}_T$) is equal to GHI on horizontal surfaces. Solar PV output power is defined by the equation below [59], [62]:

$$P_{PV} = Y_{PV} f_{PV} \left(\frac{\bar{G}_T}{\bar{G}_{T,STC}} \right) \quad 3\text{-}11$$

Where Y_{PV} is the rated capacity of PV array, and $\bar{G}_{T,STC}$ is the incident radiation at standard test conditions, which is equal to 1 kW/m^2, and f_{PV} is the derating factor. PV array output is affected by few factors such as the slope of panels, temperature of PV cell, weather conditions, soiling, shading and efficiency losses of the system, etc. [63]. The impacts of all these parameters are included in the derating factor. The temperature effect is not shown in equation 3-11. Instead, it's considered in derating factor. In this work, the derating factor was defined as 80 percent.

3.1.4. Diesel Generator

In diesel generators, the internal combustion engine consumes diesel and produces electricity. In the studies, a linear relationship between diesel generator rated capacity and output was used to obtain fuel consumption [64], [65]. The following equation shows the HOMER's model [59]:

$$F_d = F_0 Y_{gen} + F_1 P_{gen} \quad 3\text{-}12$$

Where F_d is diesel generator fuel consumption (L/h), F_0 is the fuel curve intercept (L/h.kW$_{rated}$), F_1 is the fuel curve slope (L/h.kW), Y_{gen} is the rated capacity of the diesel generator (kW), and P_{gen} is the output power of the generator (kW) at each time step. If the generator doesn't operate, fuel consumption will be zero. Fuel curve intercept and slope are defined based on the rated capacity of the diesel generator using the following equations [57], [58]:

$$F_0 = 0.0940 \times Y_{gen}^{-0.2735} \quad 3\text{-}13$$

$$F_1 = 0.3062 \times Y_{gen}^{-0.0370} \quad \text{3-14}$$

3.2. Energy system Cost

One of the most important factors that determine the feasibility of an energy system is the economic value of that system. In order to evaluate this value, the total cost of the system over its lifetime must be anticipated. Energy systems have some types of costs, such as capital cost of the grid components, O&M costs, fuel cost, replacement cost. These types of expenditures have been considered in this modeling, and they are described as the cost models of the microgrid system.

3.2.1. Net Present Cost of the System

Net Present Cost (NPC) of a system includes all kinds of costs and cash flows over the project lifetime, which are converted to their present value by discounting all these costs through the discount rate [66]. The following equation shows the NPC of the microgrid.

$$NPC = \sum_{t=0}^{n} \frac{C_t}{(1 + d_r)^t} \quad \text{3-15}$$

Where C_t is the cost of the system at time t, including the capital, O&M, fuel, carbon tax, and replacement costs, and d_r is the discount rate. In this study, the real discount rate was used to calculate the net present value of the future costs. The real discount rate is determined by the equation below [59]:

$$d_{r,real} = \frac{d_{r,N} - f}{1 + f} \quad \text{3-16}$$

Where $d_{r,real}$ and $d_{r,N}$ are the real and nominal discount rate, and f is the inflation rate. Nominal discount is the actual rate and doesn't include and adjust for the inflation rate,

but real discount rate considers the inflation effect, which is more realistic and accurate in calculating the future/present value of annualized costs.

3.2.2. Levelized Cost of Energy

The cost of energy is the other significant economic factor that helps the decision-makers and investors by demonstrating the feasibility and economic value of an energy system. LCOE is determined by the NPC of the system divided by the total energy production/served over the project lifetime. In this microgrid modeling, total served energy is the diesel generation, RE production, and ZAFB discharge from which diesel dump load and RE curtailment are subtracted. The following equation describes the LCOE [26]:

$$LCOE = \frac{\sum_{i=0}^{m} NPC_i}{\sum_{1}^{n} \frac{E_{served}\ (t)}{(1+d_r)^t}} \quad \text{3-17}$$

Where m is the microgrid component, E_{served} (kWh) is the total delivered energy over the project lifetime.

3.2.3. Wind Turbine Cost model

The capital cost of wind turbine per kW can be calculated by the scaling model below as a function of rated capacity [57], [58]. Figure 3-5 shows how equation 3-18 can predict the CAPEX.

$$C_{capital-kW} = 4525 \times e^{\left(\frac{1}{3}\times \ln\left(\frac{4000}{4525}\right)\times P_r\right)} + 2000 \quad \text{3-18}$$

Where $C_{capital-kW}$ is the capital cost per kW ($/kW), P_r is the rated capacity of the wind turbine (kW). CAPEX of the wind turbine is obtained by the following equation.

$$C_{capital} = C_{capital-kW} \times P_r \quad \text{3-19}$$

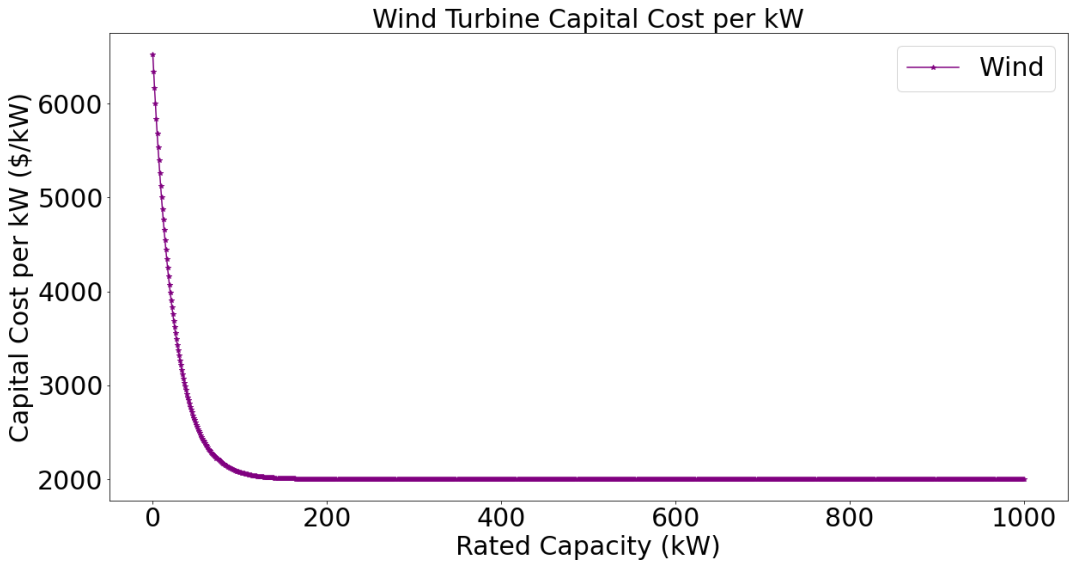

Figure 3.5 Wind Turbine CAPEX per kW

The wind turbine's operation and maintenance cost per kWh energy production is assumed 0.05 ($/kWh) [57], [58]. Annual Operational Expenditure (OPEX) of the wind turbine is determined by the equation below:

$$C_{O\&M-annual} = E_{annual} \times C_{O\&M-kWh} \quad \text{3-20}$$

Where E_{annual} is the total annual energy production. Due to the structure and technologies of the turbines, there is no replacement cost for wind turbines during the project's lifetime. The following equation describes the NPC of this system over its lifetime:

$$NPC_{Wind} = C_{capital} + \sum_{1}^{n} NPV_{O\&M} \quad \text{3-21}$$

3.2.4. Tidal Turbine Cost model

In order to calculate the capital cost of the tidal turbine, the generic model below is used to determine the CAPEX per kW [58], [59], [67]. This equation is the function of the rated capacity of the turbine. Figure 3.6 shows the CAPEX per kW using this equation. The capital cost of the tidal turbine is obtained by equation 3-19.

$$C_{capital-kW} = 4497 \times e^{\left(\frac{1}{5000}\times \ln\left(\frac{4023}{4497}\right)\times P_r\right)} + 2000 \quad \text{3-22}$$

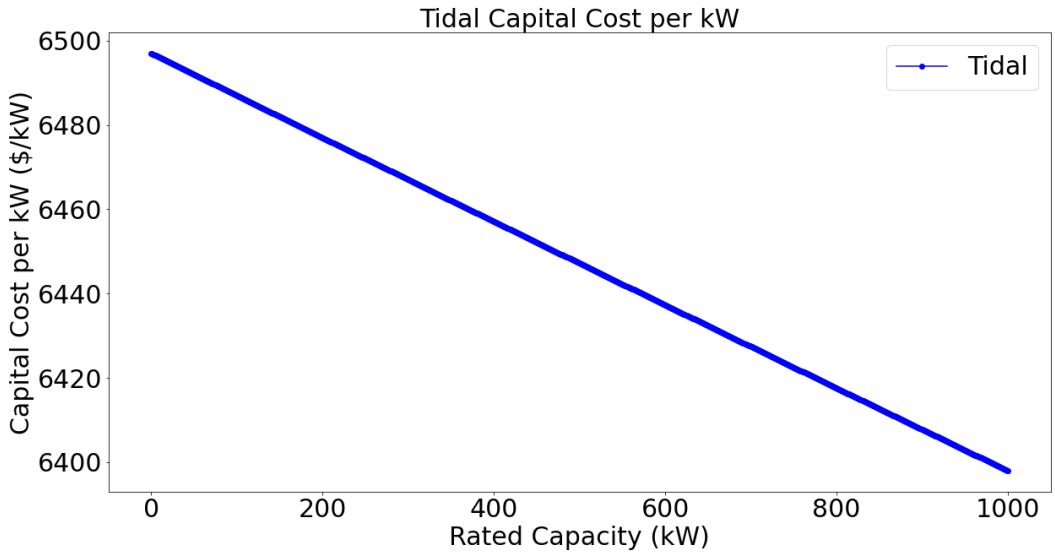

Figure 3.6 Tidal turbine CAPEX per kW

The tidal turbine's operation and maintenance cost per kWh energy production is 0.05 ($/kWh) [57], [58]. The annual O&M cost of the tidal turbine is calculated by the equation 3-20. Same as the wind turbine, the replacement cost of the tidal turbine during the project lifetime is neglected. Using the following equation, the NPC of the turbine can be obtained.

$$NPC_{Tidal} = C_{capital} + \sum_{1}^{n} NPV_{O\&M} \quad \text{3-23}$$

3.2.5. Solar PV Cost Model

The capital cost of solar PV per kW is calculated using the following equation, which is the function of the rated capacity of the PV array [58], [59]. As shown in figure 3.7, CAPEX per kW is reduced from $2520 to $770 by increase the rated capacity. The capital cost of solar PV is defined by equation 3-19.

$$C_{capital-kW} = 1750 \times e^{\left(\frac{1}{3}\times\ln\left(\frac{4000}{4525}\right)\times P_r\right)} + 770 \quad \text{3-24}$$

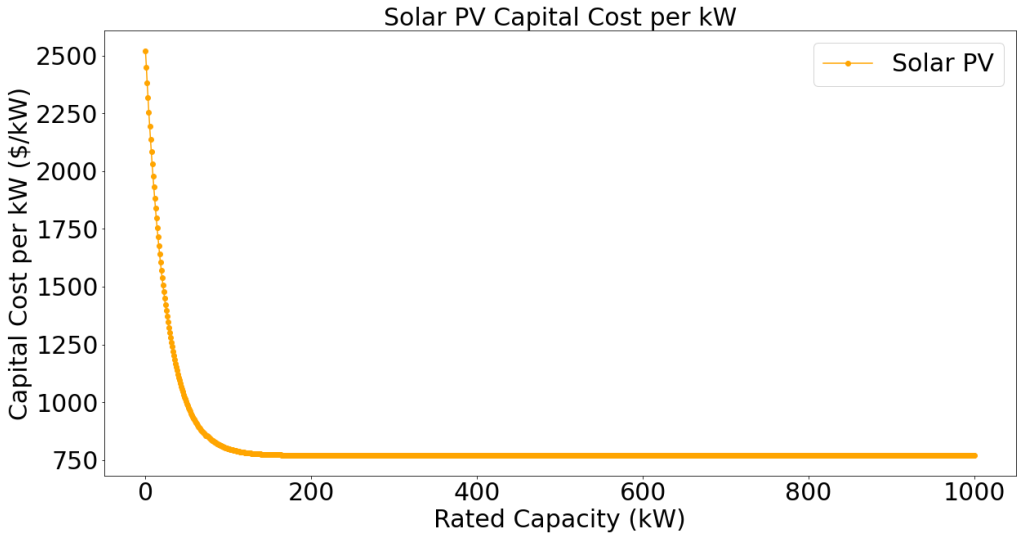

Figure 3.7. Solar PV CAPEX per kW

The O&M cost of solar PV per unit energy production is 0.01 ($/kWh). Equation 3-20 is used to calculate the annual OPEX of the solar PV array. Solar PV technologies are mature now, and replacement is not necessary during its lifetime. So, the replacement cost of solar PV is zero in this modeling. Solar PV's NPC over the project lifetime is shown below:

$$NPC_{solar} = C_{capital} + \sum_{1}^{n} NPV_{O\&M} \quad \text{3-25}$$

3.2.6. Diesel Generator Cost Model

Over the lifetime, the cost of diesel generator includes the capital, fuel, replacement, and carbon tax expenditures. Based on the generic model below, CAPEX per kW of diesel generator is obtained for different rated capacities [58], [59]. As shown in figure 3.8, the capital cost per kW is reduced by increasing the generator's rated capacity. Equations 3-19 and 3-26 are used to calculate the CAPEX.

$$C_{capital-kW} = 150 \times e^{\left(\frac{1}{5000}\times\ln\left(\frac{22}{150}\right)\times P_r\right)} + 400 \quad \text{3-26}$$

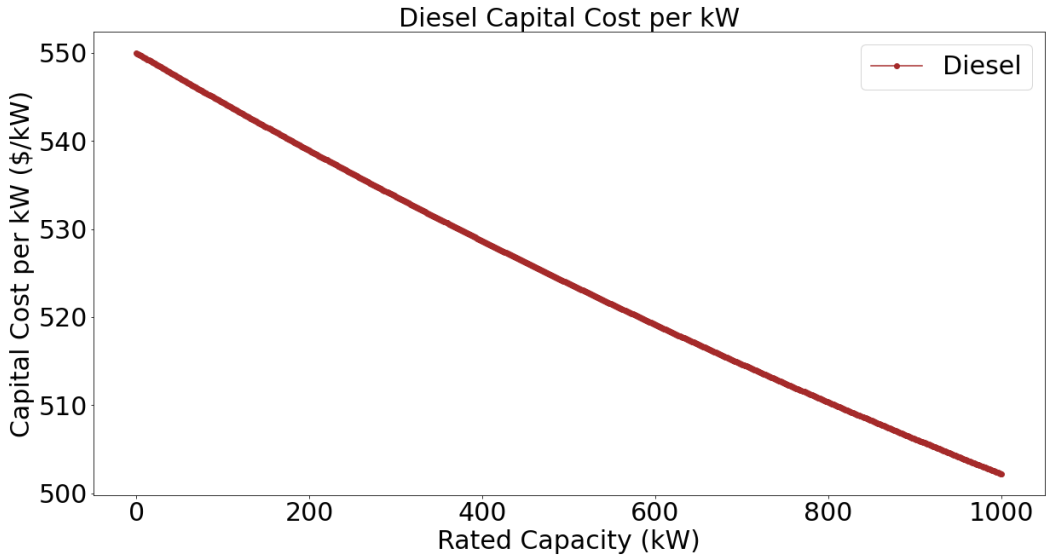

Figure 3.8 Diesel generator CAPEX per kW

The O&M cost of the diesel generator per unit energy generation ($/kWh) is obtained by the mathematical expression below [58], [59], and figure 3.9 shows the variation of the OPEX per kWh with respect to the rated power capacity of the generator using this generic model. Total annual O&M cost is determined by equation 3-20.

$$C_{O\&M-kWh} = 0.03 \times e^{\left(\frac{1}{5000}\times\ln\left(\frac{1}{30}\right)\times P_r\right)} + 0.01 \quad \text{3-27}$$

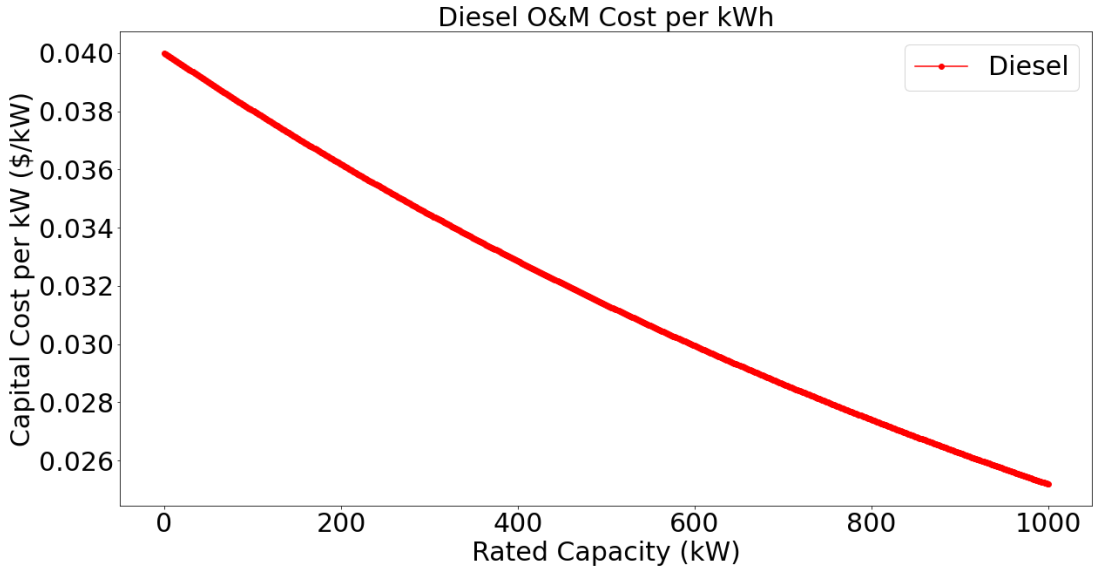

Figure 3.9. Diesel Generator O&M cost per kWh

As mentioned earlier, diesel generator fuel consumption is obtained through a linear equation and fuel curve intercept and slope. By having the annual fuel consumption and fuel price, fuel cost can easily be calculated. In this modeling, a constant fuel escalation rate was considered, which means fuel price increased yearly by this rate.

$$C_{Fuel-annual} = F_{annual} \times Fuel\ Price \quad 3\text{-}28$$

Where F_{annual} is the total annual fuel consumption (L). The future value of fuel price is determined by the mathematical expression below:

$$FV_{n,fuel} = Present\ Fuel\ Price \times \left(1 + \mathrm{i}_{fuel}\right)^{n} \quad 3\text{-}29$$

Where $FV_{n,fuel}$ is the future value of fuel price ($/L), n represents the future years and i_{fuel} is the fuel escalation rate.

In this modeling, carbon tax cost related to diesel generator CO_2 emission was considered. Equation 3-30 and 3-31 are used to calculate the carbon tax cost. A yearly increase rate ($5) was considered for the carbon tax rate.

$$Annual\ CO_2\ Emission\ \ (tonne)\ =\ F_{annual} \times 2.64\ (kg\ CO_2/L) \times 10^{-3} \quad 3\text{-}30$$

$$C_{carbon\ tax} = Annual\ CO_2\ Emission\ (tonne) \times\ Carbon\ tax\ rate\ (\$/tonne) \quad 3\text{-}31$$

Internal combustion engines have a high replacement cost. Diesel generators must be replaced after defined running hours. The mathematical expression below is used to calculate the replacement cost [58], [59].

$$C_{Replacement} = C_{capital-kW} \times P_r^{0.95} \quad 3\text{-}32$$

NPC of diesel generator includes the CAPEX and net present value of all O&M, fuel, carbon tax, and replacement costs over the project lifetime. The following equation describes this definition.

$$NPC_{Diesel} = C_{capital} + \sum_{1}^{n} NPV_{O\&M} + \sum_{1}^{n} NPV_{Fuel\ Consumption} + \sum_{1}^{n} NPV_{Carbon\ Tax} + \sum_{1}^{n} NPV_{Replacement} \quad 3\text{-}33$$

3.3. Modeling & Optimization Approach

The sizing and control of microgrid components are the two most important parts of the modeling, which must be evaluated technically and economically. This microgrid modeling tool was developed to find the optimal microgrid design and optimal operation control by incorporating the ZAFB model. This modeling was developed to apply for Canadian off-grid communities of any size in which diesel is the main energy source. As shown in figure 3.10, a bilevel optimization process was defined, the upper level is responsible for microgrid sizing, and the inner level is doing the energy management.

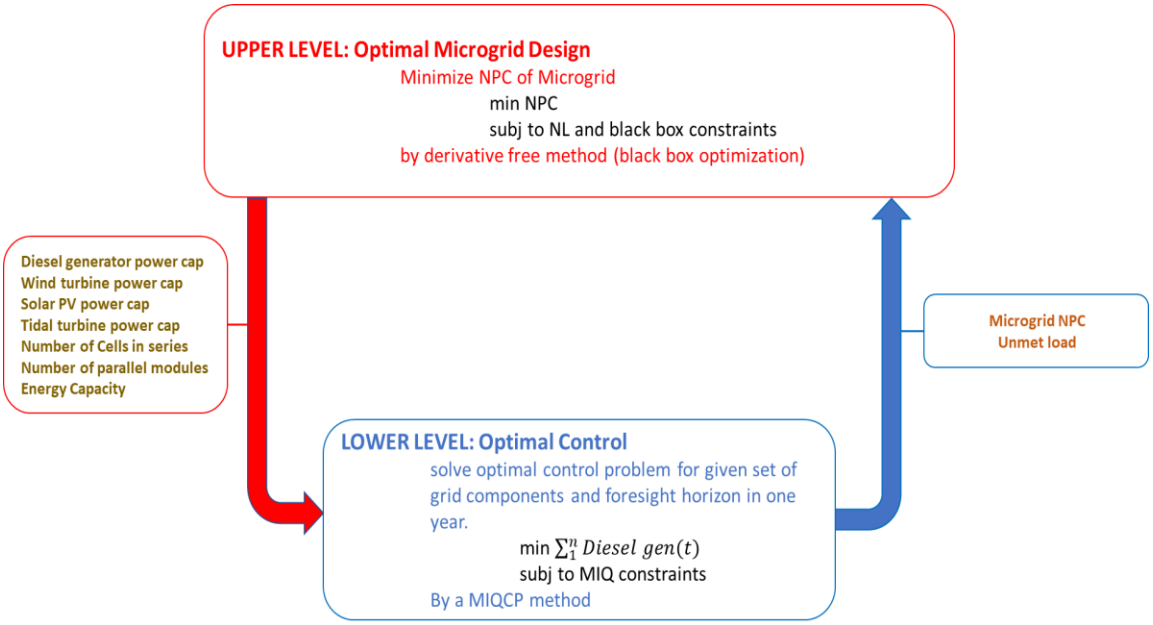

Figure 3.10 flow chart of microgrid modeling tool

The outer loop optimizes the system NPC. Microgrid configuration such as the number of cells in series in each stack of ZAFB charge unit (regenerator), the number of parallel modules of the regenerator, the number of cells in series in each stack of ZAFB discharge unit (generator), the number of parallel modules of ZAFB generator, the capacity of ZAFB energy storage, the capacity of the wind turbine, solar PV, tidal turbine and diesel generator are determined in the upper level. The optimal control model (lower level) minimizes the diesel output power based on a given grid design from the upper level and the user-defined foresight horizon for the whole year, then calculates the system costs over the project lifetime and then returns the system NPC and other information to the upper level. The code of this modeling was written in Python 3.7 programming language using the Jupyter Notebook.

3.3.1. Optimal Design Model (Upper Level)

Since this approach is a nested optimization, the economic aspect of microgrid modeling is assessed and optimized in the outer loop, and the optimal size of microgrid components is determined at this level. The NPC of the system over the project lifetime is the objective function that is minimized by the optimal size of the grid components.

$$Objective\ Function:\ min \quad NPC_{system}$$

The control model, a callable function in the optimal design model, is called at each iteration of the upper loop. The NPC value is computed through the control model (lower level) for the given microgrid components size at each iteration. Decision variables in the optimal design model are as below:

- Power capacity of the wind turbine
- Power capacity of the solar PV
- Power capacity of the tidal turbine
- Power capacity of diesel generator
- The number of cells in series of the ZAFB regenerator
- The number of parallel stacks of the ZAFB regenerator
- The number of cells in series of the ZAFB generator
- The number of parallel stacks of the ZAFB generator
- Energy storage capacity of ZAFB

Constraints:

A set of design constraints were considered at the upper level to control the sizing optimization. Due to the solver structure, only inequality constraints can be defined in this process. These constraints are as follows:

- ZAFB energy storage must be able to provide at least four hours discharging at maximum capacity
- ZAFB energy storage must have enough capacity for at least four hours charging at maximum capacity
- ZAFB discharge power capacity (generator capacity) must be less than the peak load (for hybrid cases)
- Unsatisfied load demand in the microgrid must be zero

The first constraint controls the size of discharge and energy storage units in ZAFB. In other words, it determines the minimum discharge duration. The second one controls the charge and storage tank capacity. The third constraint determines the maximum capacity

of the generator in the ZAFB, which is used for hybrid modes. The last one, which is the most important one, controls the size of microgrid components so that there is no unmet load demand. The first three constraints related to ZAFB sizing are nonlinear ones because of ZAFB nonlinear performance model. The last one, which is related to energy management, is a black-box constraint because the unmet load is one of the outputs returned by the inner loop (control model). Any other constraints can be defined for RE sizes or ZAFB manufacturing limitation, or LCOE at this level. Since there is no information regarding the manufacturing restrictions for the allowable number of cells in each stack, the allowable number of parallel stacks, maximum current, etc., any constraints related to the number of cells and stacks weren't defined in the design model. They were only limited by the assumptions for their upper bound in the search domain. However, these sets of manufacturing constraints can be easily defined if the manufacturer provides the information.

Scenarios:

In order to evaluate the ZAFB impact and RE sources on the fuel consumption and system NPC, different RE penetration scenarios were tested through this modeling tool. These scenarios were defined by limiting the upper bound of search domain for the wind turbine, solar PV, and tidal turbine in the optimal design model (upper level), and these limits were considered in a sequence of 20%, 40%, 60%, 80%, and 100% of peak load of that off-grid community, for this reason, resultant RE penetration rate in three case studies are not the same. The optimum size of ZAFB and grid components was found for each of these cases. A hybrid renewable energy system is the case that the diesel generator is integrated with RE sources. So, in these hybrid cases, a diesel generator can show up in the microgrid structure. For this reason, the upper bound of diesel generator capacity was considered equal to peak-load demand. There is one more RE penetration scenario which is the 100% RE penetration. In this case, diesel capacity is zero, and the optimal design model picks the decent size of RE plants and ZAFB to achieve zero fuel consumption and minimum NPC.

Problem Type & Solver:

Since upper-level deals with only NPC value as the objective function and there is no information regarding the objective function derivative and hessian matrix, the optimization problem is a black-box optimization. In order to solve these kinds of problems, derivative-free solvers must be used. In this work, the performance of few solvers such as Simplicial Homology Global Optimization (SHGO), Topographical Global Optimisation (TGO), Particle Swarm Optimization (PSO), Brute, and Dual Annealing was tested to find the global optimum solution. All these solvers are used for continuous variables and search domains. However, microgrid components have a discrete domain. To solve this issue, the round-off technique was used for discretizing the continuous domains. But the biggest problems with the mentioned solvers were the high run time and convergence. Finally, after all these, a derivative-free algorithm framework developed by Liuzzi et al. [68] to solve constrained black-box optimization problems with integer variables was picked. Their proposed strategy is based on using primitive directions combined with non-monotone line search.

3.3.2. Optimal Control Model (Inner Level)

Energy management, grid components output optimization, and calculation of the system costs are done at the inner level in this modeling tool. The inner loop includes two stages: the optimization stage in which the control problem is solved using Model Predictive Control (MPC) method for one year based on user-defined foresight horizon for the given microgrid design values by the upper level. In the MPC method, also known as the Receding Horizon Control method, the optimizer solves the control problem for each foresight horizon, and it decides about the future changes of microgrid components operation based on the load demand, RE resources information of that horizon, and battery SoC of the previous horizon. Then control model goes to the next horizon and solves the optimization problem. This iteration process goes on for the whole year. In The post-processing stage, microgrid costs are calculated over the lifetime based on first stage results. Figure 3.11 shows the inner level. This control model controls the power output

of microgrid components, voltage and frequency control in microgrid were not considered in this model and it was assumed that voltage and frequency are always controlled by the inverters in the defined and acceptable ranges. This point will be discussed in detailed in future works.

Inputs of the inner level are as below:

- Size of Microgrid components
- Load demand profile
- Wind speed data
- Solar radiation data
- Tidal speed data
- Foresight horizon
- Initial SoC of ZAFB
- Project lifetime
- Nominal discount rate
- Inflation rate
- Fuel price and fuel escalation rate
- Carbon tax rate and its annual increase rate

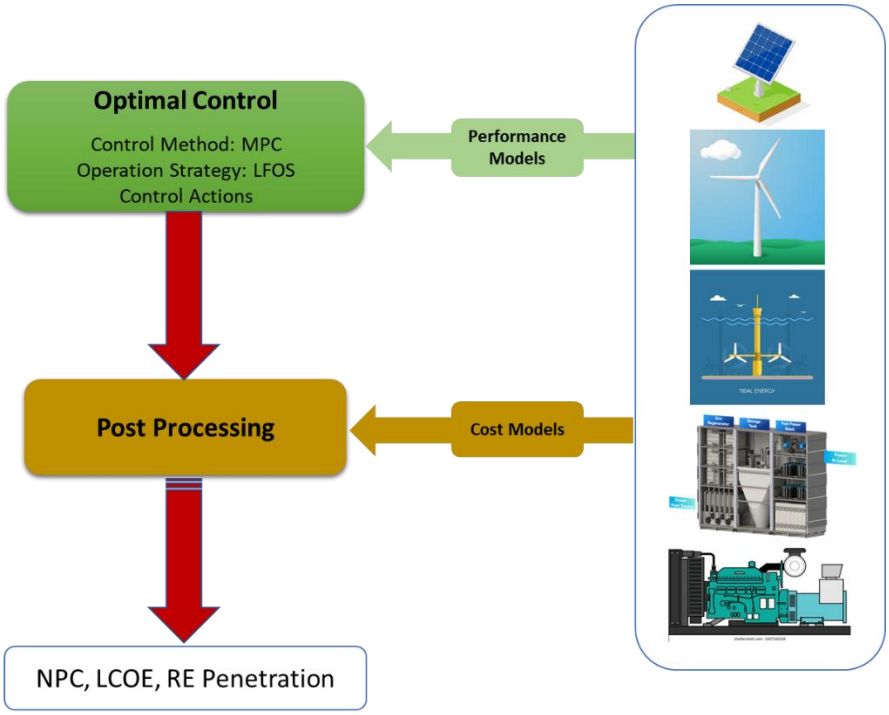

Figure 3.11 Flow chart of the optimal control model (inner level)

Optimization stage:

Using the MPC method, the optimal control model controls the system operation by solving a Mixed Integer Quadratically Constrained Programming (MIQCP) problem. At first, the control model was a Mixed Integer Nonlinear Programming (MINLP) because

of the ZAFB nonlinear performance and efficiency models. However, solving the MINLP was computationally expensive, especially for longer foresight horizons, and dealing with binary variables which control the operation, was challenging and sometimes resulted in infeasibility. These issues were solved by using the ZAFB nonlinear performance model at the upper level to calculate the maximum allowable charge and discharge power instead of using it in the inner loop and having a linear efficiency model instead of a nonlinear one in the control model. In this way, MINLP was converted to MIQCP. The optimization model was developed in Pyomo 6.0.1, which is an open-source and Python-based optimization modeling tool [69], [70], and implemented using the Jupyter Notebook. In this model, the diesel generator output power is the objective function of the control model, which is minimized at each time step. In addition, all performance models of microgrid components were implemented in this stage.

$$Objective\ Function:\ \ min \quad \sum_{t=1}^{n} P_{diesel\ gen}(t)$$

Decision variables defined at each time step in the optimization process are as below:

- Diesel Generator output power
- Charge power which is taken from the grid side
- Discharge power which ZAFB delivers to the grid
- Energy of the battery (SoC)
- Free variable for RE curtailment, diesel dump load, and unmet load
- Binary variables for the control actions

In this control model, using the MPC method (Receding Horizon Control method), the whole year is divided into a number of horizons (time windows), then the optimizer solves the MIQCP for each foresight horizon, and using the control actions, it decides to use the RE sources and run the diesel generator or charge or discharge the ZAFB at each time step based on the RE resources and energy demand data of that foresight horizon and SoC of ZAFB from the previous horizon. The optimization procedure is iterated for

each foresight horizon in a sequence that forms a year. The only information transferred from the previous horizon to the next one is the SoC of ZAFB. The final SoC of the previous horizon is considered as the initial SoC of the next horizon.

Solver:

At first, in order to solve the nonlinear optimal control problem (MINLP), many solvers such as IPOPT, BONMIN, SCIP, and COUENNE were tested. IPOPT is a solver for nonlinear programming (NLP) and cannot solve the problem with discrete variables. BONMIN, SCIP, and COUENNE can solve the MINLP, but there are some issues with them. The first one is the higher run time, especially for a longer foresight horizon. The second one, they cannot handle the binary variable very well, and sometimes they have convergence issues. As mentioned above, the optimal control problem was converted to MIQCP, which was solved by CPLEX and GUROBI solvers. CPLEX was accurate and fast enough, but GUROBI was more accurate and faster. After all iterations and tests, GUROBI was selected to solve the optimal control model in the inner loop. GUROBI is a closed source commercial optimization solver for convex and non-convex Mixed Integer Linear Programming (MILP), Mixed Integer Quadratic Programming (MIQP), and MIQCP [71]. In this study, GUROBI was used under an academic license.

Operation Strategy & Control Actions:

Since this modeling aims to reduce or eliminate the diesel fuel consumption from Canadian off-grid communities and substitute it with clean energies and longer duration ZAFB, the Load Following Operation Strategy (LFOS) is the best option to minimize the diesel operation time. In LFOS, the diesel generator runs when it’s necessary and generates as much energy as to meet the primary load demand, and lower priority demands like charging the battery are satisfied by RE sources instead of diesel generator, and the battery can help to reduce the diesel generator output/operation time by discharging critical time steps. Using LFOS can assure that diesel generator will be used for future high load demands. For this reason, LFOS was implemented in the control

model in this study. Also, there will be some diesel generator dump load (excess generation) when load demand is less than the minimum load of the diesel generator and it has to run to satisfy the load. This dump load is used to charge the battery in this control model. There is another operation strategy known as Cycle Charging Operation Strategy (CCOS), which is not a good choice for achieving the minimum diesel consumption. In CCOS, when it's needed, the diesel generator has to run at full load (rated capacity) to meet the primary loads and charge the battery. Using CCOS provides more charging energy to the battery, making it possible for the diesel generator not to run for future low load demands. Therefore, it is not possible to achieve the lowest or zero diesel fuel consumption by CCOS.

Control Actions:

As mentioned earlier, the optimal control problem is solved for each foresight horizon using the MPC method. The optimizer decides about future changes of microgrid components output (diesel generator output, battery charge/discharge) to meet the load demand by taking some control actions and using the information of demand, SoC of the battery, and available RE resources in that foresight horizon. Then it shifts forward to the next horizon and decides about the operation of components until the end of the year.

Based on the information of foresight horizon (load demand, RE sources, initial SoC of the battery), some control actions are taken to charge/discharge the ZAFB or run the diesel generator in an optimum way to have minimum diesel generator output at that horizon. Control actions are defined by some constraints in which binary variables control the system operation. The control actions implemented in the optimal control model at each horizon are as below:

- If RE production is more than load demand, then the optimizer decides to charge the battery or curtail this excess production.

- If RE production is less than load demand, then the optimal control model decides to discharge the battery (if it has enough charge) or run the diesel generator. If the diesel generator is needed to operate, it must run at a higher than its minimum load.
    - If the unmet load (load demand - RE production) is greater than the diesel generator minimum load, the optimizer will decide to discharge the battery to satisfy the demand or run the diesel generator and discharge the battery simultaneously to help to minimize the diesel generator output.
    - If the unmet load (load demand - RE production) is less than the diesel generator minimum load, the optimizer will decide to discharge the battery or run the diesel generator at a minimum load to satisfy the rest of the load demand. If diesel operates, there will be excess energy generation, and the optimal control model will decide to use this excess energy for charging the battery or dump it.

Post Processing:

In the post-processing stage, microgrid costs over the project lifetime are computed using the results of the optimization stage. For this purpose, components operation results for a year are used for the next years to calculate the net present value of the CAPEX, OPEX, fuel cost, carbon tax cost, replacement cost, and NPC and LCOE of the system over the project lifetime. All cost models of the components described earlier were used in the post-processing stage.

Diesel generator annual fuel consumption is calculated and used to obtain the fuel consumption cost and carbon tax cost. Fuel price and carbon tax are updated for the future years based on the defined fuel escalation rate and annual increase rate of the carbon tax rate. Diesel generator working hours during the project lifetime are counted, and whenever it reaches the replacement time (30000 hours), the replacement cost is considered, which is converted to its net present value. ZAFB charge and discharge power of each time step are summed over the project lifetime, and when they reach the defined replacement time (after 20000 hours working at maximum power), the replacement costs of the cathodes are added to NPC of the ZAFB.

NPC of the microgrid is obtained after calculating the NPV of all costs of the grid components, including diesel generator, wind turbine, solar PV, tidal turbine, and ZAFB. Then, LCOE is determined using the NPC value and total delivered energy by the grid components over the project lifetime. Finally, NPC, LCOE, RE penetration rate, and annual unmet load values are returned to the upper level.

Chapter 4

4. Results and Discussion

4.1. Verification and Sensitivity Analysis

The developed microgrid modeling tool and proposed ZAFB model were tested through a generic hourly load demand profile with 500 kW peak load and RE resources data provided by PRIMED, to verify its functionality and sensitivity. Three penetration scenarios were evaluated by limiting the upper limit of wind turbine and solar PV capacity in the search domain, and each scenario includes four cases. These scenarios and test cases are as below.

RE Capacity Limits:

I. Upper limits: wind turbine= 400 kW, solar PV= 400 kW
II. Upper limits: wind turbine= 500 kW, solar PV= 500 kW
III. Upper limits: wind turbine= 600 kW, solar PV= 600 kW

Cases:

- Case 1: Real ZAFB costs were applied in modeling.
- Case 2: ZAFB costs, including regenerator, generator CAPEX, and replacement cost, were doubled
- Case 3: ZAFB regenerator and generator costs were doubled, and the cost of energy storage was tripled.
- Case 4: Real ZAFB costs were applied in modeling, but the upper limit of ZAFB energy capacity was 500 kWh

The results of the three penetration scenarios are shown in tables 4-1 – 4-3. As shown in table 4-1, by doubling or tripling the ZAFB cost and limiting the energy capacity in cases 2, 3, and 4, system NPC, which is the objective function of the upper lever (optimal design model), increased. Consequently, the cost of energy increased, and RE penetration decreased because the optimizer picked smaller battery components, and the diesel generator had to run more. By doubling the ZAFB cost ($/kW) and tripling the energy

storage cost ($/kWh), the size of the tank was reduced. Consequently, a smaller regenerator and generator were needed for smaller energy capacity.

Table 4-1 Sensitivity analysis I, upper limit: wind= 400 kW, solar= 400 kW, diesel= 600 kW

	Case 1	**Case 2**	**Case 3**	**Case 4**
RE penetration (%)	80.21	77.58	77.1	74.79
System NPC (CAD $M)	7.23	7.83	7.93	7.67
LCOE (CAD $/MWh)	178.6	201.5	206	207.9
Diesel (kW)	473	473	473	473
Wind (kW)	400	400	400	400
Solar (kW)	400	400	400	393
ZAFB Regen (kW)	225	120	113	110
ZAFB gen (kW)	224	170	164	122
Tank Capacity (kWh)	4200	1689	1362	498

Table 4-2 shows the results of scenario II for four cases. In this scenario, increasing the ZAFB costs resulted in smaller ZAFB in hybrid microgrid and higher NPC and LCOE. Wind energy is available more often than solar energy, making it a better source for charging the battery. Therefore, wind turbine capacity was reduced a bit in cases 2, 3, and 4 because the optimizer picked smaller ZAFB, and there is no need for a larger wind turbine to charge the battery. On the other hand, since solar PV has a higher limit in the search domain than the previous scenario and solar PV is the cheapest RE technology, a larger solar PV array was picked to compensate for the lack of a larger battery and wind turbine.

Table 4-2 Sensitivity analysis II, upper limit: wind= 500 kW, solar= 500 kW, diesel= 600 kW

	Case 1	**Case 2**	**Case 3**	**Case 4**
RE penetration (%)	87.22	80.78	79.73	77.86
System NPC (CAD $M)	6.732	7.64	7.75	7.54
LCOE (CAD $/MWh)	155.2	193.01	200.22	202.12
Diesel (kW)	471	471	471	471
Wind (kW)	500	442	446	450
Solar (kW)	478	497	497	493
ZAFB Regenerator (kW)	250	130	112	117
ZAFB generator (kW)	301	177	159	123
Tank Capacity (kWh)	4264	1613	1043	500

The results of scenario III are shown in table 4-3. It can be seen that with an expensive battery, a smaller battery was picked by the optimizer (case 2 and 3), and for limited energy capacity (500 kWh, case 4) smaller power unit and regenerator were chosen. Smaller battery leads to lower RE penetration because diesel generator must operate more often in this case. In cases 2, 3, and 4, wind turbine capacity was reduced due to the smaller battery and NPC of the system, and LCOE was increased due to higher fuel consumption. Since upper limits of wind turbine capacity and solar PV capacity in the search domain are higher than scenario II, larger turbine and solar PV arrays were picked, particularly in case 2. For this reason, ZAFB power and energy capacities are larger than the ones in scenario II.

Table 4-3 Sensitivity analysis III, upper limit: wind= 600 kW, solar= 600 kW, diesel= 600 kW

	Case 1	**Case 2**	**Case 3**	**Case 4**
RE penetration (%)	88.15	84.83	81.92	78.16
System NPC (CAD $M)	6.735	7.55	7.72	7.52
LCOE (CAD $/MWh)	154.49	181.34	193.63	201.69
Diesel (kW)	469	469	469	469
Wind (kW)	518	484	459	446
Solar (kW)	557	568	557	555
ZAFB Regenerator (kW)	227	192	137	122
ZAFB generator (kW)	324	231	181	124
Tank Capacity (kWh)	4102	2386	1523	500

From these results, it’s obvious that the optimizer picks a smaller battery size when the battery is expensive. And for smaller storage tanks (kWh), smaller power units (regenerator and generator) are selected. A smaller battery means more diesel generator operation time, therefore, NPC and LCOE are increased, and RE penetration is reduced. It’s concluded from these results that the modeling tool works appropriately, and optimal design and optimal control model have excellent sensitivity to the cost of components.

4.2. Case Studies

As a part of CleanBC, the Province of B.C.'s Renewable Energy for Remote Communities (RERC) Program aims to reduce reliance on diesel by funding the capital

costs of renewable electricity projects. The strategy targets the largest diesel generating stations in B.C. and aims to reduce province-wide diesel consumption for generating electricity in remote communities by 80% by 2030. $16.5 million funding is allocated for these projects [72]. In order to test the performance and functionality of the developed microgrid modeling tool and evaluation of ZAFB impact, three real-world test cases with different sizes (small, medium, and large) in British Columbia were studied. These case studies are Blind Channel, Hot Spring Cove, and Moresby Island.

4.2.1. Modeling Inputs

The hourly load demand profiles of these off-grid communities in B.C. are recorded onsite, which were provided by PRIMED [57]. Wind resource data used in this modeling was collected from Environment and Climate Change Canada's Wind Atlas [73]. Based on the latitude and longitude of each mentioned location, wind speed data was gathered. Wind speed data at three altitudes were available in this database, 80 m, 100 m, and 120 m. Because of the size of likely wind turbines in these areas, data of 80 m height was used for Blind channel and Hot Spring Cove, and data of 100 m was used for Moresby Island. Solar radiation data was collected from Natural Resource Canada (NRCan). Some of the datasets of this database are publicly available for free, like SUNY. The source of SUNY is the GOES satellite. SUNY dataset with hourly time resolution was used for each case study. Latitude and longitude were used for data collecting from this source. For tidal resource inputs, tidal stream data from all over the coast of B.C. were collected from Fisheries and Oceans Canada [74]. Then a generic scaling resource series was constructed for the coast of B.C. This generic series was developed at PRIMED by A. Truelove et al. [57], used in this study. Other input parameters of this modeling are shown in table 4.1.

Table 4-4 Input parameters

Parameter	Value
Foresight horizon	24 hours
Initial SoC of ZAFB	50 %

Discount rate	5 % [75]
Inflation rate	2 % [75]
Diesel generator minimum load	30 %
Fuel price	1.2 $/L [76]
Fuel escalation rate	3 %
Carbon Tax rate	$45/Tonne CO_2 [77]
Carbon tax increase rate	$5 [77]
Project lifetime	20 years

4.2.2. Case Study I: Blind Channel

Blind Channel is a recreational center located on West Thurlow Island in the heart of British Columbia's wild coast that provides marina services including dock, aircraft dock, a fuel dock, accommodation, and adventure packages for visitors [78]. This place has a 62 kW peak load and 143.68 MWh annual energy demand. Figure 4.1 shows the load demand profile of blind Channel throughout the year.

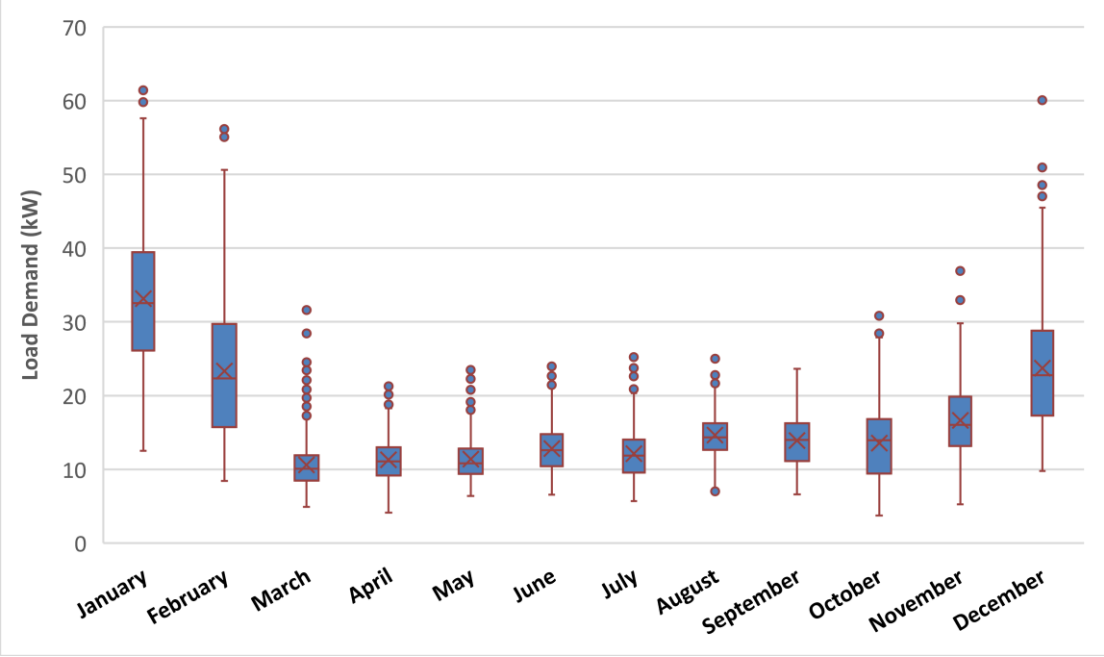

Figure 4.1 Load demand profile of Blind Channel (mean, median, 1st and 3rd quartiles, outliers, and minimum and maximum values)

As mentioned earlier, different RE penetration scenarios were defined by limiting the upper bound of the search domain in the optimal design model (upper level). The size of microgrid components for Blind Channel is shown in table 4-5.

Table 4-5 Size of components of Blind Channel microgrid in different RE penetration scenarios

	Components limit	RE Penetration (%)	Diesel (kW)	Wind (kW)	Solar (kW)	Tidal (kW)	ZAFB Charge power (kW)	ZAFB Discharge power (kW)	Tank Capacity (kWh)
Case 1	**Wind=0kW Solar=0kW Tidal=0kW Diesel=70kW**	**0**	**62**	**-**	**-**	**-**	**-**	**-**	**-**
Case 2	**Wind=5kW Solar=5kW Tidal=5kW Diesel=70kW**	**22.84**	**60**	**5**	**5**	**5**	**20**	**29**	**129**
Case 3	**Wind=10kW Solar=10kW Tidal=10kW Diesel=70kW**	**54.45**	**60**	**10**	**10**	**10**	**17**	**24**	**125**
Case 4	**Wind=15kW Solar=15kW Tidal=15kW Diesel=70kW**	**71.5**	**60**	**15**	**15**	**15**	**14**	**21**	**213**
Case 5	**Wind=25kW Solar=25kW Tidal=25kW Diesel=70kW**	**81.09**	**60**	**25**	**0**	**18**	**18**	**20**	**290**
Case 6	**Wind=35kW Solar=35kW Tidal=35kW Diesel=70kW**	**82.52**	**60**	**35**	**0**	**11**	**23**	**20**	**441**
Case 7	**Wind=50kW Solar=50kW Tidal=50kW Diesel=70kW**	**83.29**	**60**	**38**	**0**	**10**	**23**	**22**	**449**
Case 8	**Wind=65kW Solar=65kW Tidal=65kW Diesel=70kW**	**83.68**	**60**	**40**	**0**	**9**	**24**	**22**	**496**
Case 9	**Wind=100kW Solar=100kW Tidal=100kW Diesel=0kW**	**100**	**0**	**98**	**0**	**10**	**83**	**94**	**4999**

From table 4-5, it can be seen that, by increasing the RE penetration, the battery's energy capacity is increased, which means that a larger battery was preferred to capture

the excess RE production. In case 2 and case 3, wind and tidal turbines and solar PV showed up, and their capacities are equal to the upper limit. However, in case 5 – case 8, because the upper limit of the wind turbine is large enough, it was preferred as the main and cheapest energy source, and then a small but expensive tidal turbine appears to satisfy the load demand. The tidal turbine was preferred to solar PV due to the availability of tidal power compared with solar radiation. It seems that wind and tidal technologies are more preferable in the optimization process to solar PV because they are available most of the times over the year. In case 4 – case 9, by increasing the RE penetration, a larger regenerator was picked to get more charge from RE excess production. However, in case 2 and case 3, the RE penetration rate is less than case 4, the regenerator is larger than in case 4. It's related to the characteristics of the load profile of Blind Channel. Most of the time, the load is less than the diesel generator minimum load, so at lower penetrations like case 2 and case 3, the diesel generator has to run at least at minimum load, and excess generation (dump load) is used to charge the battery.

In the case of HRES (case 2 – case 8), a significantly large diesel generator shows up in the microgrid structure as a spinning reserve source. Particularly in cases 6 – case 8, although RE sources (wind, tidal, solar) have high upper limits in their search domain, but optimizer prefers to have a larger wind turbine with a small tidal turbine and large diesel generator because using the diesel generator for satisfying the load demand at critical time steps is cheaper than having larger RE sources in the system. Since NPC of the system is the objective function of upper level optimizer always picks the cheapest configuration. However, the diesel generator was eliminated in the 100% RE penetration scenario. A large wind turbine with 94 kW capacity and a large ZAFB with 4999 kWh energy capacity, and a small tidal turbine (10kW) were included. In this case, the wind turbine is responsible for satisfying most of the load, and a small tidal turbine helps to improve the reliability of RE in this microgrid. Large ZAFB are responsible for capturing the excess production of the wind turbine to charge and discharge it at critical time steps. For this reason, the power capacity of the regenerator increased significantly from 24 kW in case 8 (hybrid system) to 83 kW in case 9 (100% RE). Figure 4.2 shows the NPC of the system and LCOE in the Blind channel at different RE penetration scenarios. This

figure shows that NPC and LCOE are reduced by RE penetration increment, and the lowest NPC and LCOE occur in the hybrid case at 83.7 % penetration. However, NPC and LCOE are increased at 100% RE penetration due to the requirement of larger wind turbine and ZAFB. NPC value of each scenario was calculated by microgrid design (size of components) found by the optimization process. NPC of diesel generator includes the CAPEX, O&M, replacement, fuel, and carbon tax cost. NPC of solar PV, wind, and tidal turbines include the CAPEX and O&M cost. NPC of ZAFB includes the CAPEX, O&M, and replacement costs. The cost breakdown of each RE penetration scenario is available in Appendix A.

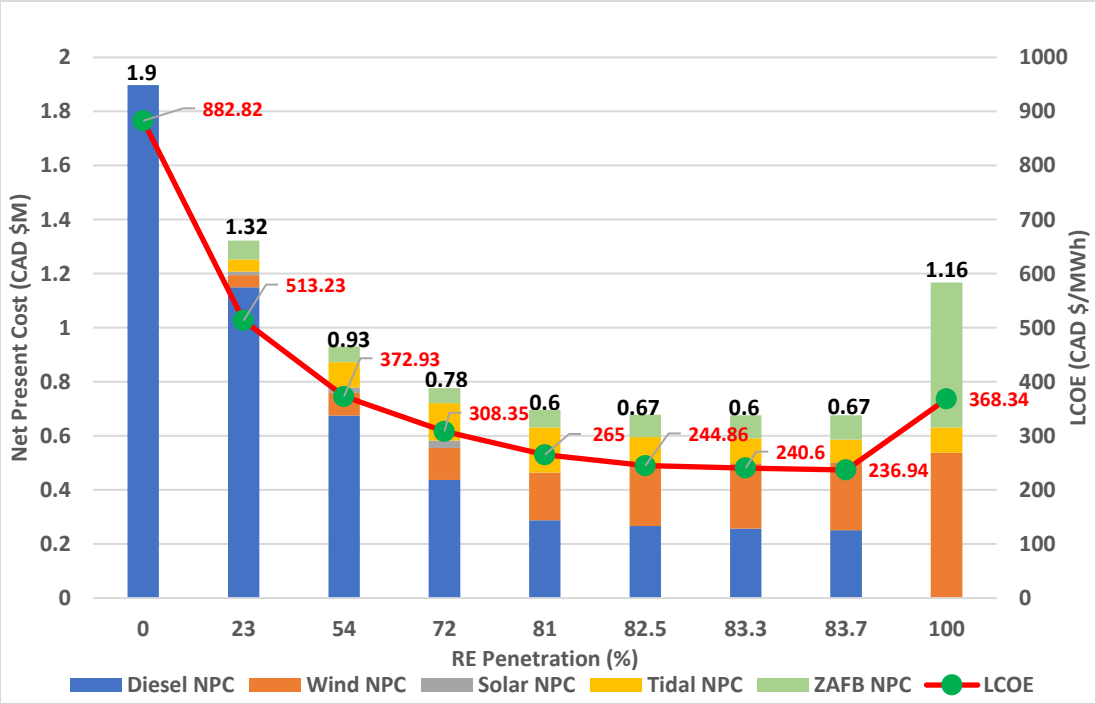

Figure 4.2 NPC & LCOE of Blind Channel

As shown in figure 4.3, to eliminate the diesel generator, a longer duration ZAFB is needed, and it must be able to provide 53.2 hours discharge at maximum power. But in HRES cases, ZAFB can have a shorter duration. For example, in hybrid case 8 (83.7 % RE penetration rate), the storage tank must have a capacity for 22.5 hours discharge. Also, larger energy storage is needed when increasing the RE penetration. Figure 4.4 shows the ratio of ZAFB discharge and annual energy demand. By raising the RE

penetration, ZAFB satisfies a larger portion of energy demand. As mentioned earlier, the battery size of case 2 (23% RE penetration) is larger than the energy capacity of case 3-case 5. For this reason, this ratio in case 2 is greater than case 3-case 5. A considerable portion of demand (23.3%) is satisfied by ZAFB in the 100% RE penetration scenario, and 76.7% of demand is met by the wind and tidal power when they are available, and their excess production is used to charge the battery. So it's clear that ZAFB has a significant role in achieving 100% RE and eliminating diesel from Blind Channel. In this case (100% scenario), the round trip efficiency of ZAFB is around 49%. Overpotentials of the regenerator and generator (battery) lead to low roundtrip efficiency, which is the biggest issue with this battery.

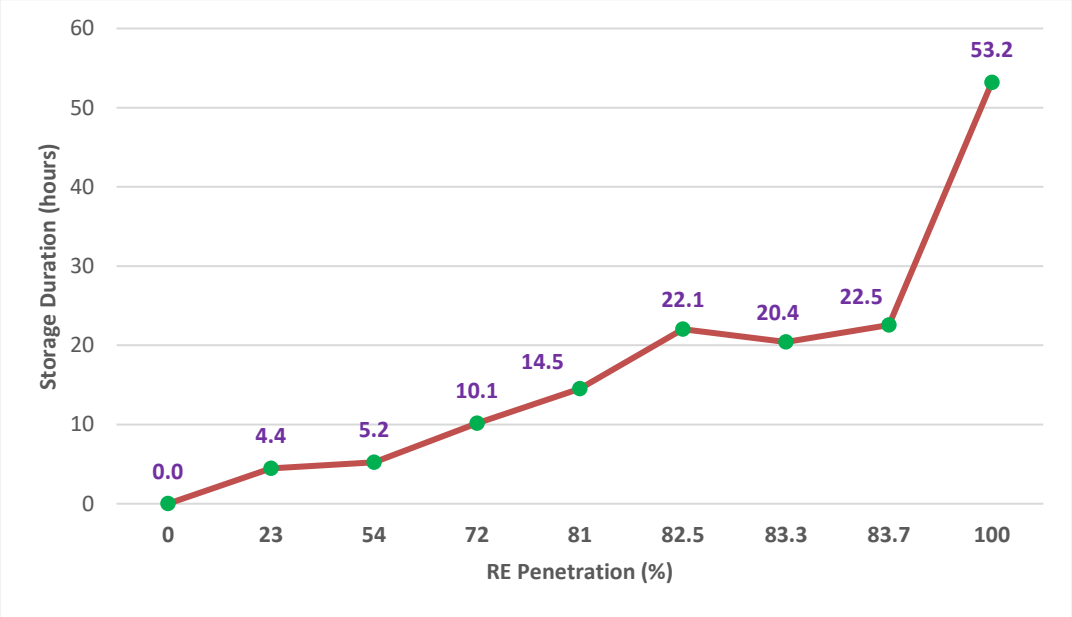

Figure 4.3 Storage duration of ZAFB at peak load hours at different scenarios in Blind Channel

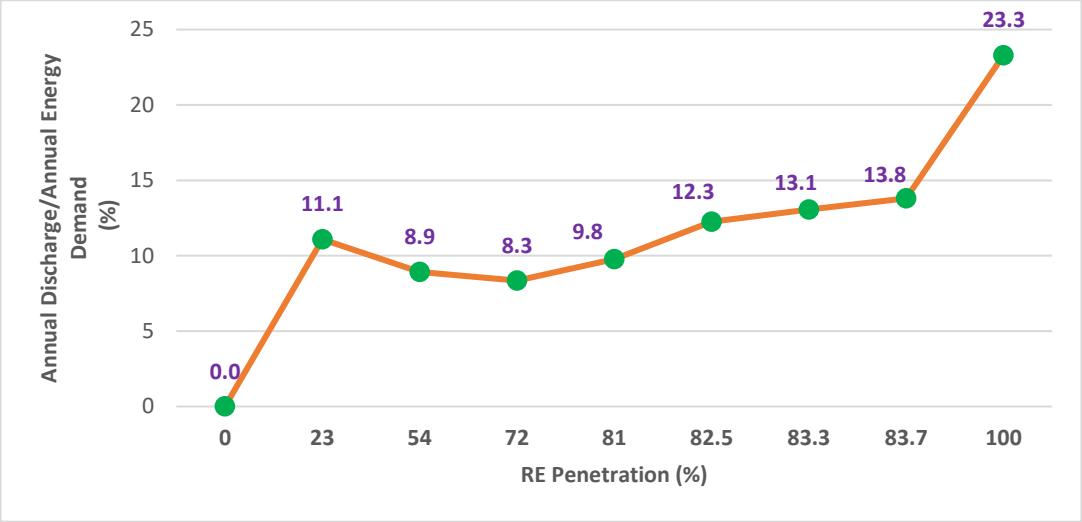

Figure 4.4 ZAFB contribution to total annual energy demand for Blind Channel

Annual fuel consumption and CO_2 emission of the Blind Channel microgrid are shown in Figures 4.5 and 4.6. It can be seen that zero-emission and zero fuel consumption are possible in this off-grid area by a microgrid in which wind energy is the main energy source, and a small tidal turbine and a large ZAFB compensate for the intermittency of wind energy. Due to the necessity of running the diesel generator as a reserve source in HRES at critical time steps, there are some fuel consumption and emission. They are reduced by penetrating more RE in the structure of the microgrid. Their lowest values appear in the hybrid system at 83.7 % RE penetration scenario. There is an 87.6 % reduction in fuel consumption and CO_2 emission in this scenario compared with the base case in which only a diesel generator operates to satisfy the demand.

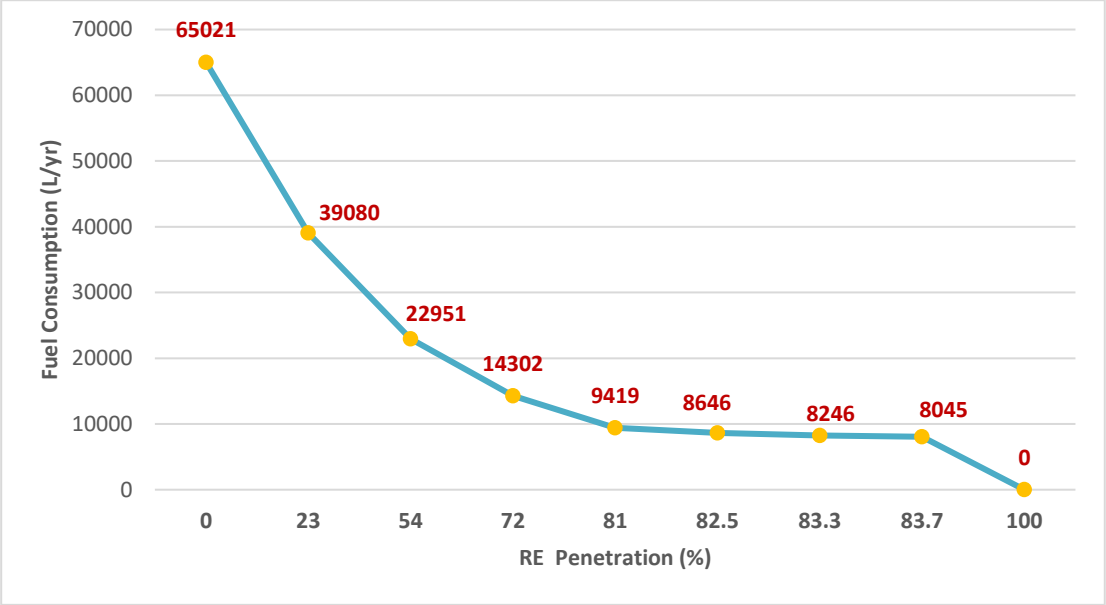

Figure 4.5 Fuel consumption for different RE penetration scenarios in Blind Channel

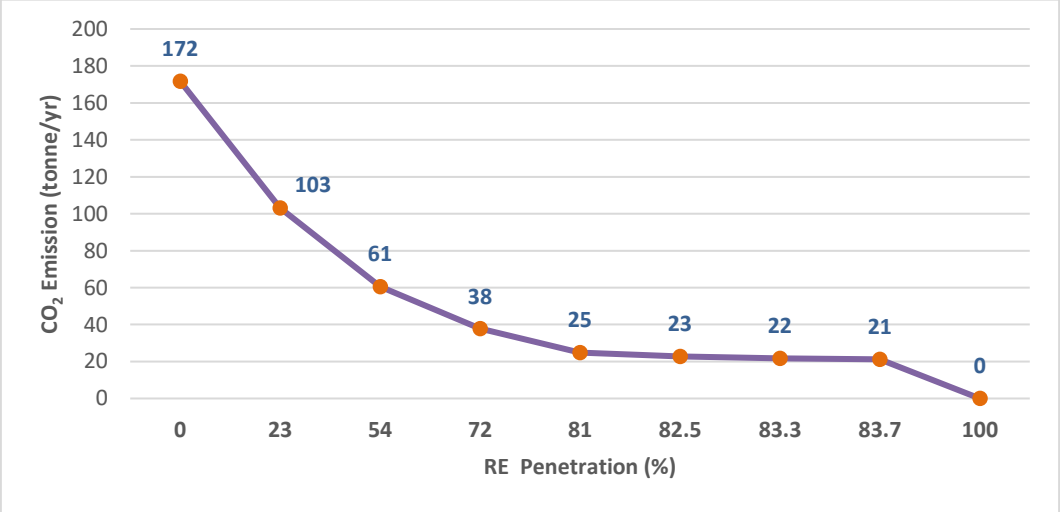

Figure 4.6 CO_2 emission for different RE penetration scenarios in Blind Channel

As discussed earlier, a large diesel generator shows up as a reserve spinning source in the microgrid configuration in Blind Channel in hybrid systems (case 2- case 8); even in a higher RE penetration rate like case 8 (83.7 % penetration), a large one was picked by the optimizer. Figure 4.7 shows the diesel output over a year. It can be seen that diesel generator runs at some peak loads when RE sources are not available, and load demands are met by RE and ZAFB most of the times. Figure 4.8 shows the critical point at which

such a large diesel generator is needed. As shown in figures 4.8 and 4.9, since there are insufficient RE resources and ZAFB doesn't have enough charge to cover the load, the diesel generator has to operate and satisfy the load demand. Maximum output occurs at this point which determines the capacity of the diesel generator. The reason for preferring to run the diesel generator at some critical peak loads instead of using larger RE and ZAFB by the optimizer is that it's the cheapest way to have a minimum NPC.

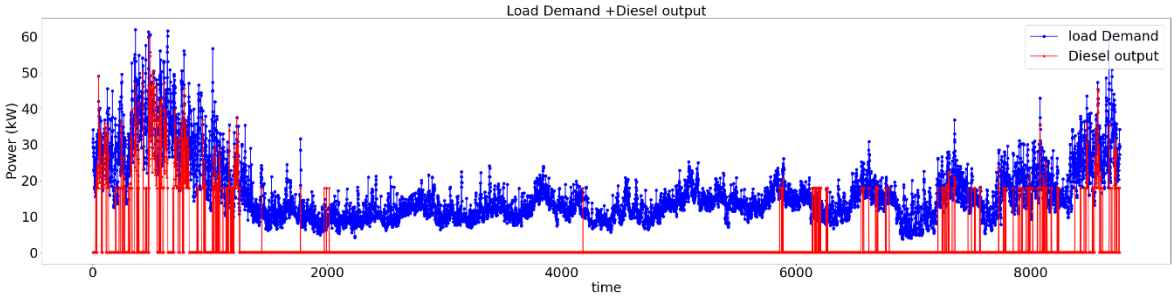

Figure 4.7 Load demand and diesel generator output over a year in Blind Channel (case 8)

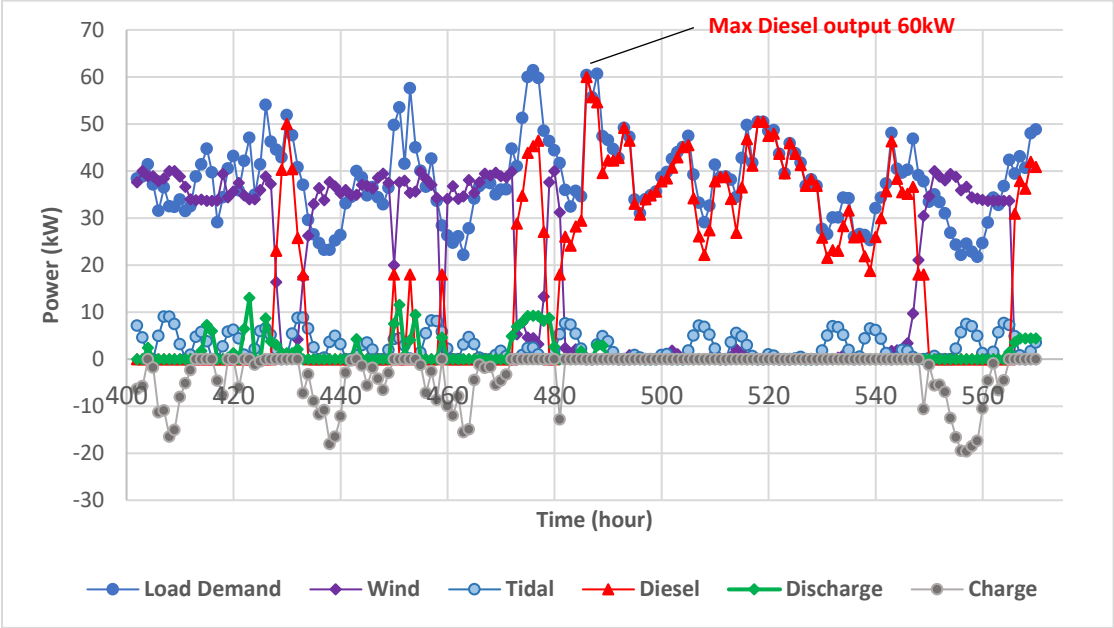

Figure 4.8 Critical point of diesel generator output (case 8)

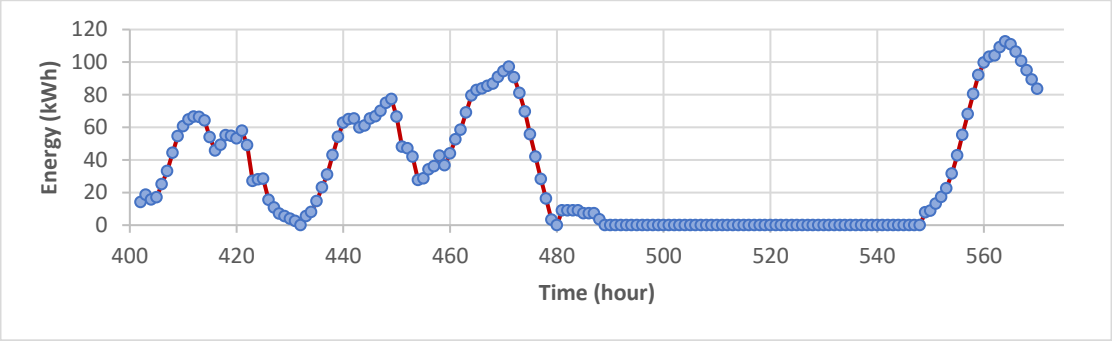

Figure 4.9 SoC of ZAFB at the critical point (case 8)

To demonstrate the operation control of a microgrid by optimal control model and using MPC method (inner level) in different seasons with different load demand profiles and RE resources, the first weeks of February and August were selected as the representatives of winter and summer, respectively. As shown in figure 4.10, RE sources are not enough to cover the demand at several time steps in winter (Feb 1^{st}-7^{th}), and ZAFB doesn't have enough charge to compensate for the lack of RE sources, so diesel generator has to run at these points to meet the rest of unmet load demand. However, when wind and tidal turbines have excess production and ZAFB has enough room for charging, the control model decides to get this excess production to charge the battery for future discharge at the next horizons. In summer (August 1^{st} – 7^{th}), as shown in figure 4-11, the load is lower than winter, and wind and tidal turbines have excess production, but ZAFB is already full of charge and can take no more charge. Hence, the control model has to consider this excess production as RE curtailment. So, it's not necessary to run the diesel generator. This figure clearly shows how energy management is done by the optimal control model by choosing the optimum operation of components to minimize the diesel generator output.

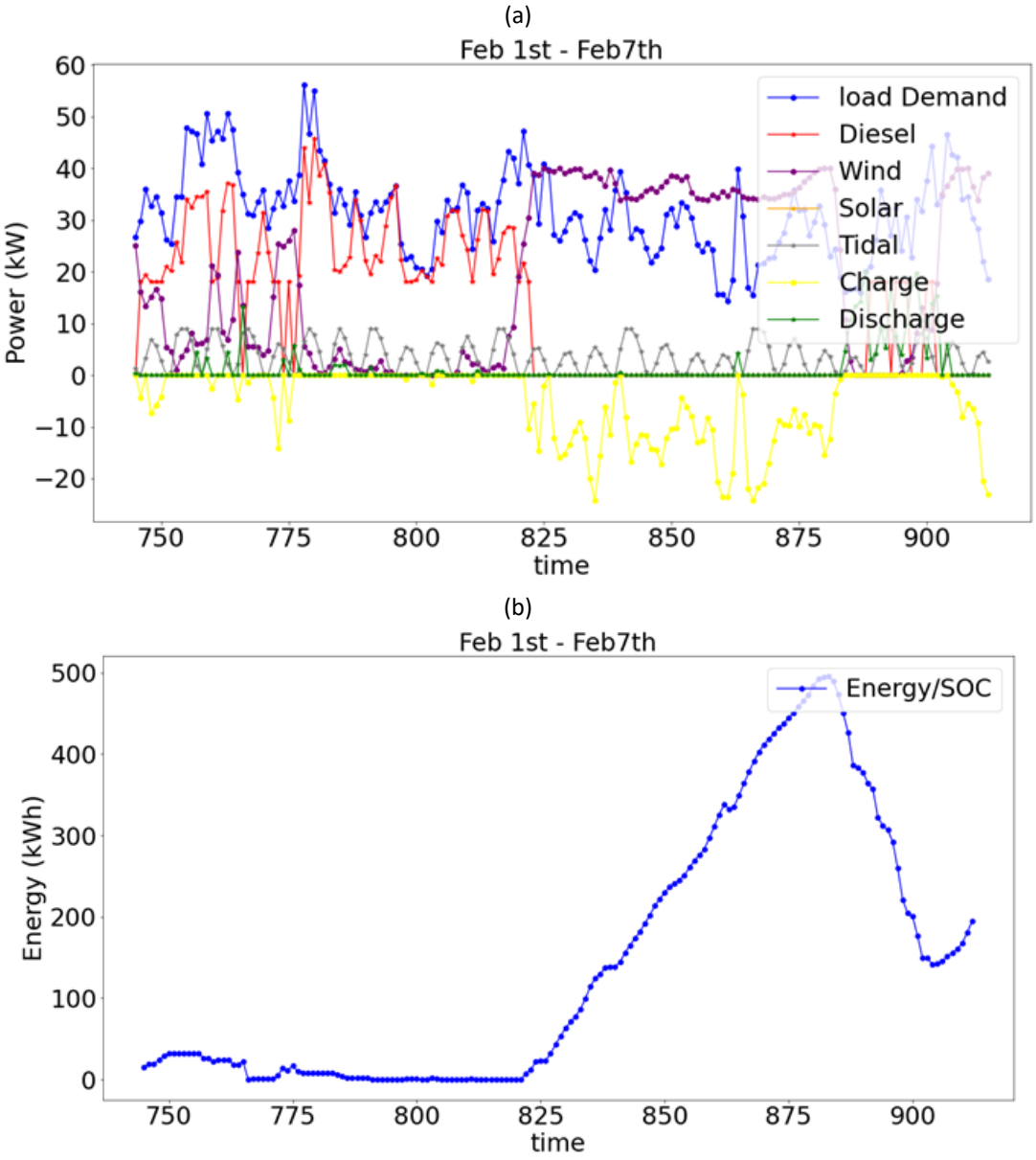

Figure 4.10 Energy management by the control model in winter in Blind Channel (a) components output (b) ZAFB SoC (Case 8)

(a)

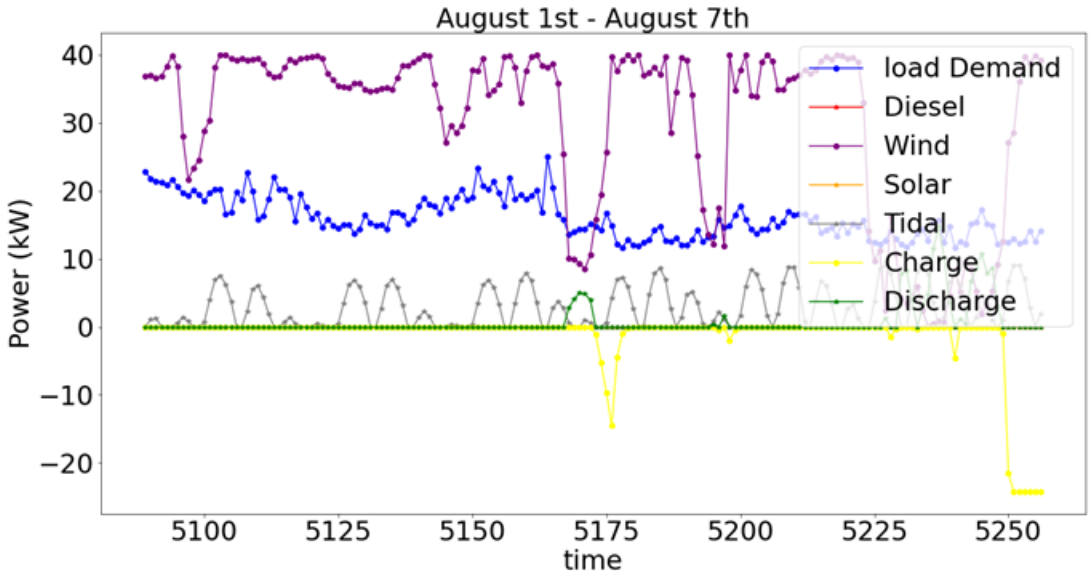

(b)

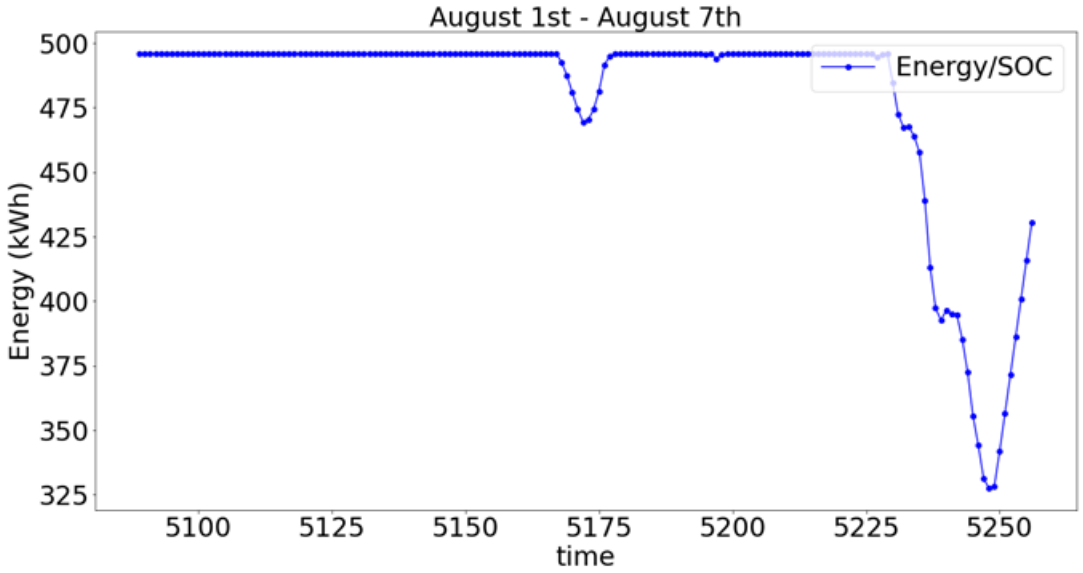

Figure 4.11 Energy management by the control model in summer in Blind Channel (a) components output (b) ZAFB SoC (Case 8)

4.2.3. Case Study II: Hot Springs Cove

Hot Springs Cove, also known as Refuge Cove, is located in Maquinna Provincial Marine Park at the remote northern end of Clayoquot Sound, north of Tofino on the west coast of Vancouver Island. This place has a population of 44. The peak load demand of

this area is 195 kW, and its annual energy demand is 873.44 MWh. Figure 4.12 shows the monthly minimum, maximum, median, and mean load demand.

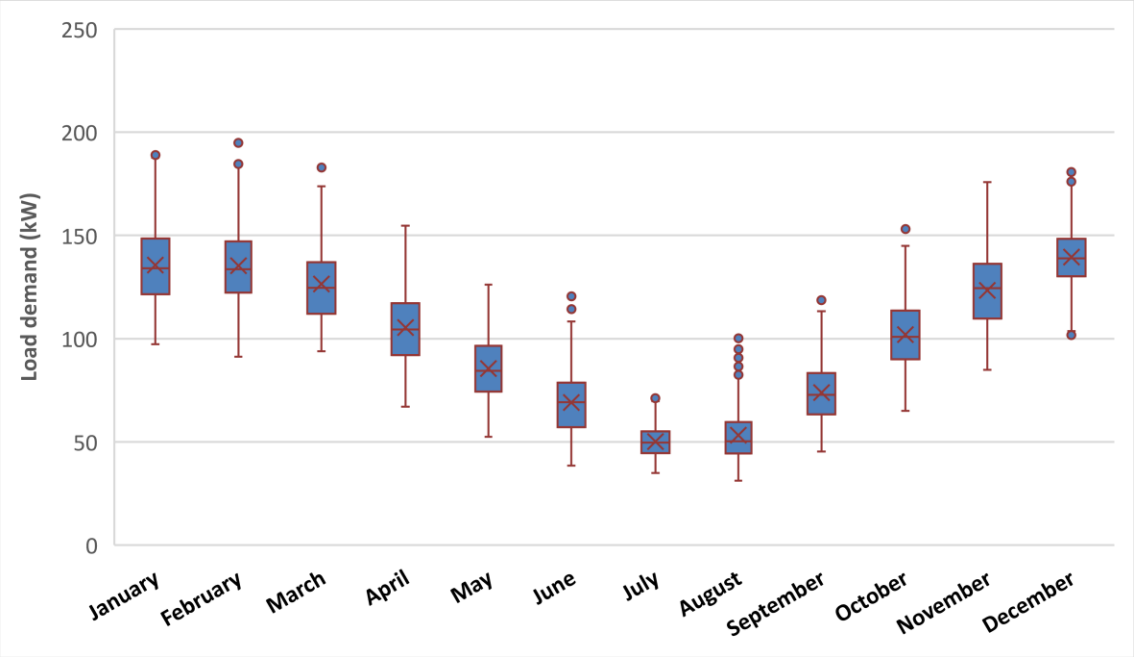

Figure 4.12 Hot Springs Cove monthly load demand (mean, median, 1st and 3rd quartiles, outliers, and minimum and maximum values)

In this case study, seven RE penetration scenarios were evaluated using this microgrid modeling tool. The first scenario is the base case in which a diesel generator of 195 kW power capacity is used to meet the load demand. Scenarios 2 – 6 were defined by setting the upper bound of each RE plant (wind, tidal turbines, and solar PV) in their search domain to 20%, 40%, 60%, 80%, and 100% of peak load. Table 4-6 shows the configuration of microgrids in these scenarios. It can be seen that in cases 2 to 4, where the RE limits are not large enough, all RE sources hit the upper bound for their capacity. Maximum allowable capacity was picked for the wind turbine and solar PV, but a smaller tidal turbine was showed up in the microgrid for cases 5 and 6. By increasing the wind turbine and solar PV capacity in case 6, tidal turbine capacity is reduced from 108 kW to 78 kW. Also, a large diesel generator shows up in the microgrid structure in the hybrid cases, which will be discussed later. In general, cheaper renewable technologies like wind turbine and solar PV are preferred to more expensive ones like the tidal turbine in hybrid systems because the diesel generator and ZAFB compensate for the lack of wind and

solar resources at critical points. However, priorities are totally different for 100% penetration. Because a reserve energy source is not available in this scenario, the RE sources that have enough production and are available most of the time should be selected. For this reason, expensive tidal technology is preferred to cheap solar PV technology because of the availability of tidal power compared with solar power. Wind energy is typically the primary source. By penetrating more RE in the microgrid structure, larger batteries are needed to get the RE excess production and improve the system reliability. So, a larger tank is needed as the energy storage for capturing more charge, and longer duration discharge and a larger regenerator is necessary to get more charge from the RE sources, and a larger generator (power unit) is needed to provide more discharge power at those critical points to minimize the diesel output power. Eliminating the diesel in Hot Spring Cove is possible by having a 100 % RE microgrid of 200 kW wind turbine, 200 kW tidal turbine, and a large ZAFB with 9764 kWh energy capacity.

Figure 4.13 shows the NPC and LCOE of different RE penetration scenarios in Hot Spring Cove. Given that a considerable portion of NPC belongs to diesel fuel consumption in the generator over the project lifetime along with the replacement cost and carbon tax, by increasing the RE penetration, most of the energy demand is satisfied by RE sources which leads to a significant reduction in fuel consumption, NPC and the cost of energy. The lowest NPC and LCOE appear in HRES at 90% RE penetration rate (case 6), and there are 57.6 % and 67.7% reduction in NPC and LCOE compared with the base case in which only diesel generator runs to meet the load demands. As mentioned earlier and shown in figure 4.13, solar PV shows up in the hybrid system (RE penetration< 100 %) and has the lowest NPC among the other technologies. In the 100% RE penetration scenario, NPC and LCOE are increased compared with case 6 (90% penetration) due to applying a larger tidal turbine and larger energy capacity and power units of ZAFB. Nevertheless, NPC and LCOE are reduced by 46% and 60% compared with the base case. As mentioned earlier, NPC values at different RE penetration rates were determined by the optimum size of components. The cost breakdown of the Hot springs Cove microgrid for each scenario is available in Appendix A.

Table 4-6 Size of components of Hot Springs Cove microgrid in different RE penetration scenarios

	Components limit	RE penetration (%)	Diesel (kW)	Wind (kW)	Solar (kW)	Tidal (kW)	ZAFB Charge power (kW)	ZAFB Discharge power (kW)	Tank Capacity (kWh)
Case 1	**Wind=0kW Solar=0kW Tidal=0kW Diesel=200kW**	-	**195**	-	-	-	-	-	-
Case 2	**Wind=40kW Solar=40kW Tidal=40kW Diesel=200kW**	**35.44**	**175**	**40**	**40**	**40**	**41**	**39**	**213**
Case 3	**Wind=80kW Solar=80kW Tidal=80kW Diesel=200kW**	**65.19**	**174**	**80**	**80**	**80**	**58**	**63**	**479**
Case 4	**Wind=120kW Solar=120kW Tidal=120kW Diesel=200kW**	**83.85**	**174**	**120**	**118**	**120**	**99**	**96**	**929**
Case 5	**Wind=160kW Solar=160kW Tidal=160kW Diesel=200kW**	**88.45**	**174**	**160**	**147**	**108**	**116**	**124**	**1643**
Case 6	**Wind=200kW Solar=200kW Tidal=200kW Diesel=200kW**	**89.64**	**174**	**200**	**199**	**78**	**140**	**142**	**2249**
Case 7	**Wind=400kW Solar=400kW Tidal=400kW Diesel=1kW**	**100**	**0**	**200**	**0**	**200**	**164**	**354**	**9764**

Storage duration of ZAFB for different RE penetration scenarios in Hot Springs Cove is shown in figure 4.14. Storage duration increased by penetrating more RE in the system, which means that the battery can get more charge from excess production of RE sources and provide more discharge to the grid, so energy storage must provide a longer duration of discharge. For a 100% RE penetration scenario (case 7) in Hot Spring Cove, ZAFB must have 50 hours storage duration and provide longer duration discharge at maximum power to cover the demands at critical time steps in which there are insufficient RE resources. But for the hybrid systems, for instance, in case 6 (90% penetration), ZAFB can have a smaller energy storage tank and provide a shorter discharge duration of 16 hours.

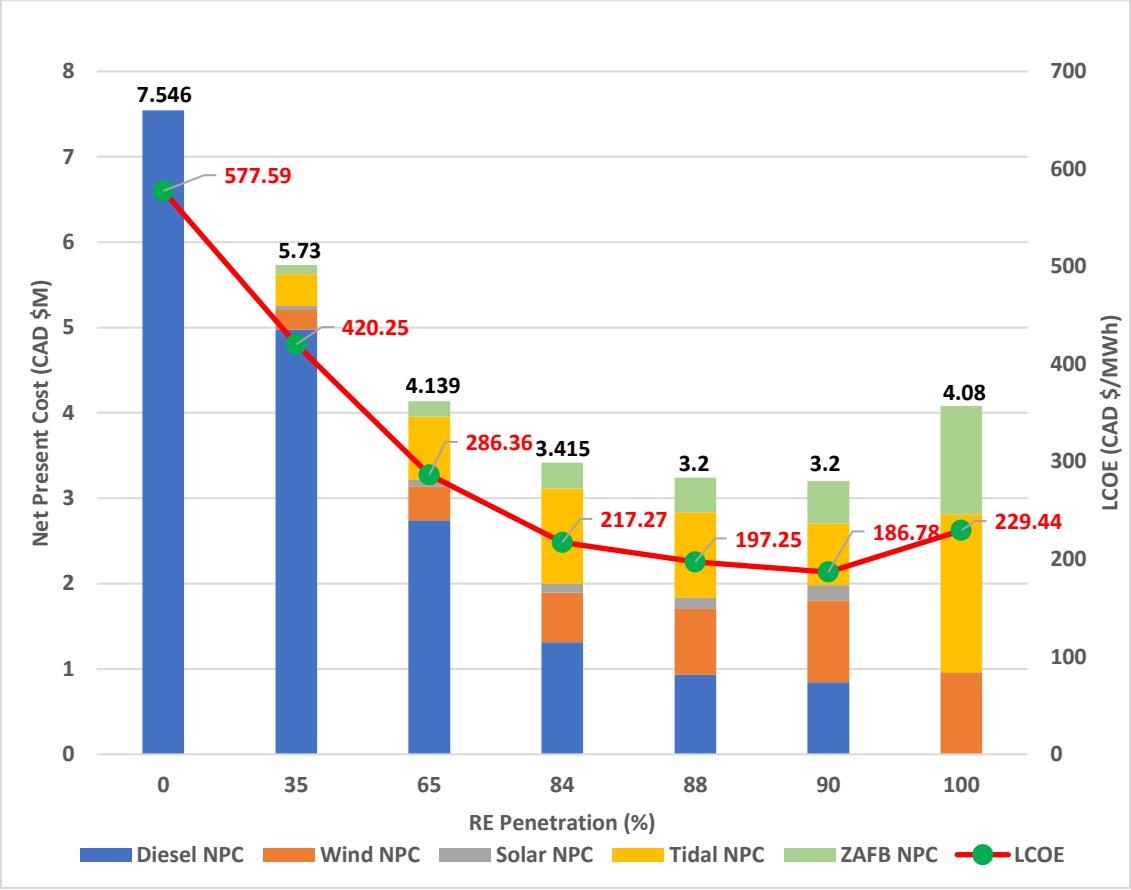

Figure 4.13 NPC (CAPEX+OPEX+Replacement+Fuel+Carbon tax costs) & LCOE of Hot Springs Cove

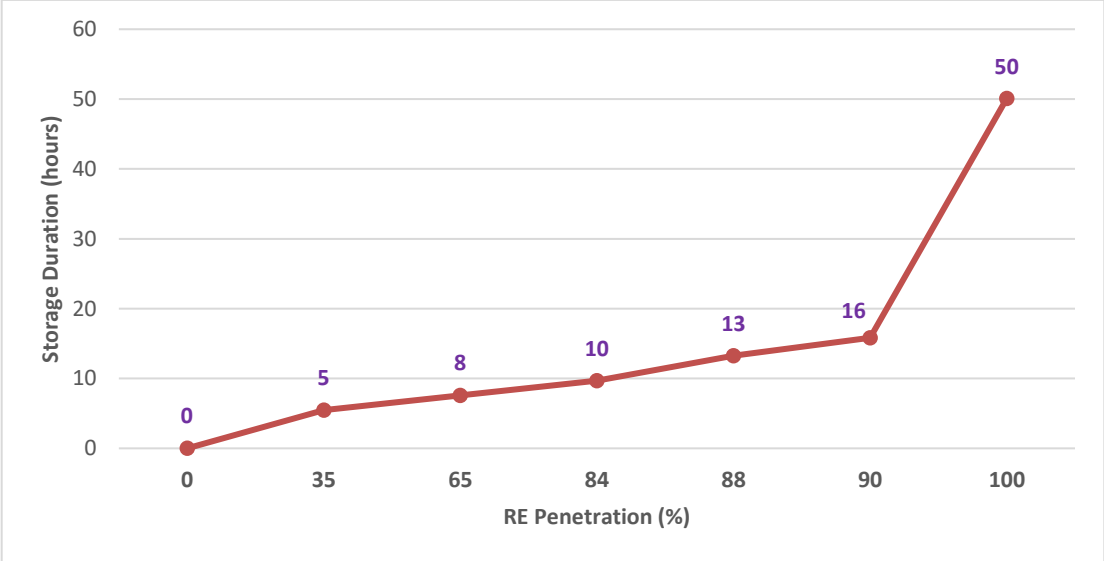

Figure 4.14 Storage duration of ZAFB at different scenarios in Hot Springs Cove

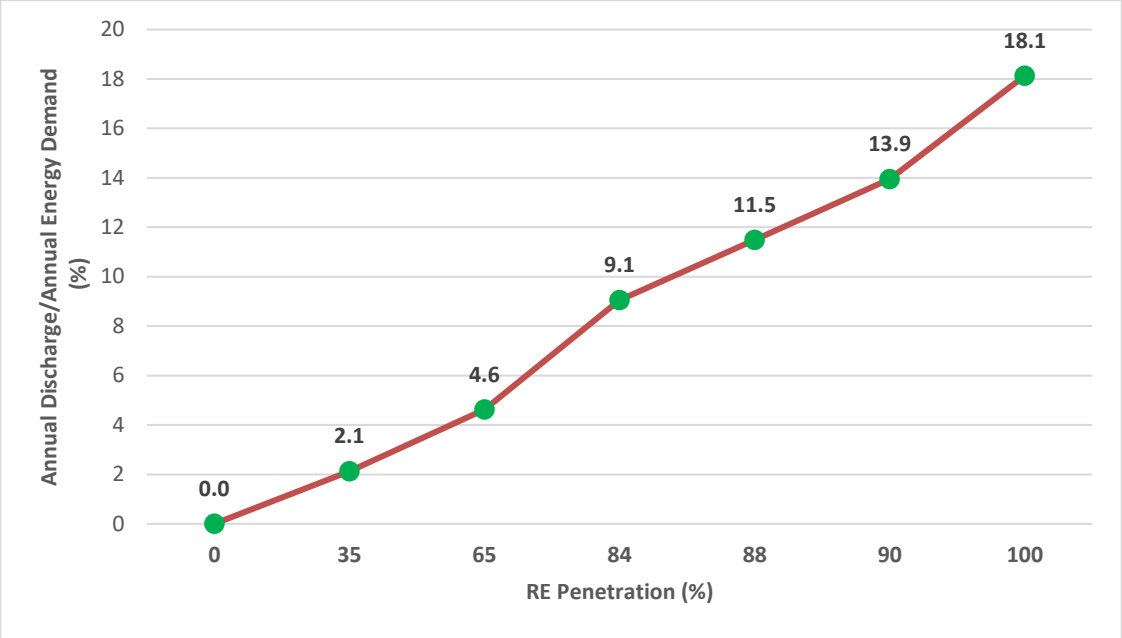

Figure 4.15 ZAFB contribution in total annual energy demand of Hot Spring Cove

The battery has a significant role in 100% RE microgrids by buffering the intermittency of the RE sources, covering the energy demand at critical points, and improving the microgrid's reliability. As shown in Figure 4.13, 18.1% of the total energy demand in Hot Spring Cove is satisfied by ZAFB in the 100% RE penetration scenario (case 8), which means that the rest of it (81.9 %) is met by wind and tidal turbines and their excess production is used to charge the battery. But in hybrid cases, due to the availability of reserve sources, a smaller portion of annual energy demand can be met by ZAFB. In the 100% RE scenario, the round-trip efficiency of ZAFB is around 50%, which means that lots of input energy are wasted due to overpotentials inside the regenerator and power unit (battery).

Diesel fuel consumption and CO_2 emission in Hot Springs Cove are reduced by penetrating more RE in the microgrid. It can be seen in figures 4.16 and 4.17 that zero fuel consumption and emission are achieved in the 100% RE penetration scenario (case 7) by applying wind and tidal turbines and large ZAFB. Case 6 (90% RE penetration) has the lowest consumption and emission among the hybrid cases (case 2-case 6). Annual

diesel fuel consumption and CO_2 emissions are reduced by 89% in case 6 (27613 L/yr, 72.9 tonnes CO_2/yr) compared with the base case (261726 L/yr, 691 tonnes CO_2/yr).

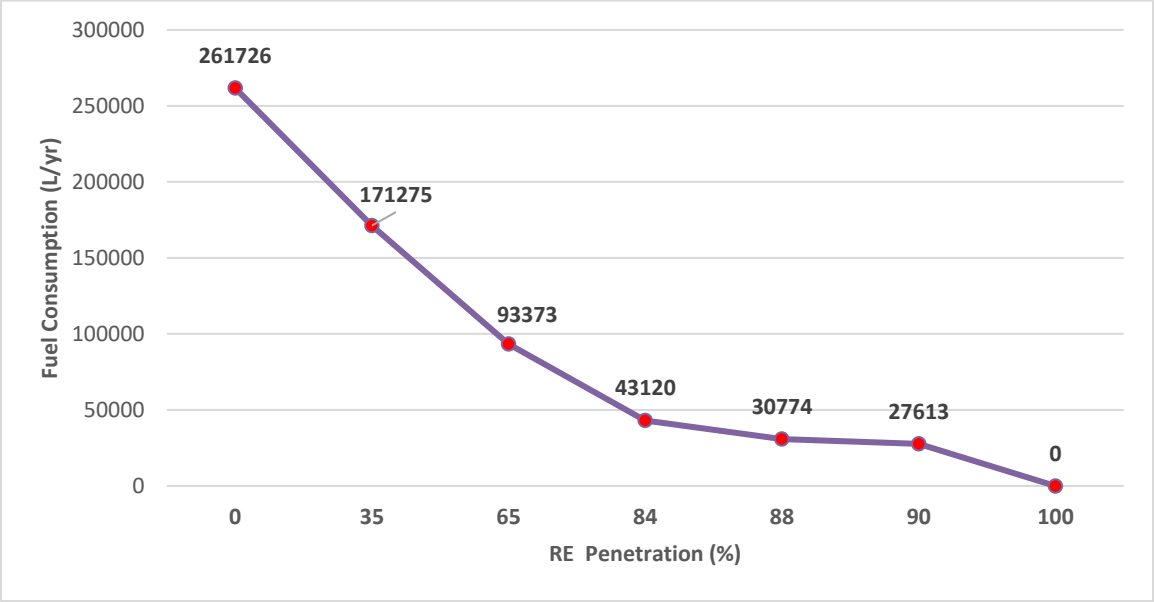

Figure 4.16 Annual Fuel consumption for different RE penetration scenarios in Hot Springs Cove

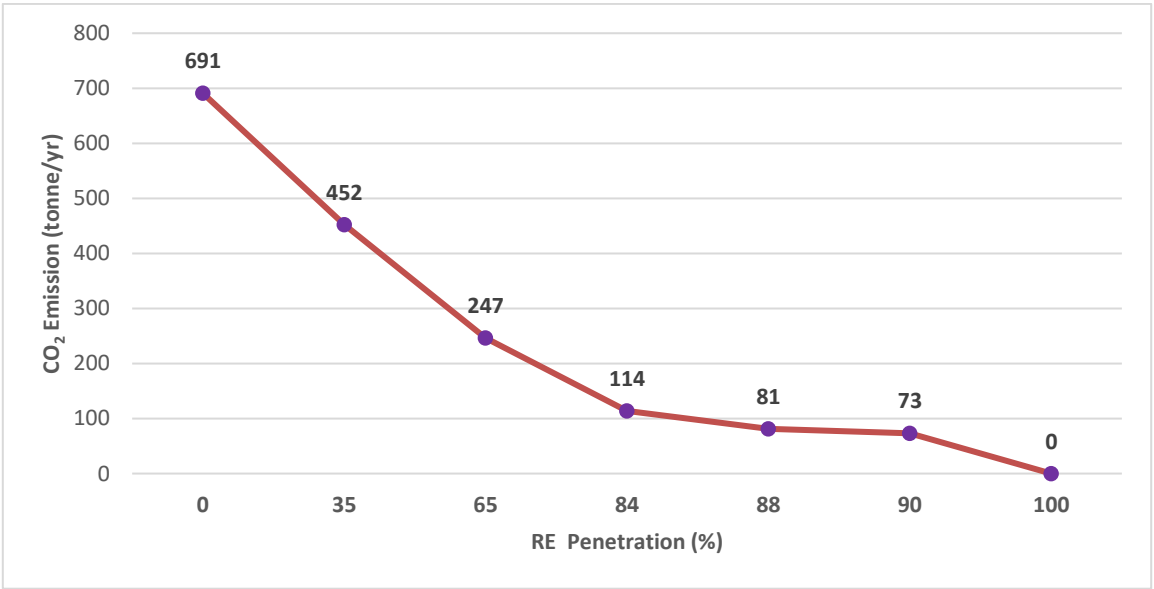

Figure 4.17 Annual CO_2 emission for different RE penetration scenarios in Hot Springs Cove

As shown in table 4-6, a large diesel generator shows up as a reserve source in all hybrid system scenarios (case 2-case 6). Figure 4.18 shows the diesel generator output

over a year. It can be seen that it runs at some peak loads during the winter to compensate for the lack of RE sources. Figures 4.19 and 4.20 can justify why such a large generator is required for Hot Spring Cove. The critical point of case 6 with 90% RE penetration, which determines the rated capacity of the diesel generator, is shown in figure 4.19. There are no RE resources at time step 287 hours, and SoC of ZAFB is zero, so load demand of 174kW must be satisfied by another energy source because of a strict constraint of zero unmet load demand. The diesel generator has to run at critical time steps to meet the whole demand or the rest of the unmet load demand. The maximum output power occurs at this point which determines the rated capacity of 174 kW. Running the diesel generator as a reserve source to meet the peak loads when RE are unavailable or insufficient and ZAFB doesn't have enough charge is the optimum way to have the minimum NPC instead of having larger RE sources and ZAFB.

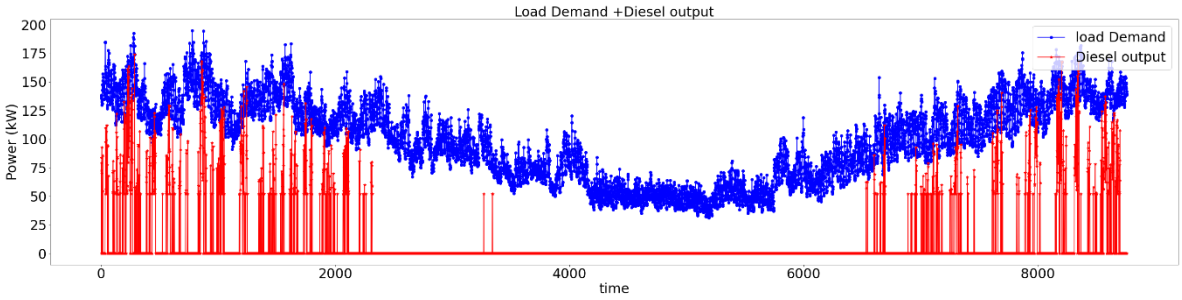

Figure 4.18 Load demand and diesel generator output over a year in Hot Springs Cove (case 6)

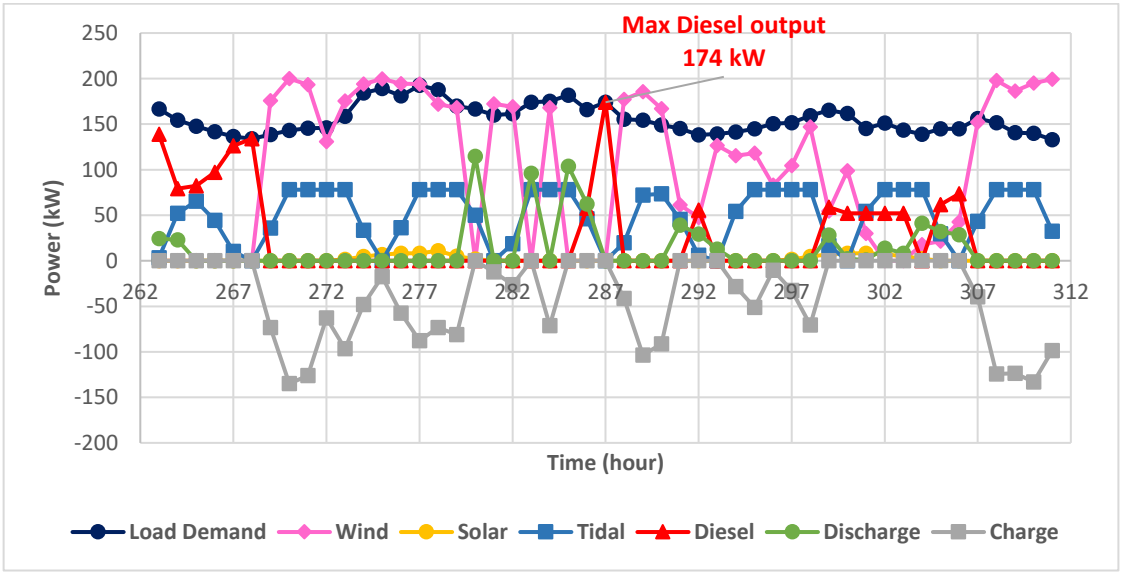

Figure 4.19 Critical point of diesel generator output (case 6)

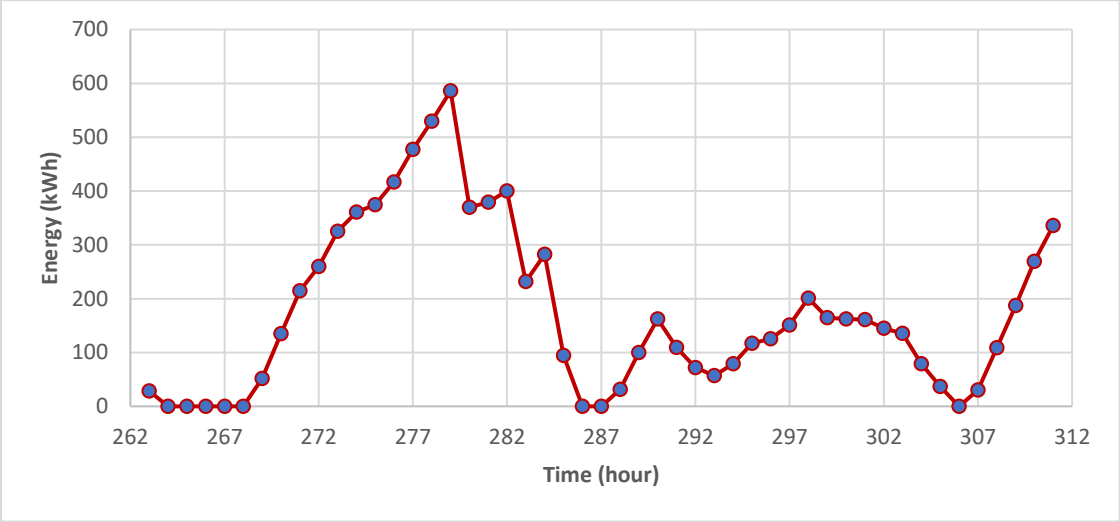

Figure 4.20 SoC of ZAFB at the critical point (case 6)

The performance of the microgrid control model in winter and summer in Hot Spring Cove is shown in figures 4.21 and 4.22 for case 6 with a 90% RE penetration rate. It can be seen that load demands in the first week of February are much higher than in the first week of August. In Feb 1st-7th, the optimal control model decides to charge the battery when there is excess RE production using the receding horizon control method and based on the information of load demand, RE resources, and SoC of the battery. On the other hand, it decides to operate the diesel generator when there are no RE and ZAFB doesn't have enough charge. Also, ZAFB delivers discharge to the grid at several time steps to help to minimize the diesel output power. In August 1st – 7th, ZAFB plays an important role in the microgrid by discharging most of the time. It helps other energy sources to let the diesel generator not run during the whole week. All these control actions and energy management throughout the year are done by the optimal control model.

(a)

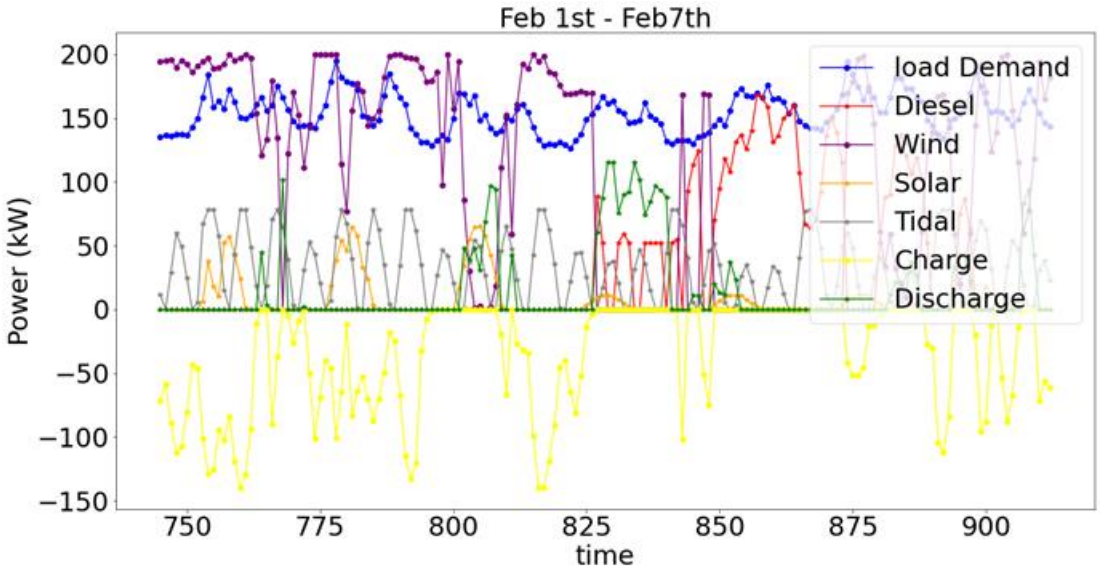

(b)

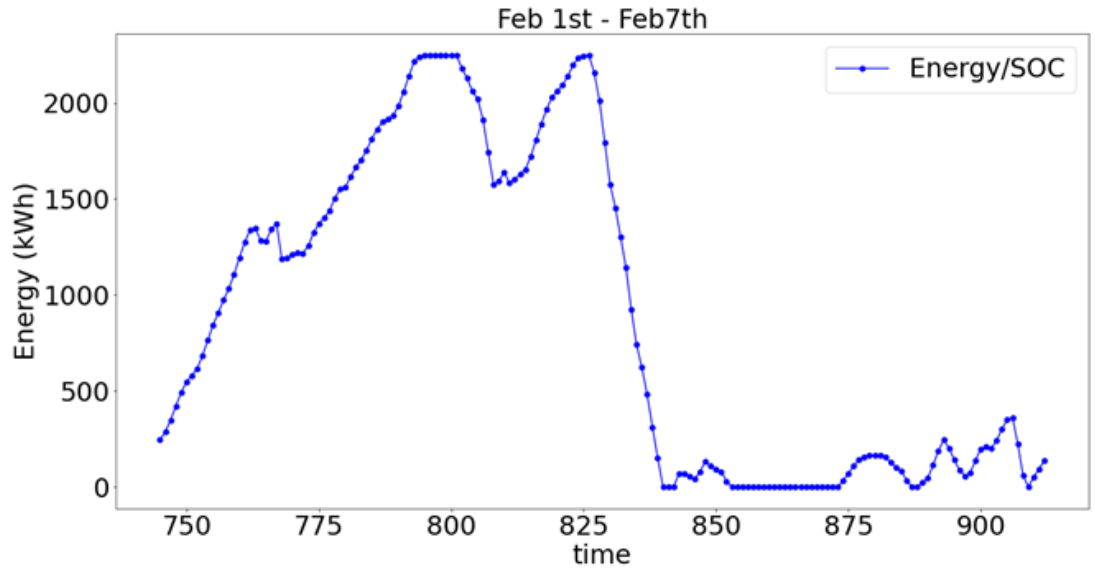

Figure 4.21 Energy management by the control model in winter in Hot Springs Cove (a) components output (b) ZAFB SoC (Case 6)

(a)

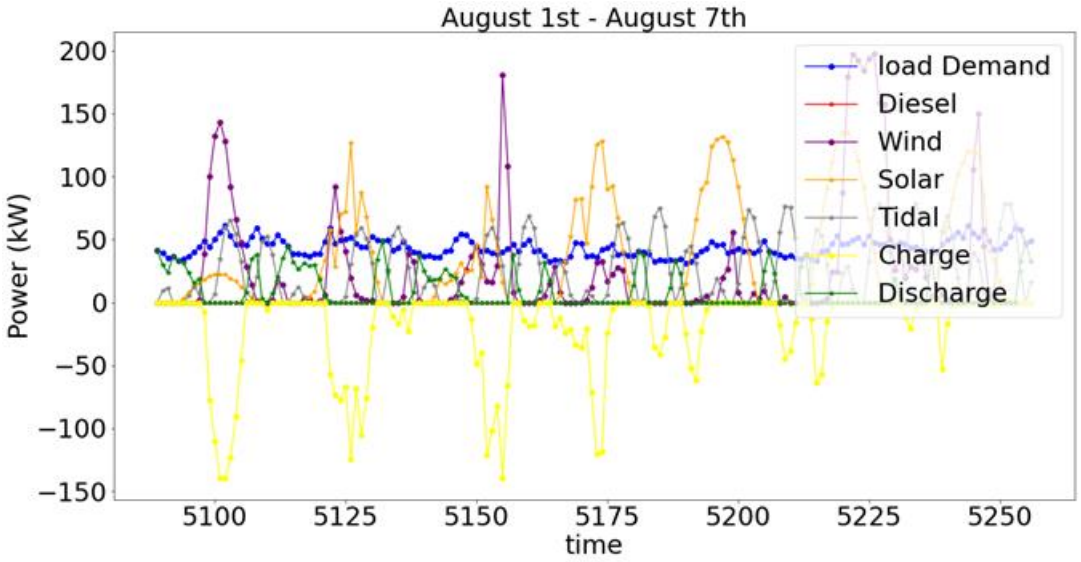

(b)

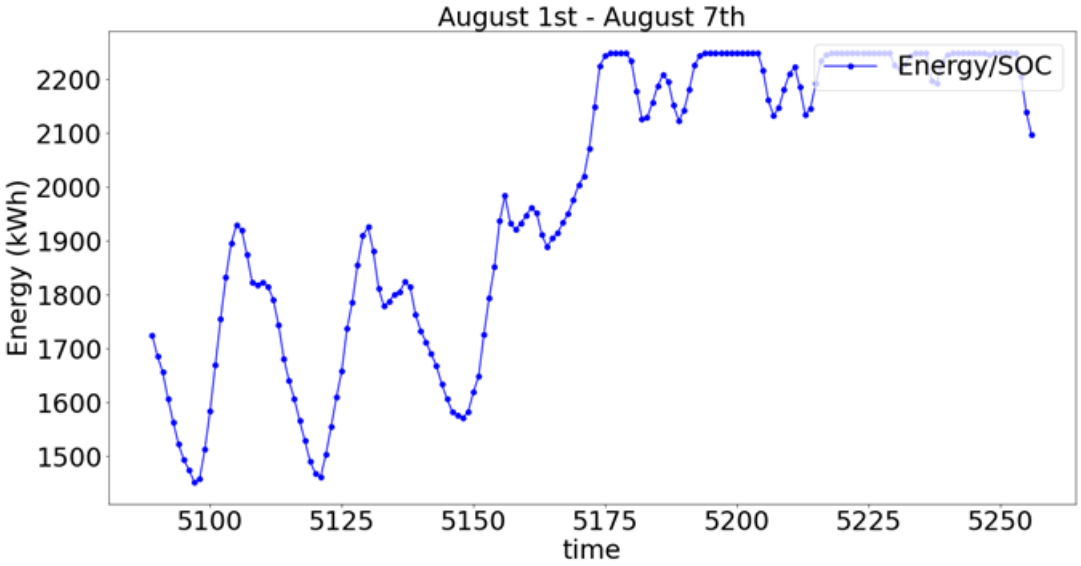

Figure 4.22 Energy management by the control model in summer in Hot Springs Cove (a) components output (b) ZAFB SoC (Case 6)

4.2.4. Case Study III: Moresby Island

Moresby Island is one of the large islands of the Haida Gwaii archipelago located south of Skidegate Inlet and Skidegate Channel that separates the two main islands of the Queen Charlotte Archipelago. It has a population of 1000 [79]. Peak load and annual

energy demand of Moresby Island are 5800 kW and 28.7 GWh. The monthly load demand of this area is shown in Figure 4.23.

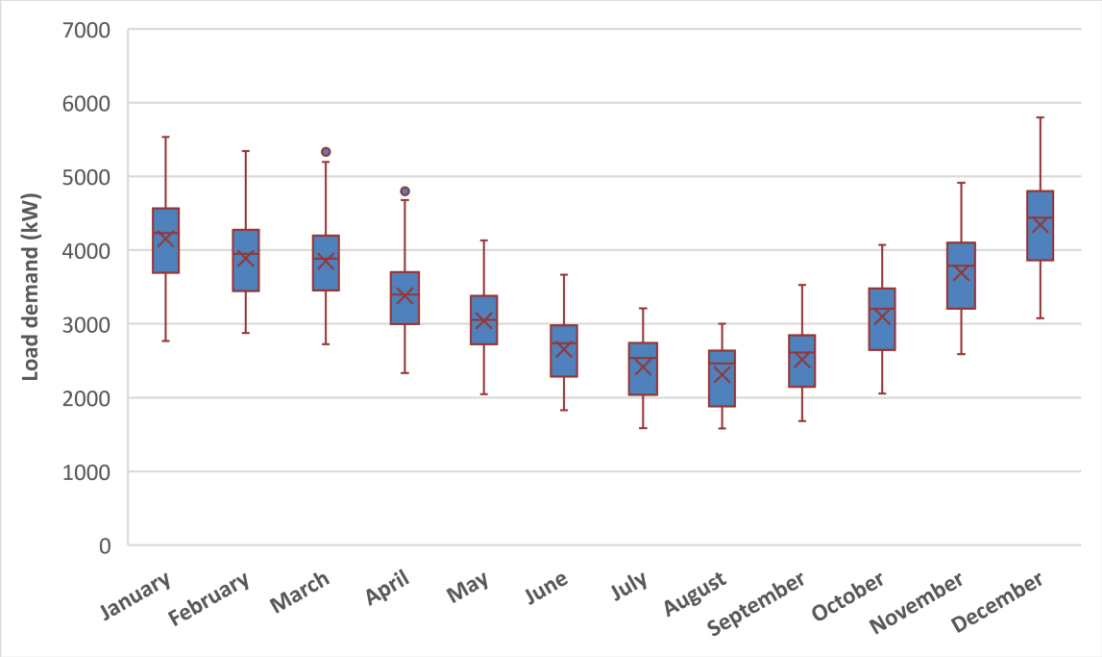

Figure 4.23 Moresby Island monthly load demand (mean, median, 1st and 3rd quartiles, outliers, and minimum and maximum values)

Moresby Island is the largest of all three case studies. Different RE penetration scenarios were evaluated in this case study using the microgrid modeling tool. Case 1 is the base case in which a diesel generator of 5800 kW rated capacity is the main source of energy generation. Other scenarios of HRES were defined in cases 2 - 6 by limiting the upper bound of each RE sources search domain in optimal design model: 10%, 20%, 40%, 80%, 100% of peak load, and case 7 is the 100% RE penetration scenario. Table 4-7 shows the microgrid design of Moresby Island in these scenarios. First of all, it can be seen that by raising the RE penetration in the system, ZAFB will have a larger energy storage for delivering discharge to the grid for a longer duration and a larger regenerator to get the maximum charge power from available RE excess production and a larger power unit to provide more discharge power at critical time steps. In cases 2 – 4, the optimizer picked the upper limits for wind and tidal turbine and solar PV because having the highest RE penetration is preferable in hybrid systems to minimize the diesel

operation time. But in case 5, by having a larger search domain, wind and solar energies were chosen as the main energy source because they are the cheapest technologies, and a smaller expensive tidal turbine of 1010 kW capacity was picked along with them. Also, the optimizer tripled the energy capacity and chose the larger regenerator and generator because there was enough excess RE production to charge the battery by having a larger wind turbine and solar PV in case 5. The capacity of wind turbine and solar PV were chosen close to their upper limit by the optimal design model, and a very small tidal turbine showed up in the system design in case 6. A larger storage tank (66693 kWh) and larger power units (2348 kW regenerator, 3022 generator) were selected in this case (83.98 % RE penetration) because of having more RE sources compared with case 5. In cases 2 – 6, a large diesel generator showed up as the reserve source in all hybrid system scenarios, which will be discussed later. It's obvious that cheaper RE technologies like wind and solar are preferred to expensive ones like tidal power in HRES (case 5 and 6), where there is no concern about meeting the unmet load demand because diesel generators are available to satisfy the demands at critical time steps. But in the 100% RE penetration scenario, priority is the system's reliability, so it can be seen that tidal turbine was preferred to solar PV because tidal power is available most of the time compared with intermittent solar power, so the upper limit was selected for the wind turbine, and a tidal turbine of 3003 kW capacity appeared in the structure of the microgrid of Moresby Island. In order to achieve 100% RE penetration in this off-grid territory, a large ZAFB of 339384 kWh energy capacity was applied to buffer the intermittency of wind and tidal power and meet the load demands at critical points.

NPC and LCOE in Moresby Island microgrid at different RE penetration scenarios are shown in figure 4.24. NPC of the system over the project lifetime in the base case in which only diesel generator operates is 186.76 $M; fuel cost includes the biggest portion of this value (151.96 $M), and carbon tax also has the significant portion (22.23 $M). LCOE of the base case is 435.07 $/MWh. It can be seen that NPC and LCOE are reducing by penetrating more RE sources because diesel is replaced by these clean energy sources. This reduction trend goes on by 83.98 % RE penetration rate (case 6), and the lowest NPC and LCOE occur in this case, 81.65 $M and 155.65 $/MWh,

respectively. In case 6, there are 56.3 % and 64.2 % reductions in NPC and LCOE compared with the base case, wind turbine and diesel generator have the highest costs, and solar PV has the lowest cost. However, a larger tidal turbine and ZAFB are required for the 100% penetration scenario (case 7), so NPC of the system is increased, and consequently, the cost of energy is raised. By increasing the RE penetration rate in the Moresby Island microgrid, the NPC of the ZAFB is increased because a larger ZAFB is applied in the configuration of the microgrid. In order to calculate the NPC of the system for each scenario, the final optimum microgrid design (components size) was used. The cost breakdown of the Moresby Island microgrid for each scenario is shown in tables A-17 – A-23 (Appendix A).

Table 4-7 Size of components of Moresby Island microgrid in different RE penetration scenarios

	Components limit	RE penetration (%)	Diesel (kW)	Wind (kW)	Solar (kW)	Tidal (kW)	ZAFB Charge power (kW)	ZAFB Discharge power (kW)	Tank Capacity (kWh)
Case 1	**Wind=0kW Solar=0kW Tidal=0kW Diesel=6000kW**	**0**	**5800**	**-**	**-**	**-**	**-**	**-**	**-**
Case 2	**Wind=600kW Solar=600kW Tidal=600kW Diesel=6000kW**	**20.19**	**5623**	**600**	**600**	**600**	**1.3**	**0.6**	**8**
Case 3	**Wind=1200kW Solar=1200kW Tidal=1200kW Diesel=6000kW**	**38.07**	**5465**	**1200**	**1200**	**1200**	**1192**	**890**	**4806**
Case 4	**Wind=2400kW Solar=2400kW Tidal=2400kW Diesel=6000kW**	**71.53**	**5450**	**2400**	**2400**	**2400**	**1485**	**1881**	**13935**
Case 5	**Wind=4600kW Solar=4600kW Tidal=4600kW Diesel=6000kW**	**83.68**	**5502**	**4592**	**4548**	**1010**	**2273**	**2405**	**43036**
Case 6	**Wind=5800kW Solar=5800kW Tidal=5800kW Diesel=6000kW**	**83.98**	**5794**	**5486**	**5790**	**25**	**2348**	**3022**	**66693**
Case 7	**Wind=6000kW Solar=6000kW Tidal=6000kW Diesel=1kW**	**100**	**0**	**6000**	**0**	**3003**	**8601**	**12987**	**339384**

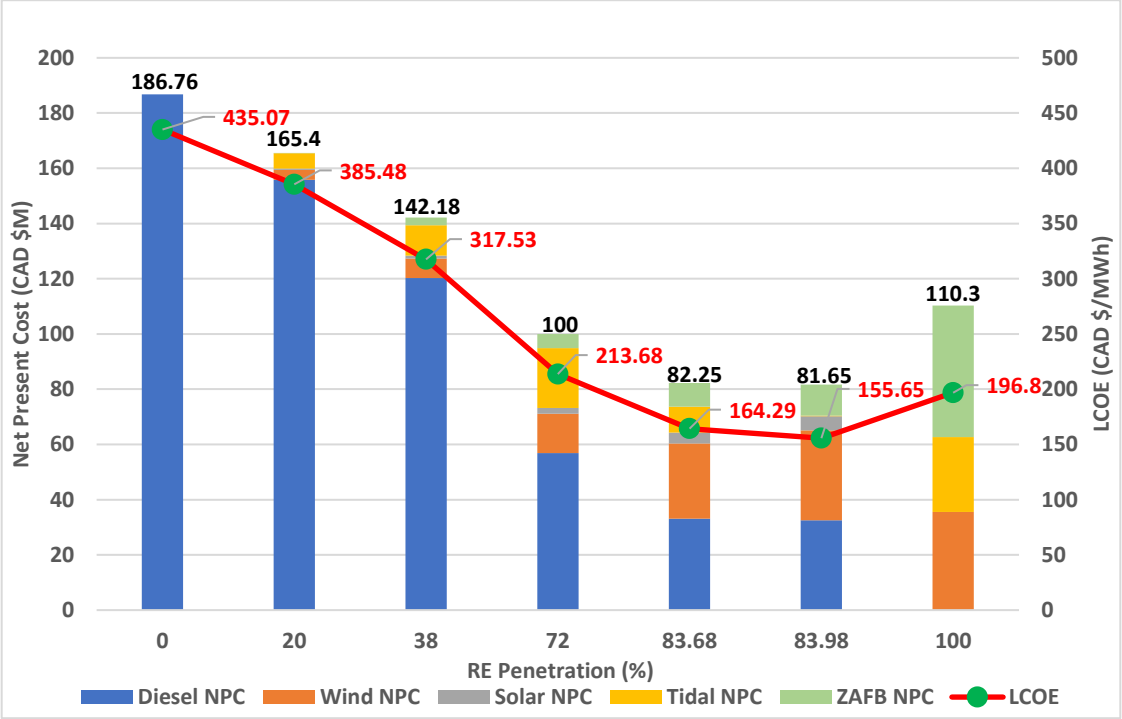

Figure 4.24 NPC (CAPEX+OPEX+Replacement+Fuel+Carbon tax costs) & LCOE of Moresby Island

The storage duration of ZAFB at different RE penetration rates in Moresby Island is shown in figure 4.25. As mentioned earlier, the size of ZAFB components is increased by applying more RE sources in the microgrid. This figure shows that ZAFB has a shorter storage duration in HRES (case 3- case 6) compared with the 100% penetration scenario. For example, in case 6, a hybrid system with the highest RE penetration rate (83.98), a storage tank must be able to provide 22 hours discharge to the grid. But for achieving 100% RE penetration in Moresby Island, ZAFB must have 59 hours storage duration.

Figure 4.26 demonstrates the contribution of ZAFB in satisfying the annual energy demand of Moresby Island in different penetration scenarios. By having a larger battery and more RE sources, ZAFB can have a bigger portion. 16.96% of annual energy demand is met by ZAFB in Moresby Island, which means 4865.9 MWh of energy per year is delivered to the microgrid by ZAFB, and the rest of it (23830.7 MWh) is met by wind and solar power, and excess production of these sources are used to charge the battery. So it's obvious that ZAFB plays a significant role in having a 100% RE microgrid in this remote off-grid area. However, ZAFB suffers from low round trip efficiency due to the

losses inside the system. In the 100% penetration scenario, the round-trip efficiency of the ZAFB is around 55%.

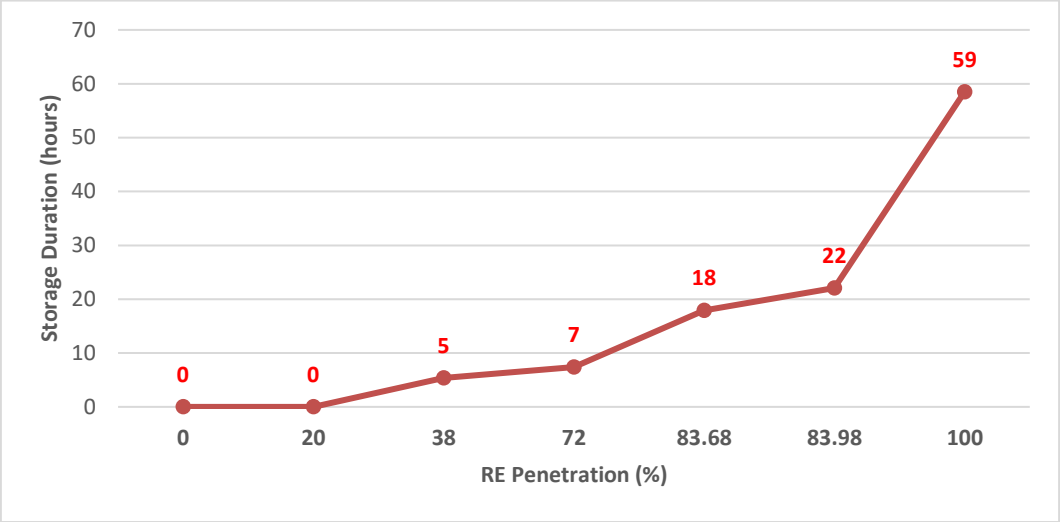

Figure 4.25 Storage duration of ZAFB at different scenarios in Moresby Island

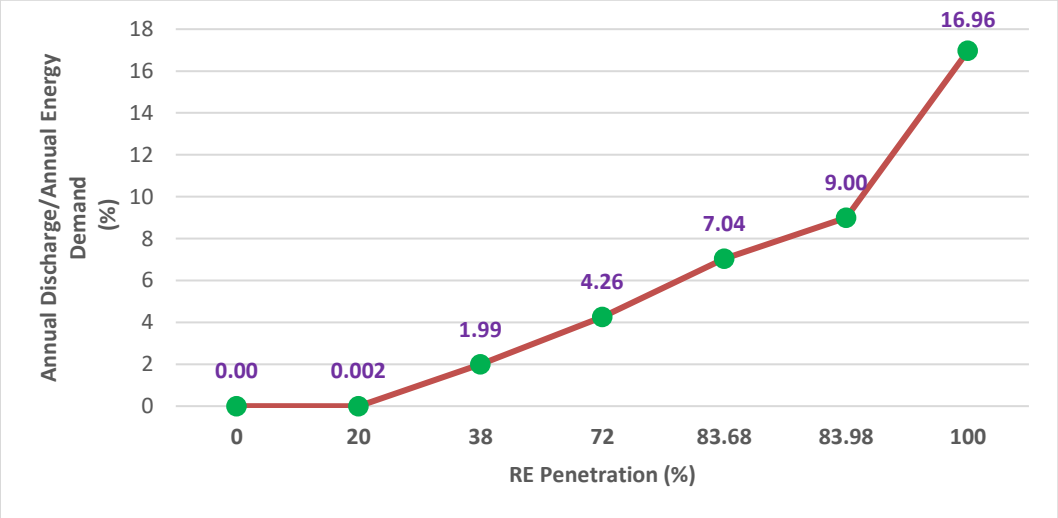

Figure 4.26 ZAFB contribution in total annual energy demand of Moresby Island

Annual diesel fuel consumption of Moresby Island in different scenarios is shown in figure 4.27. Diesel generator in this off-grid community consumes 6.826 ML per year, costing 151.96 $M over the lifetime, and it's 81.37% of NPC of the system in the base case. But it can be seen that by penetrating more RE sources in the microgrid and using larger ZAFB, the operation time of the diesel generator is reduced and, consequently, fuel

consumption. In case 6, hybrid system with 83.98 % RE penetration, annual fuel consumption is decreased by 83.65% compared with the base case. CO_2 emission is directly related to fuel consumption. As shown in figure 4.28, CO_2 emission is reduced at a higher penetration rate. In the base case, diesel generator releases 18 Mtonne CO_2 per year, and such a large amount of emission costs 22.23 $M, which is 12% of NPC of the grid over the lifetime. Obviously, a 100% RE microgrid in Moresby Island, which relies on a wind turbine of 6MW capacity, tidal turbine of 3 MW capacity, and a large battery of 339 MWh energy capacity, can lead to zero fuel consumption and zero-emission.

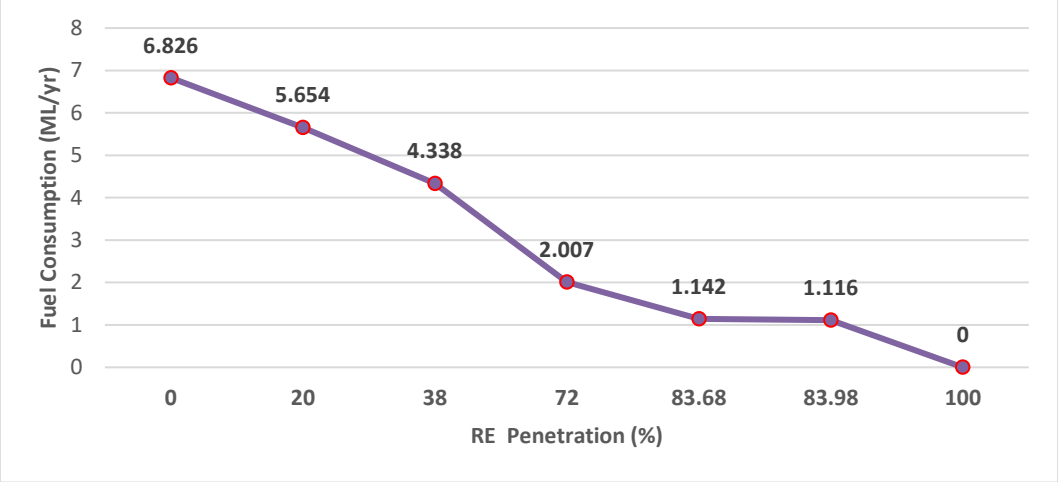

Figure 4.27 Annual Fuel consumption for different RE penetration scenarios in Moresby Island

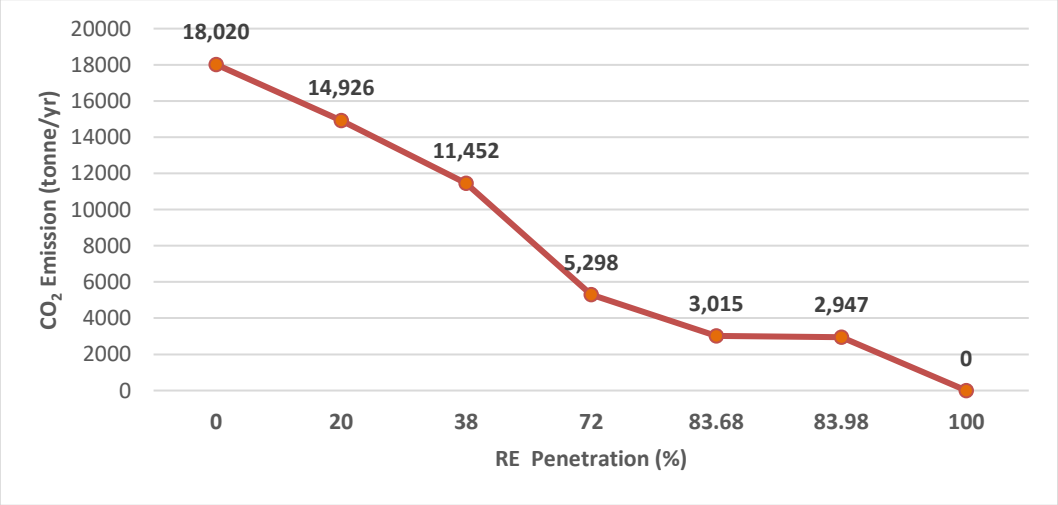

Figure 4.28 Annual CO_2 emission for different RE penetration scenarios in Moresby Island

HRES includes a combination of RE sources, diesel generator, and battery. As shown in table 4-7, a large diesel generator showed up at different RE penetration scenarios (case 2- case6). Figure 4.29 shows the diesel generator output over a year in Moresby Island (Case 6). It can be seen that the diesel generator has to run at peak loads when RE sources don't have enough production. Figure 4.30 demonstrates why a large diesel generator of 5794 kW rated capacity is required in the configuration of the Moresby Island microgrid in case 6 with an 83.98 % RE penetration rate. The reason for such a large diesel generator appearing in the microgrid structure is the lack of RE resources and SoC of the ZAFB at a few critical time steps. As shown in figures 4.30 and 4.31, there is no solar, wind, and tidal power, and ZAFB SoC is zero, so the load demand of 5794 kW must be satisfied by the diesel generator. This critical point determines the rated capacity of the generator. Using the diesel generator at critical peak loads is preferred to adding larger RE sources to the system by the optimizer because it is the optimum way to minimize the NPC.

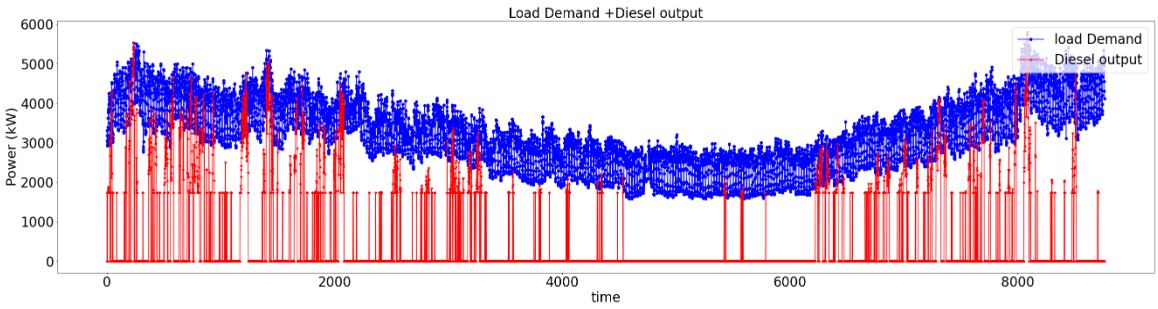

Figure 4.29 Load demand and diesel generator output over a year in Hot Springs Cove (case 6)

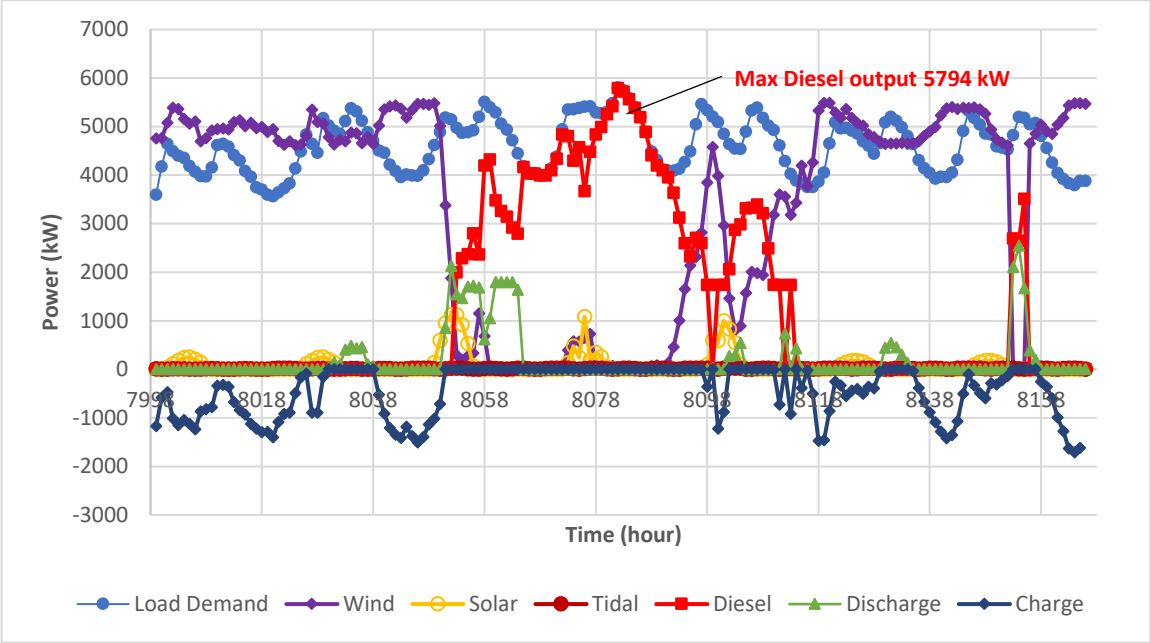

Figure 4.30 Critical point of diesel generator output (case 6)

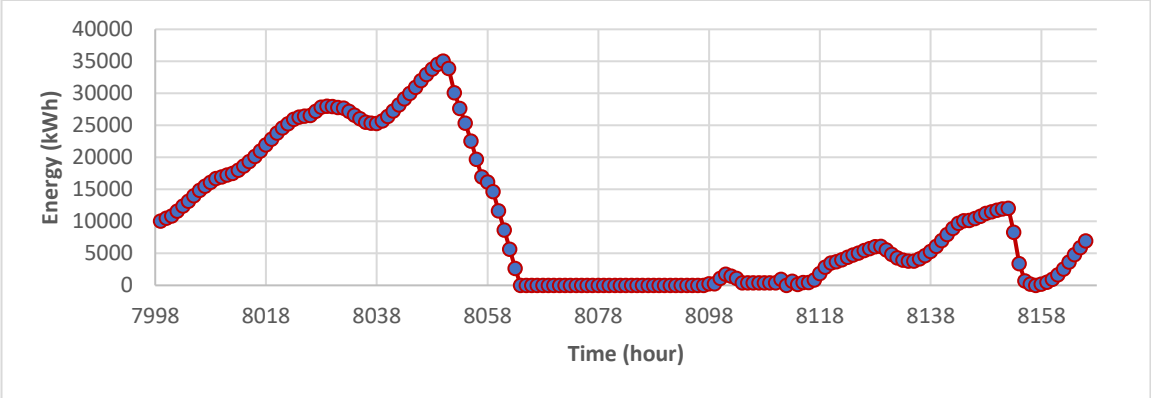

Figure 4.31 SoC of ZAFB at the critical point (case 6)

Energy management is the most important part of the microgrid, which is done by the optimal control model using the receding horizon control method (MPC) in this modeling tool. Because the energy demand and RE resources are not the same in different seasons of the year, the control model must take different control actions. Figures 4.32 and 4.33 show the operation control of components in the Moresby Island microgrid (case 6, 83.98% RE penetration) in the first week of February and August. Load demand in winter is much higher than in summer. On the other hand, RE resources in winter are less than in summer. So, it can be seen that in Feb 1st – Feb 7th, the control model decided to run the

diesel generator to satisfy the demand when RE sources are not sufficient, and ZAFB doesn't have enough charge. But from August 1st – August 7th, the optimal control model decided not to operate the diesel generator. Also, it's obvious that the control model decides to charge the battery when there is excess RE production and discharge the battery to minimize the diesel operation time when necessary, and the battery has enough charge.

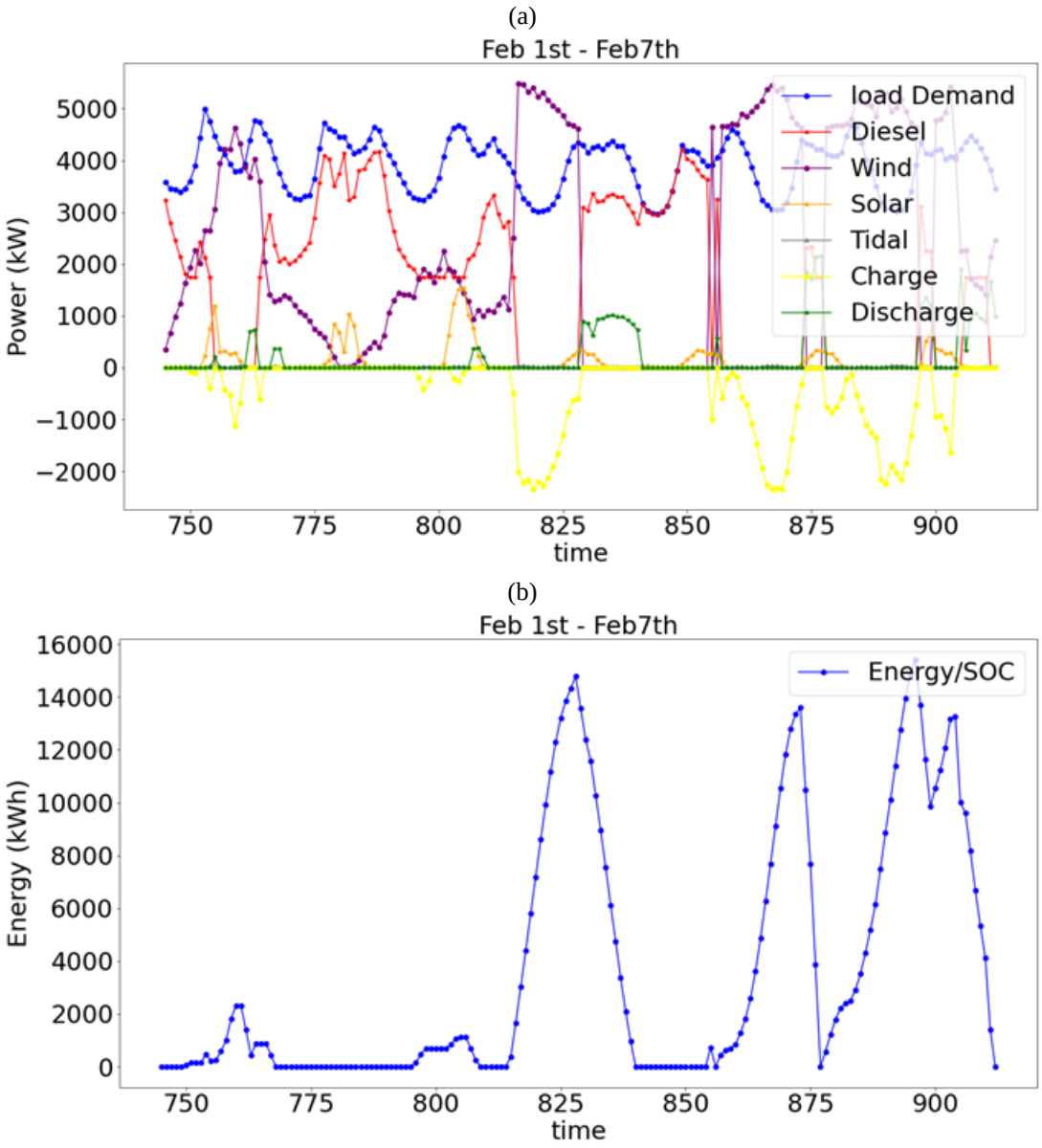

Figure 4.32 Energy management by the control model in winter in Moresby Island (a) components output (b) ZAFB SoC (Case 6)

(a)

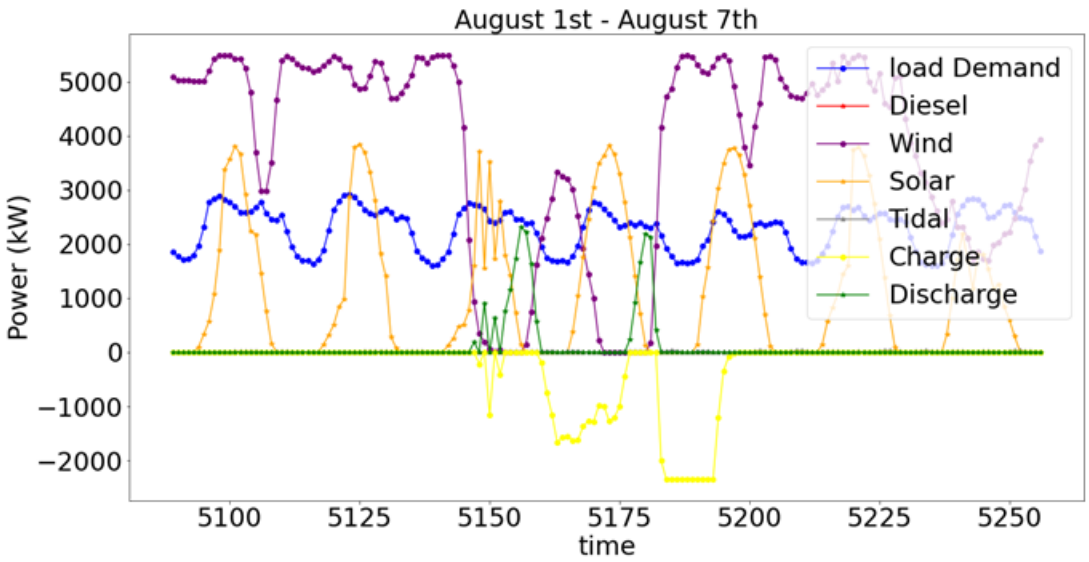

(b)

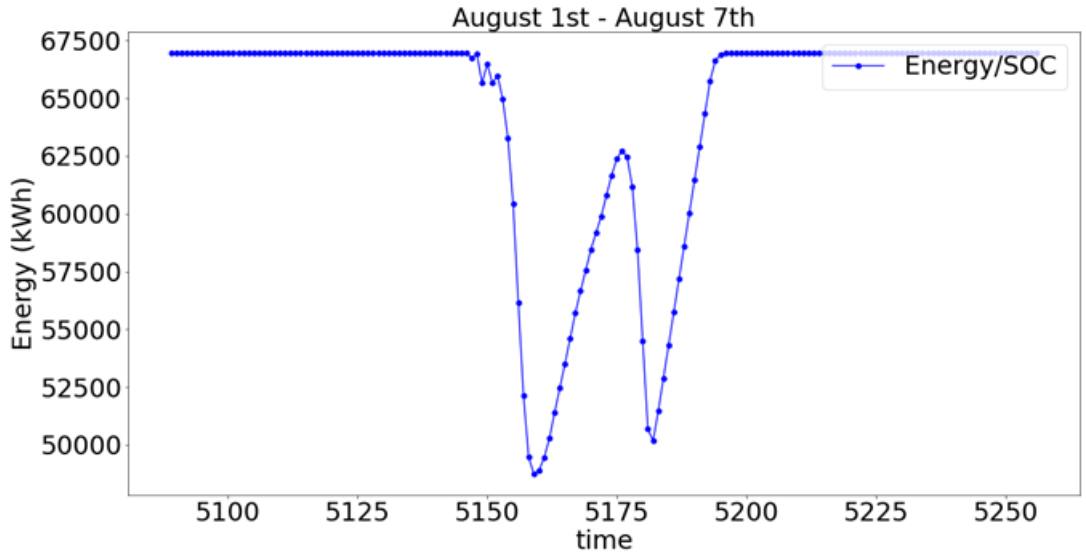

Figure 4.33 Energy management by the control model in summer in Moresby Island (a) components output (b) ZAFB SoC (Case 6)

4.3. ZAFB vs. Li-ion Battery

In this section, ZAFB is compared with Li-ion batteries. For this comparison, three common types of Li-ion batteries which are used in stationary applications were selected. These Li-ion technologies include NMC (lithium nickel, manganese, and cobalt), NCA (lithium nickel, cobalt, and aluminum oxides), LFP (lithium, iron, and phosphate). Table 4-8 shows the specifications of these three types [80], [81].

Table 4-8 Specifications of three types of Li-ion batteries

	Li-ion Battery Cell Data-sheet		
Manufacturer	Samsung	Panasonic	Murata
Cell Chemistry	NMC:C	NCA:C	LFP:C
Cell Format	Prismatic	Cylindrical	Cylindrical
Energy Density	355 Wh/L	676 Wh/L	278 Wh/L
Power Capacity (C-rate, Dch/Ch)	3C/1C	2C/0.5C	6C/1C
Cell Capacity (Ah)	94	3.2	3
Voltage Range (V)	2.7 – 4.15	2.5 – 4.2	2 – 3.6
Capital Cost (CAD $/kWh)	385.67	401.44	507.02

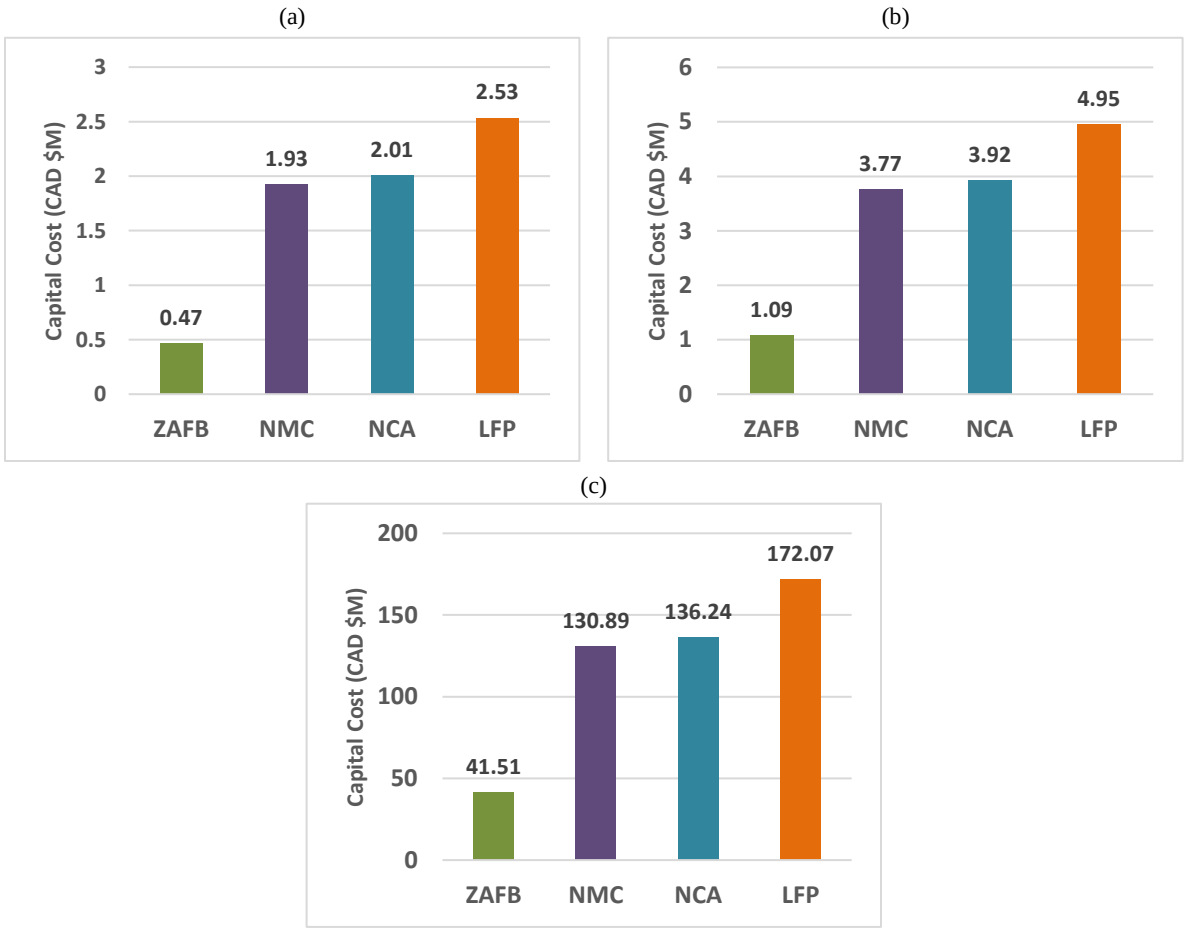

Figure 4.34 Capital cost of different batteries in 100% RE in (a) Blind Channel (b) Hot Spring Cove (c) Moresby Island

The capital cost of ZAFB derived from the optimization process of the microgrid modeling tool was compared with the capital cost of Li-ion batteries with the same energy capacity using their capital cost per kWh. Figure 4.34 shows the capital cost of ZAFB compared with three Li-ion technologies in three case studies in the 100% RE scenario. It can be seen that the CAPEX of ZAFB is much cheaper than Li-ion batteries, 68 – 75% less NMC CAPEX, 69 – 76% less than NCA CAPEX, and 76 – 81% less than LFP CAPEX.

As another comparison, CAPEX per kWh of ZAFB was compared with three Li-ion batteries. Using the capital cost and energy storage capacities of ZAFB and Li-ion batteries, the capital cost per kWh of these batteries at different RE penetration rates in three case studies were determined and are shown in figure 4.35. As shown, the capital cost per kWh of Li-ion batteries is the same for all scenarios because of the structure of these types of batteries in which power and storage are coupled. In contrast, CAPEX per kWh of ZAFB is reduced by increasing RE penetration rate and applying a larger battery due to decoupled feature of this flow battery. Many Li-ion battery cells have to be used when a larger battery is needed in higher RE penetration rates, and each cell has a constant capital cost. But in ZAFB, power units (regenerator, generator) can be scalable separately, and the energy capacity of this battery is very cheap, so when a battery with a larger energy capacity is needed, it will have a lower capital cost per kWh.

Table 4-9 Charge (CH) & discharge (DCH) power capacity of ZAFB and Li-ion batteries in three case studies' 100% RE microgrid

	ZAFB		**NMC**		**NCA**		**LFP**	
	CH Power Capacity (kW)	DCH Power Capacity (kW)	CH Power Capacity (kW)	DCH Power Capacity (kW)	CH Power Capacity (kW)	DCH Power Capacity (kW)	CH Power Capacity (kW)	DCH Power Capacity (kW)
Blind Channel	83	94	4999	14997	2500	9998	4999	29994
Hot Springs Cove	164	354	9764	29292	4882	19528	9764	58584
Moresby Island	8601	12987	339384	1018152	169692	678768	339384	2036304

Since the power capacity of Li-ion batteries is coupled with energy capacity, it's defined by the C-rate, which is exclusive for each Li-ion battery technology. Table 4-8

shows these C-rates. Using these C-rates and energy capacity of the battery in 100% RE scenario in three case studies, rated charge and discharge power capacity of Li-ion batteries were determined and compared with the capacity of regenerator (charge unit) and generator (discharge unit). Table 4-9 shows these values. The nominal power capacities of Li-ion batteries are much higher than ZAFB's ones. In the case studies, li-ion batteries may not have such a large output power in the 100% RE microgrids. In other words, a battery with a large energy capacity is needed for 100% RE scenarios, and large energy capacity means larger power (charge/discharge) capacity in Li-ion batteries. Therefore, such a scalable battery like ZAFB with decoupled power and energy is required for microgrids of any size and 100% RE penetration.

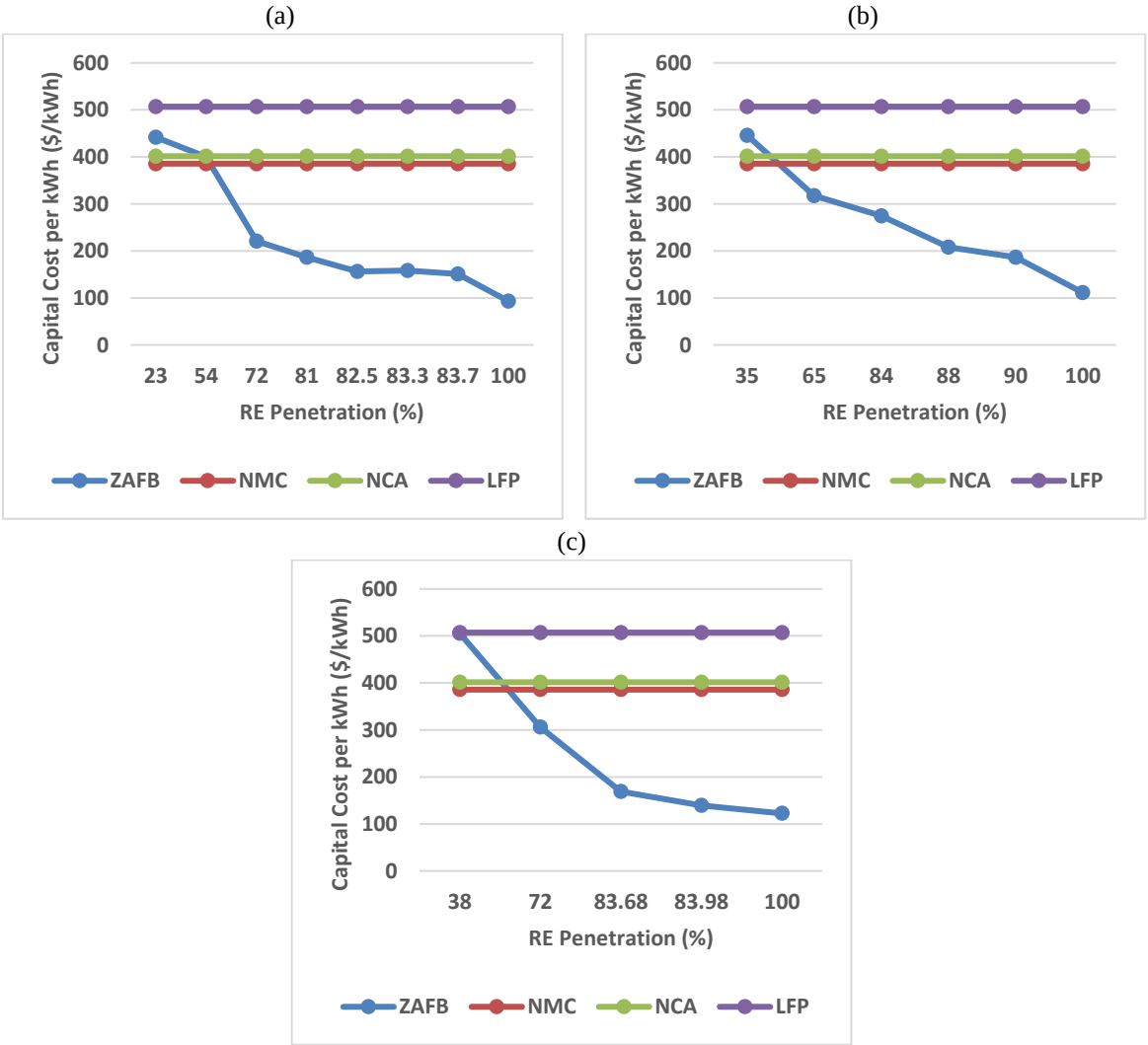

Figure 4.35 Capital cost per kWh of ZAFB & Li-ion batteries at different RE penetration rates in (a) Blind Channel (b) Hot Spring Cove (c) Moresby Island

4.4. Insights

By penetrating more RE and incorporating larger ZAFB, fuel consumption and CO_2 emission are reduced. Zero diesel consumption and CO_2 emission were achieved in the 100% RE penetration scenario in all three case studies. Figure 4.36 shows the fuel NPC and carbon tax NPC over the project lifetime for all three case studies. It can be seen that considerable savings can be made in 100% RE microgrids. For Blind Channel, $1.45M is saved by 1.3 ML fuel consumption reduction, and $0.21M is saved from carbon tax by impeding 3.44 Gtonnes of CO_2 release. For Hot Spring Cove, $5.83M is saved by eliminating 5.23 ML diesel fuel consumption over the project lifetime, and also $0.85M is saved by preventing 13.82 Gtonnes of CO_2 emission. In Moresby Island, $151.96M is saved by removing the dependency of this remote area on 136.52 ML diesel, and $22.23M is saved from carbon tax by eliminating 360.4 Gtonnes of CO_2 emission from this region.

A longer duration energy storage system is one of the most important requirements of RE 100% systems. Applying batteries with large energy storage may be impossible for costly batteries like Li-ion in which power and energy are coupled. Therefore, a cheap flow battery with scalable power and energy units that has a very low energy capacity unit price can be the best option for the longer-duration application in microgrids. Figure 4.37 demonstrates that applying a longer duration ZAFB in the microgrid in all case studies significantly reduces the capital cost per kWh of ZAFB. As shown, ZAFB should have 50 – 59 hours of storage duration in 100 RE penetration scenarios, and it will cost 93 – 122 $/kWh in these cases. It is clear that ZAFB with decoupled and scalable energy, charge and discharge units, and cheap raw material, and very low capital cost for longer duration energy storage (around 100 $/kWh) can be a good candidate for 100% RE microgrids.

(a)

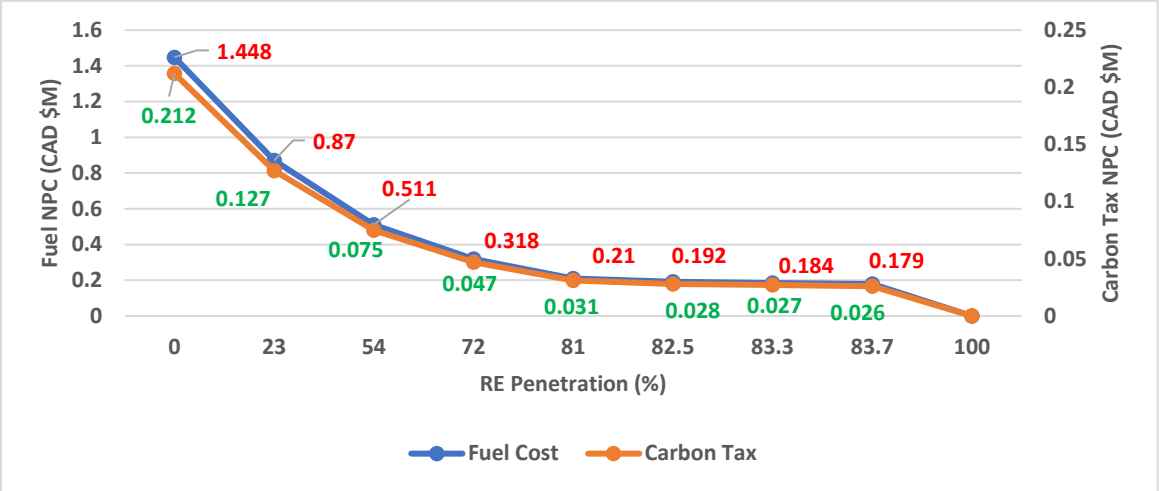

(b)

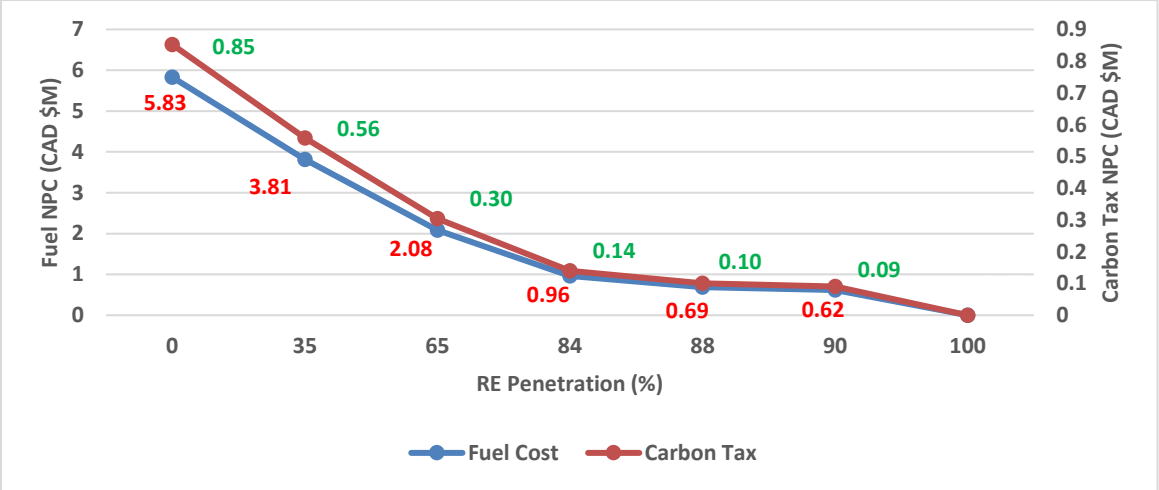

(c)

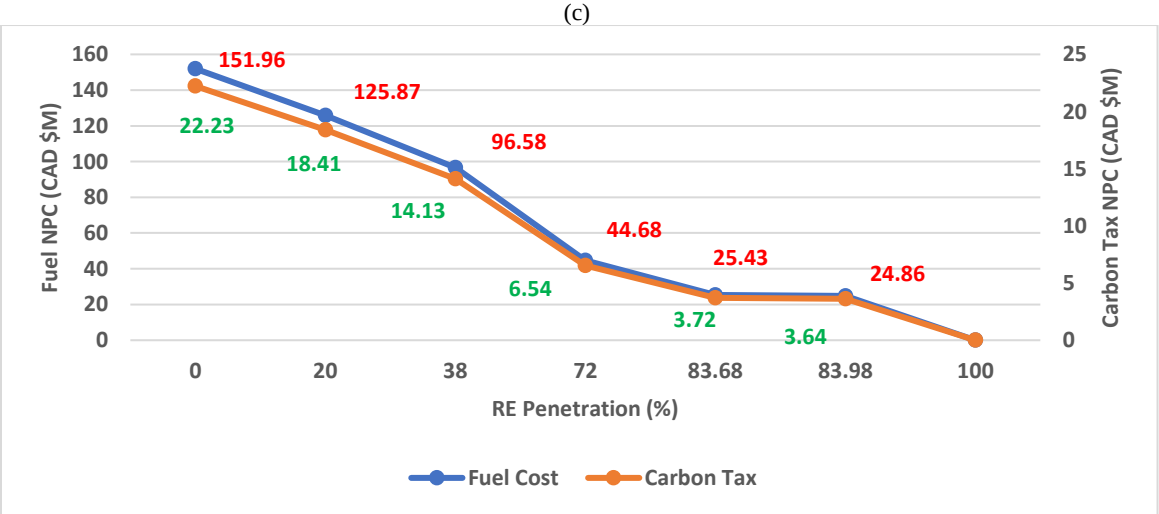

Figure 4.36 Fuel & carbon tax NPC at different RE penetration rates in (a) Blind Channel (b) Hot Spring Cove (c) Moresby Island

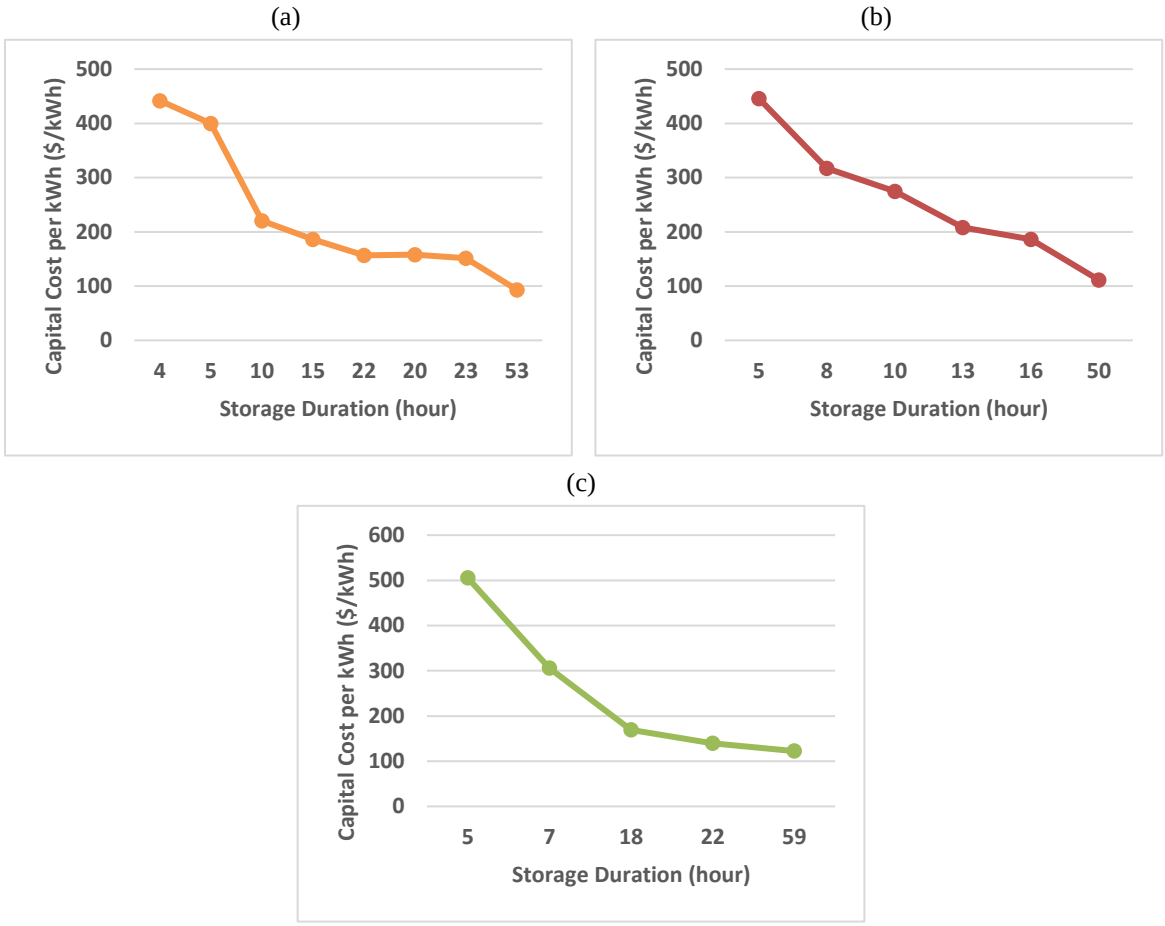

Figure 4.37 Capital cost per kWh of ZAFB at different storage durations in (a) Blind Channel (b) Hot Spring Cove (c) Moresby Island

In HRES, case studies results show that larger ZAFB, wind turbine, and solar PV show up in the microgrid structure by increasing the RE penetration rate. The tidal turbine appears only at a lower penetration rate when the upper limit of RE sources is too small, and it disappears or gets smaller at higher penetration rates. Solar PV was preferred to the tidal turbine by the optimizer because tidal power technology is costly. Solar PV shows up when a diesel generator is available as a reserve source. In hybrid systems, a large diesel generator is responsible for meeting the critical peak loads when RE sources are unavailable, and ZAFB doesn't have enough charge. Based on the results, the lowest NPC and LCOE can be achievable in HRES.

In all case studies, integration of ZAFB with microgrids led to achieving 100% RE penetration, zero diesel fuel consumption, and zero CO_2 emission. Configuration of these

microgrids includes large wind and tidal turbines with larger ZAFB. In 100% RE scenarios, RE sources that are available most of the time, show up in the microgrid structure, and they are preferred by the optimizer even if they are expensive technologies. For this reason, costly tidal power technology is preferred to cheap and mature solar PV. Also, a ZAFB with a large energy storage capacity is required for capturing as much charge power as possible from RE excess production and satisfying the load demands when RE sources are not available or enough. Obviously, the battery must have a longer duration energy storage capacity to achieve 100% RE, which is possible with ZAFB technology. Based on the case studies results and as shown in figure 4.38, ZAFB with 50 – 60 hours storage duration is needed for 100% RE microgrids, and this size of the battery can satisfy 17% - 23% of total annual energy demand in off-grid communities. The capacity of power units (charge/discharge) was determined separately by the microgrid modeling tool to get enough charge from the RE sources and deliver adequate discharge to compensate for the lack of RE sources. In addition, NPC and LCOE in 100% RE scenarios are reduced by 39 – 46 % and 55 – 60 %, respectively, compared with the base case.

(a)

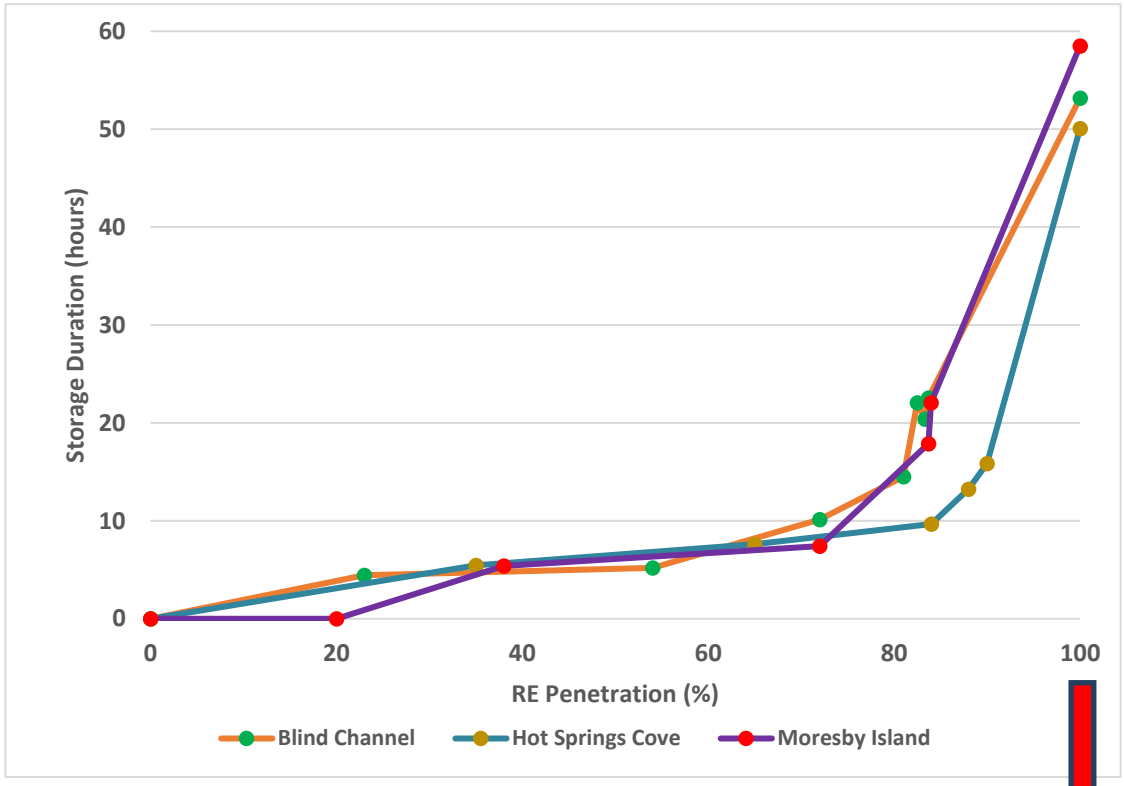

(b)

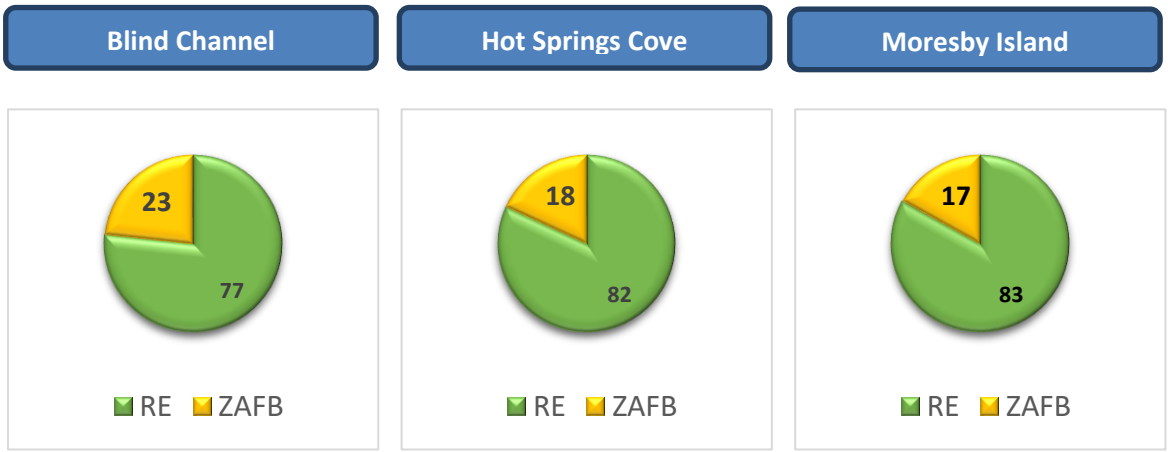

Figure 4.38 ZAFB (a) storage duration at different RE penetration (b) contribution (%) in annual energy demand (100% RE system)

Chapter 5

5. Conclusion and Future Developments

In this work, we developed a model for ZAFB, which includes a semi-empirical performance model, energy-based SoC model, efficiency and cost models. This model is accurate, efficient, and applicable for large-scale modeling. We also developed optimal design and control models for microgrids using a bilevel optimization approach to simultaneously minimize the energy system's cost and the diesel generator's operation. The optimal design model is responsible for sizing the microgrid components, and the optimal control model optimizes the operation of components using the MPC method (receding horizon control method). Incorporating the ZAFB model in this microgrid model led to a microgrid modeling tool for off-grid communities, and ZAFB evaluated techno-economically through this tool.

The functionality of the microgrid modeling tool and the impact of integrating ZAFB with RE sources like wind, tidal and solar power to reduce or eliminate the dependency of off-grid remote areas on fossil fuels were tested in three case studies in British Columbia: Blind Channel, Hot Spring Cove, Moresby Island with different RE penetration scenarios.

The results of the first case study (Blind Channel) showed that 100% RE and zero fuel consumption, and zero CO_2 emission are achievable by a microgrid in which a wind turbine of 98 kW capacity and a tidal turbine of 10 kW capacity, and a large ZAFB with 4999 kWh energy capacity, 83 kW charge power capacity and 94 kW discharge capacity are the main energy sources and the ESS, respectively. 23.3% of annual energy demand was satisfied by ZAFB in Blind Channel 100% RE microgrid. For this purpose, ZAFB must be able to provide 53.2 hours discharge at maximum power. NPC and LCOE in this 100% RE system are 1.167 $M and 368.34 $/MWh, 38.7% and 58.3% less than base case ones. The lowest NPC and LCOE appeared in HRES with 83.7% RE penetration.

In the second case study (Hot Springs Cove), we achieved 100 % RE penetration by integrating a ZAFB of 9764 kWh energy capacity with a wind turbine of 200 kW capacity and a tidal turbine of 200 kW capacity. In order to capture as much charge as possible from RE sources and meet the load demand at critical time steps, the optimum size of the regenerator and power unit (generator) was found for this microgrid. ZAFB

delivered 158.37 MWh per year to Hot Springs Cove, 18.13% of the annual energy demand. NPC (4.08 $M) and LCOE (229.44 $/MWh) in this energy system were reduced by 45.9% and 60.3% compared with the base case. HRES with 90% RE penetration had the lowest NPC and LCOE among all scenarios.

The results of the last case study (Moresby Island) demonstrated that we could have a 100% RE microgrid with zero fuel consumption and CO_2 emission even for large size off-grid communities like Moresby Island by having enough RE sources and large ZAFB. This microgrid consists of a 6 MW wind turbine, 3 MW tidal turbine, and 339 MWh ZAFB. In the 100% RE penetration scenario, the battery had 59 hours of storage duration, and 16.96 % of annual energy demand (1868 MWh) was met by ZAFB, and NPC was reduced from 186.76 $M to 110.33 $M. There was also a 54.8% reduction in LCOE compared with the base case one (435.07 $/MWh). However, the lowest NPC and LCOE were in a hybrid system with 83.98 % RE penetration.

Overall, diesel generators and fuel consumption can totally be eliminated from off-grid communities, and 100% RE penetration is achievable by incorporating large ZAFB with a longer storage duration in microgrids. For this purpose, ZAFB must have 50-60 hours of storage duration, and 17-23 % of annual energy demand can be met by ZAFB. By penetrating more RE in the system, a larger battery is picked by the optimal design model. The optimum size of energy capacity, regenerator, and generator (power unit) power capacity are selected for each RE penetration scenario via this modeling tool. Wind power is the main energy source in 100% RE microgrids. Although tidal power is an expensive technology, it's preferred to solar power in 100% RE scenarios because tidal power is available more often than solar power in coastal communities in B.C. These remote areas suffer from cloudiness and northern latitudes, and wind and tidal resources are available most of the time throughout the year and ready to harness. As a result, although solar power is the cheapest technology, it shows up only in the structure of the hybrid systems when the diesel generator is available as a reserve source to meet the demand at critical time steps. The lowest NPC and LCOE are possible in HRES. These values are a bit greater in 100% RE systems because of applying larger RE plants and ZAFB. This microgrid modeling tool is applicable for all off-grid communities of

any size, and ZAFB is a promising technology by which we can achieve 100% RE penetration and totally remove the dependency of these territories on diesel fuel.

5.1. Future Work

To further develop this modeling tool, some future works can be done in the continuation of this study. Developments can be in three sections: Accuracy, reliability, and functionality improvements.

One of the most important developments that can be done is the accuracy improvements of microgrid modeling and components models. Applying more accurate performance models is the way to have better microgrid modeling. ZAFB, as one of the microgrid components, has the potential for more development. ZAFB model can be developed more accurately by adding the mechanical losses like pumping or HVAC system and a linear or nonlinear model of open-circuit voltage as a function of SoC and considering the impact of electrolyte flow rate in the performance model. In addition, material and performance degradation models can be proposed using the experimental data and integrated with the ZAFB model. Another future work that improves the accuracy of the ZAFB and microgrid models is to add the real-world design constraints of ZAFB, such as the allowable number of cells in each stack and maximum allowable cell current density, etc. to the optimal design model (upper level).

The second type of future works can be done to improve the control model. The robustness and reliability of microgrid modeling, particularly the optimal control model, can be improved by using a robust optimization method and considering the uncertainty of load demand profile, RE resources, microgrid components failures, and fuel price. Also, the Li-ion battery and VRFB models can be added to the control model to allow the optimizer to choose the best battery technology for the microgrid. Another improvement can be made by adding voltage and frequency control to the control model. For this purpose, DC-AC inverter models using the droop control method, which is used for islanded microgrids, can be added to the control model to keep the voltage and frequency, stable and in an allowable range.

The last future works are related to functionality improvements of the microgrid modeling tool. For example, by having one more optimization stage to optimize the design of ZAFB after finding the optimum size of components, including the volume of electrolyte, initial concentration of zinc, and KOH, piping, flow rates, pumping, etc. microgrid modeling tool will be much more useful and practical. Although most of excess RE production is captured by the battery in 100% RE microgrids, a big portion of this energy source is curtailed when the battery is full of charge. All RE curtailment can be used for producing green hydrogen. For this purpose, hydrogen storage and fuel cell models should be added to the optimal control model. In this way, this modeling tool can be the best option for islanded microgrids of any size.

Bibliography

[1] "Our Energy Needs: World Energy Consumption & Demand," *CAPP*. https://www.capp.ca/energy/world-energy-needs/ (accessed Apr. 27, 2021).

[2] N. R. C. Government of Canada, "Natural Resources Canada. The Atlas of Canada. Remote Communities Energy Database," Sep. 12, 2016. https://atlas.gc.ca/rced-bdece/en/index.html (accessed Apr. 28, 2021).

[3] C. E. R. Government of Canada, "NEB – Market Snapshot: Overcoming the challenges of powering Canada's off-grid communities," Jan. 29, 2021. https://www.cer-rec.gc.ca/en/data-analysis/energy-markets/market-snapshots/2018/market-snapshot-overcoming-challenges-powering-canadas-off-grid-communities.html (accessed Apr. 28, 2021).

[4] "Frequently Asked Questions (FAQs) - U.S. Energy Information Administration (EIA)." https://www.eia.gov/tools/faqs/faq.php (accessed Apr. 28, 2021).

[5] "Wind map Canada - VORTEX." https://vortexfdc.com/knowledge/wind-map-canada/ (accessed Jun. 14, 2021).

[6] "Solar Energy Maps Canada 2021 (Every Province)." https://www.energyhub.org/solar-energy-maps-canada/ (accessed Jun. 14, 2021).

[7] "How zinc-air battery capacity might reach a cost of $45/kWh – pv magazine USA." https://pv-magazine-usa.com/2020/02/27/how-zinc-air-battery-capacity-might-reach-a-cost-of-45-kwh/ (accessed Jun. 15, 2021).

[8] C. Bloch, J. Newcomb, S. Shiledar, and M. Tyson, "Breakthrough Batteries: Powering the Era of Clean Electrification," *Rocky Mountain Institute*, 2019, [Online]. Available: http://www.rmi.org/breakthrough-batteries

[9] "Zinc-Air Regenerative Fuel Cell System - Zinc8 Energy Solutions." https://www.zinc8energy.com/technology (accessed Apr. 28, 2021).

[10] G. Mendes, C. Ioakimidis, and P. Ferrão, "On the planning and analysis of Integrated Community Energy Systems: A review and survey of available tools," *Renewable and Sustainable Energy Reviews*, vol. 15, no. 9, pp. 4836–4854, Dec. 2011, doi: 10.1016/j.rser.2011.07.067.

[11] B. Kuri and F. Li, "Distributed generation planning in the deregulated electricity supply industry," in *IEEE Power Engineering Society General Meeting, 2004.*, Denver, CO, USA, 2004, vol. 2, pp. 2085–2089. doi: 10.1109/PES.2004.1373248.

[12] "Microgrids: A solution for modern-day energy challenges," *Cushing Terrell*, Jan. 25, 2021. https://cushingterrell.com/microgrids-a-solution-for-modern-day-energy-challenges/ (accessed Apr. 28, 2021).

[13] S. Kamel, "The economics of hybrid power systems for sustainable desert agriculture in Egypt," *Energy*, vol. 30, no. 8, pp. 1271–1281, Jun. 2005, doi: 10.1016/j.energy.2004.02.004.

[14] Y. Himri, A. B. Stambouli, B. Draoui, and S. Himri, "Techno-economical study of hybrid power system for a remote village in Algeria," *Energy*, vol. 33, no. 7, pp. 1128–1136, 2008.

[15] J. G. Fantidis, D. V. Bandekas, and N. Vordos, "Techno-economical study of hybrid power system for a remote village in Greece," *Environment and Sustainable Development*, p. 6.

[16] G. Rohani and M. Nour, “Techno-economical analysis of stand-alone hybrid renewable power system for Ras Musherib in United Arab Emirates,” *Energy*, vol. 64, pp. 828–841, Jan. 2014, doi: 10.1016/j.energy.2013.10.065.
[17] S. Rehman, Md. Mahbub Alam, J. P. Meyer, and L. M. Al-Hadhrami, “Feasibility study of a wind–pv–diesel hybrid power system for a village,” *Renewable Energy*, vol. 38, no. 1, pp. 258–268, Feb. 2012, doi: 10.1016/j.renene.2011.06.028.
[18] S. K. A. Shezan, N. Das, and H. Mahmudul, “Techno-economic analysis of a smart-grid hybrid renewable energy system for Brisbane of Australia,” *Energy Procedia*, vol. 110, pp. 340–345, 2017.
[19] K. Murugaperumal and P. A. D. V. Raj, “Feasibility design and techno-economic analysis of hybrid renewable energy system for rural electrification,” *Solar Energy*, vol. 188, pp. 1068–1083, 2019.
[20] J. P. Lopes *et al.*, “Control strategies for microgrids emergency operation,” in *2005 International Conference on Future Power Systems*, 2005, p. 6 pp. – 6.
[21] A. G. Madureira and J. P. Lopes, “Coordinated voltage support in distribution networks with distributed generation and microgrids,” *IET Renewable Power Generation*, vol. 3, no. 4, pp. 439–454, 2009.
[22] L. Uwineza, H.-G. Kim, and C. K. Kim, “Feasibility study of integrating the renewable energy system in Popova Island using the Monte Carlo model and HOMER,” *Energy Strategy Reviews*, vol. 33, p. 100607, Jan. 2021, doi: 10.1016/j.esr.2020.100607.
[23] S. Mohammadi, S. Soleymani, and B. Mozafari, “Scenario-based stochastic operation management of MicroGrid including Wind, Photovoltaic, Micro-Turbine, Fuel Cell and Energy Storage Devices,” *International Journal of Electrical Power & Energy Systems*, vol. 54, pp. 525–535, Jan. 2014, doi: 10.1016/j.ijepes.2013.08.004.
[24] A. Kafetzis, C. Ziogou, K. D. Panopoulos, S. Papadopoulou, P. Seferlis, and S. Voutetakis, “Energy management strategies based on hybrid automata for islanded microgrids with renewable sources, batteries and hydrogen,” *Renewable and Sustainable Energy Reviews*, vol. 134, p. 110118, Dec. 2020, doi: 10.1016/j.rser.2020.110118.
[25] P. Firouzmakan, R.-A. Hooshmand, M. Bornapour, and A. Khodabakhshian, “A comprehensive stochastic energy management system of micro-CHP units, renewable energy sources and storage systems in microgrids considering demand response programs,” *Renewable and Sustainable Energy Reviews*, vol. 108, pp. 355–368, Jul. 2019, doi: 10.1016/j.rser.2019.04.001.
[26] M. R. Quitoras, P. E. Campana, and C. Crawford, “Exploring electricity generation alternatives for Canadian Arctic communities using a multi-objective genetic algorithm approach,” *Energy Conversion and Management*, vol. 210, p. 112471, Apr. 2020, doi: 10.1016/j.enconman.2020.112471.
[27] B. S. Borowy and Z. M. Salameh, “Methodology for optimally sizing the combination of a battery bank and PV array in a wind/PV hybrid system,” *IEEE Transactions on energy conversion*, vol. 11, no. 2, pp. 367–375, 1996.
[28] M. A. Elhadidy and S. M. Shaahid, “Optimal sizing of battery storage for hybrid (wind+ diesel) power systems,” *Renewable Energy*, vol. 18, no. 1, pp. 77–86, 1999.

[29] P. Arun, R. Banerjee, and S. Bandyopadhyay, “Optimum sizing of battery-integrated diesel generator for remote electrification through design-space approach,” *Energy*, vol. 33, no. 7, pp. 1155–1168, 2008.
[30] M. R. Aghamohammadi and H. Abdolahinia, “A new approach for optimal sizing of battery energy storage system for primary frequency control of islanded microgrid,” *International Journal of Electrical Power & Energy Systems*, vol. 54, pp. 325–333, 2014.
[31] T. A. Nguyen, M. L. Crow, and A. C. Elmore, “Optimal sizing of a vanadium redox battery system for microgrid systems,” *IEEE transactions on sustainable energy*, vol. 6, no. 3, pp. 729–737, 2015.
[32] G. He, Q. Chen, C. Kang, and Q. Xia, “Optimal operating strategy and revenue estimates for the arbitrage of a vanadium redox flow battery considering dynamic efficiencies and capacity loss,” *IET Generation, Transmission & Distribution*, vol. 10, no. 5, pp. 1278–1285, 2016.
[33] T. Sarkar, A. Bhattacharjee, H. Samanta, K. Bhattacharya, and H. Saha, “Optimal design and implementation of solar PV-wind-biogas-VRFB storage integrated smart hybrid microgrid for ensuring zero loss of power supply probability,” *Energy conversion and management*, vol. 191, pp. 102–118, 2019.
[34] M. Mohiti, M. Mazidi, N. Rezaei, and M.-H. Khooban, “Role of vanadium redox flow batteries in the energy management system of isolated microgrids,” *Journal of Energy Storage*, vol. 40, p. 102673, 2021.
[35] J. Fu *et al.*, “A flexible solid-state electrolyte for wide-scale integration of rechargeable zinc–air batteries,” *Energy & Environmental Science*, vol. 9, no. 2, pp. 663–670, 2016.
[36] S. Suren and S. Kheawhom, “Development of a high energy density flexible zinc-air battery,” *Journal of the Electrochemical Society*, vol. 163, no. 6, p. A846, 2016.
[37] J. Park, M. Park, G. Nam, J. Lee, and J. Cho, “All-solid-state cable-type flexible zinc–air battery,” *Advanced Materials*, vol. 27, no. 8, pp. 1396–1401, 2015.
[38] M. Bockelmann, U. Kunz, and T. Turek, “Electrically rechargeable zinc-oxygen flow battery with high power density,” *Electrochemistry Communications*, vol. 69, pp. 24–27, 2016.
[39] Y. Li *et al.*, “Advanced zinc-air batteries based on high-performance hybrid electrocatalysts,” *Nature communications*, vol. 4, no. 1, pp. 1–7, 2013.
[40] B. A. Gutierrez, J. A. Colborn, S. I. Smedley, and K. I. Smedley, *Particle feeding apparatus for electrochemical power source and method of making same*. Google Patents, 2000.
[41] S. I. Smedley and X. G. Zhang, “A regenerative zinc–air fuel cell,” *Journal of power sources*, vol. 165, no. 2, pp. 897–904, 2007.
[42] B. Amunátegui, A. Ibáñez, M. Sierra, and M. Pérez, “Electrochemical energy storage for renewable energy integration: zinc-air flow batteries,” *Journal of Applied Electrochemistry*, vol. 48, no. 6, pp. 627–637, 2018.
[43] Z. Mao and R. E. White, “Mathematical modeling of a primary zinc/air battery,” *Journal of the Electrochemical Society*, vol. 139, no. 4, p. 1105, 1992.
[44] E. Deiss, F. Holzer, and O. Haas, “Modeling of an electrically rechargeable alkaline Zn–air battery,” *Electrochimica acta*, vol. 47, no. 25, pp. 3995–4010, 2002.

[45] D. Schröder and U. Krewer, “Model based quantification of air-composition impact on secondary zinc air batteries,” *Electrochimica Acta*, vol. 117, pp. 541–553, 2014.
[46] K. Wang *et al.*, “Dendrite growth in the recharging process of zinc–air batteries,” *Journal of Materials Chemistry A*, vol. 3, no. 45, pp. 22648–22655, 2015.
[47] K. Wongrujipairoj, L. Poolnapol, A. Arpornwichanop, S. Suren, and S. Kheawhom, “Suppression of zinc anode corrosion for printed flexible zinc-air battery,” *physica status solidi (b)*, vol. 254, no. 2, p. 1600442, 2017.
[48] W. Lao-Atiman, K. Bumroongsil, A. Arpornwichanop, P. Bumroongsakulsawat, S. Olaru, and S. Kheawhom, “Model-based analysis of an integrated zinc-air flow battery/zinc electrolyzer system,” *Frontiers in Energy Research*, vol. 7, p. 15, 2019.
[49] M. M. Saleh, J. W. Weidner, B. E. El-Anadouli, and B. G. Ateya, “Electrowinning of Nonnoble Metals with Simultaneous Hydrogen Evolution at Flow-Through Porous Electrodes: III. Time Effects,” *Journal of the Electrochemical society*, vol. 144, no. 3, p. 922, 1997.
[50] J. Dundálek *et al.*, “Zinc electrodeposition from flowing alkaline zincate solutions: Role of hydrogen evolution reaction,” *Journal of Power Sources*, vol. 372, pp. 221–226, 2017.
[51] S. Olaru, A. Golovkina, W. Lao-atiman, and S. Kheawhom, “A Mathematical Model for Dynamic Operation of Zinc-Air Battery Cells,” *IFAC-PapersOnLine*, vol. 52, no. 17, pp. 66–71, 2019, doi: 10.1016/j.ifacol.2019.11.028.
[52] D. M. Rosewater, D. A. Copp, T. A. Nguyen, R. H. Byrne, and S. Santoso, “Battery Energy Storage Models for Optimal Control,” *IEEE Access*, vol. 7, pp. 178357–178391, 2019, doi: 10.1109/ACCESS.2019.2957698.
[53] J. O. Bockris and A. K. N. Reddy, *Modern electrochemistry: an introduction to an interdisciplinary area*. New York: Plenum, 1973.
[54] A. Abbasi, S. Hosseini, A. Somwangthanaroj, R. Cheacharoen, S. Olaru, and S. Kheawhom, “Discharge profile of a zinc-air flow battery at various electrolyte flow rates and discharge currents,” *Sci Data*, vol. 7, no. 1, p. 196, Dec. 2020, doi: 10.1038/s41597-020-0539-y.
[55] W. Lao-atiman, S. Olaru, A. Arpornwichanop, and S. Kheawhom, “Discharge performance and dynamic behavior of refuellable zinc-air battery,” *Sci Data*, vol. 6, no. 1, p. 168, Dec. 2019, doi: 10.1038/s41597-019-0178-3.
[56] W. Lao-Atiman, K. Bumroongsil, A. Arpornwichanop, P. Bumroongsakulsawat, S. Olaru, and S. Kheawhom, “Model-based analysis of an integrated zinc-air flow battery/zinc electrolyzer system,” *Frontiers in Energy Research*, vol. 7, p. 15, 2019.
[57] “Pacific Regional Institute for Marine Energy Discovery.” https://onlineacademiccommunity.uvic.ca/primed/
[58] Anthony Truelove, Brad Buckham, Curran Crawford, and Clayton Hiles, “Scaling Technology Models for HOMER Pro,” PRIMED, Unpublished report, 2020.
[59] HOMER Energy, *HOMER Pro*. 2018. [Online]. Available: https://www.homerenergy.com/
[60] J. A. Duffie and W. A. Beckman, “Solar Engineering of Thermal Processes John Wiley & Sons,” *Inc. New York*, 1991.

[61] D. G. Erbs, S. A. Klein, and J. A. Duffie, “Estimation of the diffuse radiation fraction for hourly, daily and monthly-average global radiation,” *Solar energy*, vol. 28, no. 4, pp. 293–302, 1982.
[62] J. J. Roberts, A. A. Mendiburu Zevallos, and A. M. Cassula, “Assessment of photovoltaic performance models for system simulation,” *Renewable and Sustainable Energy Reviews*, vol. 72, pp. 1104–1123, May 2017, doi: 10.1016/j.rser.2016.10.022.
[63] D. E. Franklin, “Calculations for a Grid-Connected Solar Energy System,” p. 8.
[64] T. Lambert, P. Gilman, and P. Lilienthal, “Micropower system modeling with HOMER,” *Integration of alternative sources of energy*, vol. 1, no. 1, pp. 379–385, 2006.
[65] E. J. Hoevenaars and C. A. Crawford, “Implications of temporal resolution for modeling renewables-based power systems,” *Renewable Energy*, vol. 41, pp. 285–293, 2012.
[66] R. Ahshan, N. Hosseinzadeh, and A. H. Al-Badi, “Economic evaluation of a remote microgrid system for an Omani island,” *IJSGCE*, pp. 495–510, 2020, doi: 10.12720/sgce.9.3.495-510.
[67] Shelley McDougall, “Commercial Potential of Marine Renewables in British Columbia,” S. L. McDougall Research & Consulting, 2019.
[68] G. Liuzzi, S. Lucidi, and F. Rinaldi, “An algorithmic framework based on primitive directions and nonmonotone line searches for black-box optimization problems with integer variables,” *Math. Prog. Comp.*, vol. 12, no. 4, pp. 673–702, Dec. 2020, doi: 10.1007/s12532-020-00182-7.
[69] M. L. Bynum *et al.*, *Pyomo—Optimization Modeling in Python*, vol. 67. Springer Nature, 2021.
[70] “Pyomo Documentation 6.0.1 — Pyomo 6.0.1 documentation.” https://pyomo.readthedocs.io/en/stable/ (accessed Jul. 13, 2021).
[71] “Gurobi - The fastest solver - Gurobi.” https://www.gurobi.com/ (accessed Jul. 13, 2021).
[72] “Renewable Energy for Remote Communities (RERC) Program - Province of British Columbia.” https://www2.gov.bc.ca/gov/content/industry/electricity-alternative-energy/community-energy-solutions/renewable-energy-remote-communities (accessed Jul. 15, 2021).
[73] “Wind Atlas - Environment and Climate Change Canada.” http://www.windatlas.ca (accessed Jul. 15, 2021).
[74] “Tides, Currents, and Water Levels.” https://tides.gc.ca/eng (accessed Jul. 16, 2021).
[75] “Discount Rate - Ontario Teachers’ Pension Plan.” https://www.otpp.com/corporate/plan-funding/funding-valuations/discount-rate (accessed Jul. 16, 2021).
[76] “Daily Average Retail Prices for Diesel in 2021 | Natural Resources Canada.” https://www2.nrcan.gc.ca/eneene/sources/pripri/prices_bycity_e.cfm?PriceYear=0&ProductID=5&LocationID=66,8,39,17#PriceGraph (accessed Jul. 16, 2021).
[77] “British Columbia’s Carbon Tax - Province of British Columbia.” https://www2.gov.bc.ca/gov/content/environment/climate-change/clean-economy/carbon-tax (accessed Jul. 16, 2021).

[78] “Blind Channel Resort.” https://www.blindchannel.com/ (accessed Jul. 19, 2021).
[79] “Moresby Island – British Columbia Travel and Adventure Vacations.” https://britishcolumbia.com/plan-your-trip/regions-and-towns/northern-bc-and-haida-gwaii/moresby-island/ (accessed Jul. 20, 2021).
[80] H. Hesse, M. Schimpe, D. Kucevic, and A. Jossen, “Lithium-Ion Battery Storage for the Grid—A Review of Stationary Battery Storage System Design Tailored for Applications in Modern Power Grids,” *Energies*, vol. 10, no. 12, p. 2107, Dec. 2017, doi: 10.3390/en10122107.
[81] G. Patry, A. Romagny, S. Martinet, and D. Froelich, “Cost modeling of lithium-ion battery cells for automotive applications,” *Energy Sci Eng*, vol. 3, no. 1, pp. 71–82, Jan. 2015, doi: 10.1002/ese3.47.

Appendix A

Blind Channel:

Table A-1 Blind Channel microgrid component size and cost breakdown in case 1 (0% Penetration)

Component	**Capacity** (kW)	**NPC** (CAD $M)	**Capital Cost** (CAD $M)	**Replacement Cost** (CAD $M)	**Fuel Cost** (CAD $M) 20yr	**VOM Cost** (CAD $M) 20yr	**Carbon Tax** (CAD $M) 20yr
Diesel gen	62	1.898	0.034	0.102	1.448	0.103	0.212
Wind T	-	-	-	-	-	-	-
Solar PV	-	-	-	-	-	-	-
Tidal T	-	-	-	-	-	-	-
Regenerator	-		-	-	-	-	-
Generator	-	-	-	-	-	-	-
Tank (kWh)	-		-	-	-	-	-

Table A-2 Blind Channel microgrid component size and cost breakdown in case 2 (23% Penetration)

Component	**Capacity** (kW)	**NPC** (CAD $M)	**Capital Cost** (CAD $M)	**Replacement Cost** (CAD $M)	**Fuel Cost** (CAD $M) 20yr	**VOM Cost** (CAD $M) 20yr	**Carbon Tax** (CAD $M) 20yr
Diesel gen	60	1.150	0.033	0.058	0.870	0.062	0.127
Wind T	5	0.045	0.028	0	-	0.017	-
Solar PV	5	0.012	0.011	0	-	0.001	-
Tidal T	5	0.046	0.032	0	-	0.014	-
Regenerator	20.464		0.021	0.002	-	0.003	-
Generator	28.564	0.069	0.029	0	-	0.004	-
Tank (kWh)	129		0.007	0	-	0.001	-

Table 0-3 Blind Channel microgrid component size and cost breakdown in case 3 (54% Penetration)

Component	**Capacity** (kW)	**NPC** (CAD $M)	**Capital Cost** (CAD $M)	**Replacement Cost** (CAD $M)	**Fuel Cost** (CAD $M) 20yr	**VOM Cost** (CAD $M) 20yr	**Carbon Tax** (CAD $M) 20yr
Diesel gen	60	0.675	0.033	0.020	0.511	0.037	0.075
Wind T	10	0.084	0.050	0	-	0.034	-
Solar PV	10	0.020	0.019	0	-	0.001	-
Tidal T	10	0.093	0.065	0	-	0.028	-
Regenerator	17.310		0.018	0.002	-	0.003	-
Generator	24.428	0.059	0.025	0	-	0.004	-
Tank (kWh)	125		0.007	0	-	0.001	-

Table A-4 Blind Channel microgrid component size and cost breakdown in case 4 (71% Penetration)

Component	Capacity (kW)	NPC (CAD $M)	Capital Cost (CAD $M)	Replacement Cost (CAD $M)	Fuel Cost (CAD $M) 20yr	VOM Cost (CAD $M) 20yr	Carbon Tax (CAD $M) 20yr
Diesel gen	60	0.437	0.033	0.017	0.318	0.023	0.047
Wind T	15	0.118	0.067	0	-	0.051	-
Solar PV	15	0.027	0.026	0	-	0.002	-
Tidal T	15	0.139	0.097	0	-	0.042	-
Regenerator	13.727		0.014	0.002	-	0.002	-
Generator	20.840	0.056	0.021	0	-	0.003	-
Tank (kWh)	213		0.012	0	-	0.002	-

Table 0-5 Blind Channel microgrid component size and cost breakdown in case 5 (81% Penetration)

Component	Capacity (kW)	NPC (CAD $M)	Capital Cost (CAD $M)	Replacement Cost (CAD $M)	Fuel Cost (CAD $M) 20yr	VOM Cost (CAD $M) 20yr	Carbon Tax (CAD $M) 20yr
Diesel gen	60	0.288	0.033	0	0.210	0.015	0.031
Wind T	25	0.176	0.090	0	-	0.085	-
Solar PV	0	0.000	0.000	0	-	0.000	-
Tidal T	18	0.167	0.117	0	-	0.050	-
Regenerator	17.678		0.018	0.002	-	0.003	-
Generator	19.505	0.065	0.020	0	-	0.003	-
Tank (kWh)	290		0.016	0	-	0.002	-

Table 0-6 Blind Channel microgrid component size and cost breakdown in case 6 (82% Penetration)

Component	Capacity (kW)	NPC (CAD $M)	Capital Cost (CAD $M)	Replacement Cost (CAD $M)	Fuel Cost (CAD $M) 20yr	VOM Cost (CAD $M) 20yr	Carbon Tax (CAD $M) 20yr
Diesel gen	60	0.267	0.033	0	0.192	0.014	0.028
Wind T	35	0.227	0.108	0	-	0.119	-
Solar PV	0	0.000	0.000	0	-	0.000	-
Tidal T	11	0.102	0.071	0	-	0.031	-
Regenerator	22.857		0.024	0.003	-	0.004	-
Generator	19.650	0.082	0.020	0	-	0.003	-
Tank (kWh)	441		0.025	0	-	0.004	-

Table A-7 Blind Channel microgrid component size and cost breakdown in case 7 (83.3% Penetration)

Component	Capacity (kW)	NPC (CAD $M)	Capital Cost (CAD $M)	Replacement Cost (CAD $M)	Fuel Cost (CAD $M) 20yr	VOM Cost (CAD $M) 20yr	Carbon Tax (CAD $M) 20yr
Diesel gen	60	0.257	0.033	0	0.184	0.013	0.027
Wind T	38	0.241	0.112	0	-	0.129	-
Solar PV	0	0	0	0	-	0	-
Tidal T	10	0.093	0.065	0	-	0.028	-
Regenerator	23.089		0.024	0.003	-	0.004	-
Generator	21.622	0.085	0.022	0	-	0.003	-
Tank (kWh)	449		0.025	0	-	0.004	-

Table 0-8 Blind Channel microgrid component size and cost breakdown in case 8 (83.7% Penetration)

Component	**Capacity** (kW)	**NPC** (CAD $M)	**Capital Cost** (CAD $M)	**Replacement Cost** (CAD $M)	**Fuel Cost** (CAD $M) 20yr	**VOM Cost** (CAD $M) 20yr	**Carbon Tax** (CAD $M) 20yr
Diesel gen	60	0.251	0.033	0	0.179	0.013	0.026
Wind T	40	0.251	0.115	0	-	0.136	-
Solar PV	0	0	0	0	-	0	-
Tidal T	9	0.084	0.058	0	-	0.025	-
Regenerator	24.250		0.025	0.003	-	0.004	-
Generator	21.760	0.090	0.022	0	-	0.003	-
Tank (kWh)	496		0.028	0	-	0.004	-

Table 0-9 Blind Channel microgrid component size and cost breakdown in case 9 (100% Penetration)

Component	**Capacity** (kW)	**NPC** (CAD $M)	**Capital Cost** (CAD $M)	**Replacement Cost** (CAD $M)	**Fuel Cost** (CAD $M) 20yr	**VOM Cost** (CAD $M) 20yr	**Carbon Tax** (CAD $M) 20yr
Diesel gen	0	0	0	0	0	0	0
Wind T	98	0.538	0.204	0	-	0.334	-
Solar PV	0	0	0	0	-	0	-
Tidal T	10	0.093	0.065	0	-	0.028	-
Regenerator	83.337		0.087	0	-	0.013	-
Generator	93.522	0.536	0.096	0	-	0.014	-
Tank (kWh)	4999		0.283	0	-	0.042	-

Hot Springs Cove:

Table 0-10 Hot Springs Cove microgrid component size and cost breakdown in case 1 (0% Penetration)

Component	Capacity (kW)	NPC (CAD $M)	Capital Cost (CAD $M)	Replacement Cost (CAD $M)	Fuel Cost (CAD $M) 20yr	VOM Cost (CAD $M) 20yr	Carbon Tax (CAD $M) 20yr
Diesel gen	195	7.546	0.105	0.298	5.827	0.464	0.852
Wind T	-	-	-	-	-	-	-
Solar PV	-	-	-	-	-	-	-
Tidal T	-	-	-	-	-	-	-
Regenerator	-		-	-	-	-	-
Generator	-	-	-	-	-	-	-
Tank	-		-	-	-	-	-

Table A-11 Hot Springs Cove microgrid component size and cost breakdown in case 2 (35% Penetration)

Component	Capacity (kW)	NPC (CAD $M)	Capital Cost (CAD $M)	Replacement Cost (CAD $M)	Fuel Cost (CAD $M) 20yr	VOM Cost (CAD $M) 20yr	Carbon Tax (CAD $M) 20yr
Diesel gen	175	4.977	0.095	0.214	3.813	0.297	0.558
Wind T	40	0.227	0.115	0	-	0.112	-
Solar PV	40	0.049	0.044	0	-	0.005	-
Tidal T	40	0.371	0.260	0	-	0.112	-
Regenerator	40.790		0.043	0	-	0.006	-
Generator	39.368	0.109	0.040	0	-	0.006	-
Tank (kWh)	213		0.012	-	-	0.002	-

Table A-12 Hot Springs Cove microgrid component size and cost breakdown in case 3 (65% Penetration)

Component	Capacity (kW)	NPC (CAD $M)	Capital Cost (CAD $M)	Replacement Cost (CAD $M)	Fuel Cost (CAD $M) 20yr	VOM Cost (CAD $M) 20yr	Carbon Tax (CAD $M) 20yr
Diesel gen	174	2.742	0.094	0.105	2.079	0.160	0.304
Wind T	80	0.397	0.174	0	-	0.224	-
Solar PV	80	0.076	0.067	0	-	0.009	-
Tidal T	80	0.742	0.519	0	-	0.223	-
Regenerator	58.047		0.061	0.006247	-	0.009	-
Generator	62.959	0.181	0.064	0	-	0.010	-
Tank (kWh)	479		0.027	-	-	0.004	-

Table A-13 Hot Springs Cove microgrid component size and cost breakdown in case 4 (84% Penetration)

Component	Capacity (kW)	NPC (CAD $M)	Capital Cost (CAD $M)	Replacement Cost (CAD $M)	Fuel Cost (CAD $M) 20yr	VOM Cost (CAD $M) 20yr	Carbon Tax (CAD $M) 20yr
Diesel gen	174	1.313	0.094	0.044	0.960	0.074	0.140
Wind T	120	0.580	0.244	0	-	0.336	-
Solar PV	118	0.106	0.092	0	-	0.014	-
Tidal T	120	1.113	0.778	0	-	0.335	-
Regenerator	99.107		0.104	0.010979	-	0.016	-
Generator	95.649	0.303	0.098	0	-	0.015	-
Tank (kWh)	929		0.053	-	-	0.008	-

Table A-14 Hot Springs Cove microgrid component size and cost breakdown in case 5 (88% Penetration)

Component	**Capacity** (kW)	**NPC** (CAD $M)	**Capital Cost** (CAD $M)	**Replacement Cost** (CAD $M)	**Fuel Cost** (CAD $M) 20yr	**VOM Cost** (CAD $M) 20yr	**Carbon Tax** (CAD $M) 20yr
Diesel gen	174	0.933	0.094	0	0.685	0.053	0.100
Wind T	160	0.769	0.321	0	-	0.448	-
Solar PV	147	0.131	0.114	0	-	0.017	-
Tidal T	108	1.002	0.701	0	-	0.301	-
Regenerator	116.375		0.122	0.013271	-	0.018	-
Generator	124.442	0.406	0.127	0	-	0.019	-
Tank (kWh)	1643		0.093	-	-	0.014	-

Table 0-15 Hot Springs Cove microgrid component size and cost breakdown in case 6 (90% Penetration)

Component	**Capacity** (kW)	**NPC** (CAD $M)	**Capital Cost** (CAD $M)	**Replacement Cost** (CAD $M)	**Fuel Cost** (CAD $M) 20yr	**VOM Cost** (CAD $M) 20yr	**Carbon Tax** (CAD $M) 20yr
Diesel gen	174	0.846	0.094	0	0.615	0.048	0.090
Wind T	200	0.960	0.400	0	-	0.560	-
Solar PV	199	0.176	0.153	0	-	0.023	-
Tidal T	78	0.724	0.506	0	-	0.218	-
Regenerator	139.724		0.146	0.015934	-	0.022	-
Generator	141.913	0.497	0.145	0	-	0.022	-
Tank (kWh)	2249		0.128	-	-	0.019	-

Table 0-16 Hot Springs Cove microgrid component size and cost breakdown in case 7 (100% Penetration)

Component	**Capacity** (kW)	**NPC** (CAD $M)	**Capital Cost** (CAD $M)	**Replacement Cost** (CAD $M)	**Fuel Cost** (CAD $M) 20yr	**VOM Cost** (CAD $M) 20yr	**Carbon Tax** (CAD $M) 20yr
Diesel gen	0	0	0	0	0	0	0
Wind T	200	0.960	0.400	0	-	0.560	-
Solar PV	0	0	0	0	-	0	-
Tidal T	200	1.853	1.295	0	-	0.558	-
Regenerator	163.932		0.171	0.018695	-	0.026	-
Generator	353.787	1.268	0.362	0	-	0.054	-
Tank (kWh)	9764		0.554	-	-	0.083	-

Moresby Island:

Table 0-17 Moresby Island microgrid component size and cost breakdown in case 1 (0% Penetration)

Component	Capacity (kW)	NPC (CAD $M)	Capital Cost (CAD $M)	Replacement Cost (CAD $M)	Fuel Cost (CAD $M) 20yr	VOM Cost (CAD $M) 20yr	Carbon Tax (CAD $M) 20yr
Diesel gen	5800	186.76	2.414	5.781	151.961	4.674	22.229
Wind T	-	-	-	-	-	-	-
Solar PV	-	-	-	-	-	-	-
Tidal T	-	-	-	-	-	-	-
Regenerator	-		-	-	-	-	-
Generator	-	-	-	-	-	-	-
Tank (kWh)	-		-	-	-	-	-

Table 0-18 Moresby Island microgrid component size and cost breakdown in case 2 (20% Penetration)

Component	Capacity (kW)	NPC (CAD $M)	Capital Cost (CAD $M)	Replacement Cost (CAD $M)	Fuel Cost (CAD $M) 20yr	VOM Cost (CAD $M) 20yr	Carbon Tax (CAD $M) 20yr
Diesel gen	5623	155.859	2.347	5.629	125.873	3.598	18.413
Wind T	600	3.560	1.200	0	-	2.360	-
Solar PV	600	0.522	0.462	0	-	0.060	-
Tidal T	600	5.536	3.862	0	-	1.674	-
Regenerator	1.322			0.0001	-	0.000	-
Generator	0.561	0.003	0.001	0	-	0.000	-
Tank (kWh)	8			0	-	0.000	-

Table 0-19 Moresby Island microgrid component size and cost breakdown in case 3 (38% Penetration)

Component	Capacity (kW)	NPC (CAD $M)	Capital Cost (CAD $M)	Replacement Cost (CAD $M)	Fuel Cost (CAD $M) 20yr	VOM Cost (CAD $M) 20yr	Carbon Tax (CAD $M) 20yr
Diesel gen	5465	120.224	2.287	4.489	96.575	2.746	14.127
Wind T	1200	7.120	2.400	0	-	4.720	-
Solar PV	1200	1.044	0.924	0	-	0.120	-
Tidal T	1200	11.002	7.654	0	-	3.348	-
Regenerator	1192.413		1.247	0	-	0.187	-
Generator	889.681	2.792	0.909	0	-	0.136	-
Tank (kWh)	4806		0.273	0	-	0.041	-

Table A-20 Moresby Island microgrid component size and cost breakdown in case 4 (71% Penetration)

Component	Capacity (kW)	NPC (CAD $M)	Capital Cost (CAD $M)	Replacement Cost (CAD $M)	Fuel Cost (CAD $M) 20yr	VOM Cost (CAD $M) 20yr	Carbon Tax (CAD $M) 20yr
Diesel gen	5450	56.870	2.281	2.109	44.681	1.263	6.536032
Wind T	2400	14.241	4.800	0	-	9.441	-
Solar PV	2400	2.089	1.848	0	-	0.241	-
Tidal T	2400	21.726	15.031	0	-	6.695	-
Regenerator	1485.057		1.553	0.165	-	0.232	-
Generator	1880.633	5.067	1.922	0	-	0.287	-
Tank (kWh)	13935		0.790	0	-	0.118	-

Table 0-21 Moresby Island microgrid component size and cost breakdown in case 5 (83% Penetration)

Component	Capacity (kW)	NPC (CAD $M)	Capital Cost (CAD $M)	Replacement Cost (CAD $M)	Fuel Cost (CAD $M) 20yr	VOM Cost (CAD $M) 20yr	Carbon Tax (CAD $M) 20yr
Diesel gen	5502	33.139	2.301	0.968	25.428	0.722	3.720
Wind T	4592	27.247	9.184	0	-	18.063	-
Solar PV	4548	3.958	3.502	0	-	0.456	-
Tidal T	1010	9.278	6.461	0	-	2.818	-
Regenerator	2273.318		2.377	0.267	-	0.356	-
Generator	2404.931	8.630	2.458	0	-	0.368	-
Tank (kWh)	43036		2.440	0	-	0.365	-

Table A-22 Moresby Island microgrid component size and cost breakdown in case 6 (84% Penetration)

Component	Capacity (kW)	NPC (CAD $M)	Capital Cost (CAD $M)	Replacement Cost (CAD $M)	Fuel Cost (CAD $M) 20yr	VOM Cost (CAD $M) 20yr	Carbon Tax (CAD $M) 20yr
Diesel gen	5794	32.558	2.412	0.955	24.855	0.701	3.636
Wind T	5486	32.552	10.972	0	-	21.580	-
Solar PV	5790	5.039	4.458	0	-	0.580	-
Tidal T	25	0.232	0.162	0	-	0.070	-
Regenerator	2347.893		2.455	0.531	-	0.367	-
Generator	3022.458	11.269	3.089	0	-	0.462	-
Tank (kWh)	66963		3.797	0	-	0.568	-

Table A-23 Moresby Island microgrid component size and cost breakdown in case 7 (100% Penetration)

Component	Capacity (kW)	NPC (CAD $M)	Capital Cost (CAD $M)	Replacement Cost (CAD $M)	Fuel Cost (CAD $M) 20yr	VOM Cost (CAD $M) 20yr	Carbon Tax (CAD $M) 20yr
Diesel gen	0	0	0	0	0	0	0
Wind T	6000	35.602	12	0	-	23.602	-
Solar PV	0	0	0	0	-	0	-
Tidal T	3003	27.014	18.637	0	-	8.377	-
Regenerator	8601.18		8.995	0	-	1.346	-
Generator	12987.27	47.719	13.271	0	-	1.985	-
Tank (kWh)	339384		19.243	0	-	2.879	-